Title	Design and Development of Magnetic Variable Transmission
Author(s)	Husain, Mustafa
Citation	大阪大学, 2013, 博士論文
Version Type	VoR
URL	https://hdl.handle.net/11094/24955
rights	
Note	

Doctoral Dissertation

Design and Development of Magnetic Variable Transmission

Mustafa Husain

January 2013

Graduate School of Engineering

OsakaUniversity

Work. Finish. Publish

        Michael Farady (1791-1867)

Dedicated to my loving parents, my lovely wife Fatima and adorable children Ali and Kawthar

Acknowledgements

Abstract

The objective of this study is the development and analysis of techniques to realize magnetic variable transmission. At the time of the beginning of this study, there were many patents and researches on magnetic transmission but no published research on magnetic variable transmission. Magnetic variable transmission is useful in many applications such as wind power generation, power tools, automotives, and so on.

The magnetic gear is contactless and quiet in operation, and it requires no lubrication. In addition, it slips when overloaded. On the other hand, the mechanical gear requires frequent maintenance and may break down when overloaded.

A high performance magnetic gear based on the concept of modulated magnetic flux was theoretically investigated by Atallah et al in 2001 based on an improved design of an old patent. The developed gear was operational at a fixed gear ratio.

In this work, several techniques have been proposed to realize magnetic variable transmission. The first technique is based on the concept of pole changing. This technique has been validated by finite element analysis (FEA) and by experiment. The second technique uses several magnetic gears with different topologies forming a multi-element magnetic gear. This method has been validated by FEA. The developed techniques are a good beginning of a new research that is predicted to grow rapidly towards industrial and commercial applications.

The theory of operation of magnetic gears has been improved using a basic model that gives a clear and simple insight into the concept

of the magnetic gearing. Torque equations that include design parameters have been derived. In addition, guidelines for the design and optimization of magnetic gears have been developed which can be used as a tool for a quick and approximate design process before making an FEA model.

Contents

List of Figures

Nomenclature

Roman Symbols

B Magnetic Field density

F_m Resultant magneto-motive force

G_r Gear ratio

H Magnetic Field intensity

I Electric current

J Electric current density

K_R Ratio of cogging torque to transmitted torque

l_a Axial length

N Number of coil turns

P_i Number of pole pairs of inner rotor

P_o Number of pole pairs of outer rotor

P_s Number of pole pieces

R_g Air-gap reluctance

T_{cog} Cogging torque

T_i Electromagnetic torque exerted on inner rotor

T_o Electromagnetic torque exerted on outer rotor

T_s Electromagnetic torque exerted on pole pieces

Greek Symbols

α_i Arc-to-pitch ratio of inner rotor

α_o Arc-to-pitch ratio of outer rotor

α_s Arc-to-pitch ratio of pole piece

Λ_g Air-gap permeance

λ_i Pitch of inner rotor

λ_o Pitch of outer rotor

λ_s Pitch of pole piece

μ Permeability of a material

μ_o Permeability of air

μ_r Relative permeability of a material

ω_i Angular speed of inner rotor

ω_o Angular speed of outer rotor

ϕ_g air-gap magnetic flux

θ_i Angular displacement of inner rotor

θ_o Angular displacement of outer rotor

θ_s Angular displacement of pole pieces

Acronyms

EVT   Electrical variable transmission

FEA   Finite element analysis

IPM   Interior permanent magnet

mmf   Magneto-motive force

MVT Magnetic variable transmission

NdFeB Permanent magnet Neodymium-Iron-Boron

RNA   Reluctance network analysis

SPM   Surface permanent magnet

Chapter 1

Introduction

1.1 Objective of magnetic gearing

The objective of studying magnetic gears is to replace mechanical gears which are noisy, require frequent maintenance and lubrication, and suffer from friction losses. In addition, the mechanical gear may break down if overloaded heavily.

Thus, to overcome the drawbacks of the mechanical gear, new technologies for power transmission need to be developed.

On the other hand, the magnetic gear is contactless and quiet in operation, and it does not require lubrication. Another attractive advantage is that it slips when overloaded.

1.2 Evolution of magnetic gearing

The operation of a spur gear (Fig.1.1) forms the founding principle of mechanical gearing. It has two wheels with different numbers of teeth, and the teeth come in direct contact with each other as the wheels rotate.

To develop an analogous gear without direct contact between the teeth implies magnetic means. The simplest way is the use of the same design of the spur gear, but with the condition that the teeth must be magnetized. The first attempt of this approach was patented in 1901 by Armstrong [Arm01]. The schematic diagram of Armstrong's prototype is reproduced in Fig.1.2a. There are two bi-
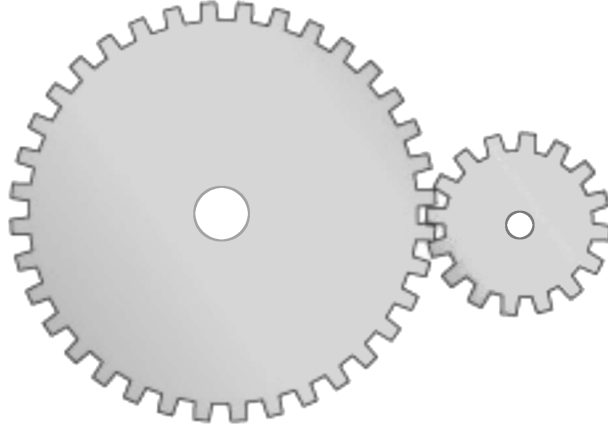
Figure 1.1: Spur gear

axial wheels of different diameters and of different numbers of teeth. The teeth
of the small wheel are magnetized with a concentrated winding that is supplied
with electric current via a pair of slip rings. When one wheel is turned, torque
is transmitted to the other teeth at a different speed. The small wheel generates
the magneto-motive force (mmf) that interacts with the air-gap permeance to
generate the magnetic flux which produces transmitted torques. The small wheel
experiences a Lorentz force while a reluctance force is exerted on the big wheel.
The transmitted torques become too small because only a few teeth are engaged
during this transfer of power due to the nature of the bi-axial design.

Another approach is to use permanent magnets instead of teeth and this was
achieved nearly three decades later by Faus [Fau41]. This is illustrated by the
schematic diagram in Fig.1.2b. This technique does not require a winding or slip
rings, and thus the efficiency of power transmission is better than the previous
method. However, the bi-axial design and the mounting method of the magnets
results in very low torque density.

Yao et al [Yao00] improved Faus's design by using surface mounted perma-
nent magnets (SPM) and a thorough optimization study was conducted. The
schematic diagram is shown in Fig.1.2c.

The concentric design is an alternative way to improve the efficiency of power
transmission. The first concentric design was patented by Neuland [Neu16].
Different designs were presented for forward and reverse speed operation. The
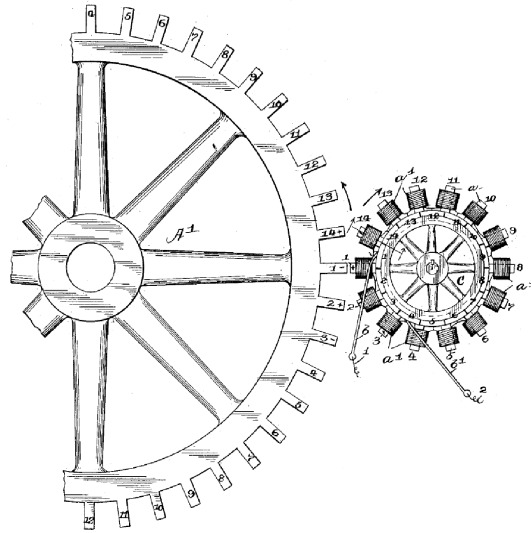
(a)
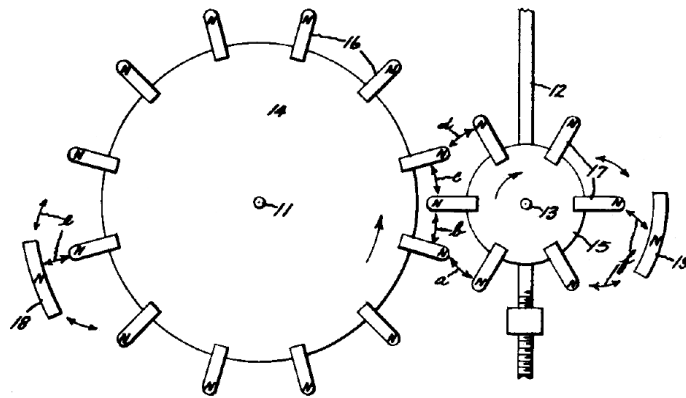
(b)
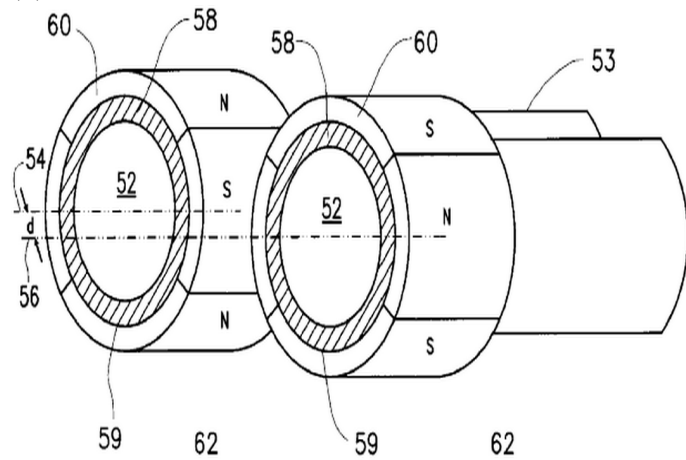
(c)

Figure 1.2: Magnetic spur gears (a) Armstrong's method [Arm01] (b) Faus's method [Fau41] (c) Yao's method [Yao00]

schematic of Fig.1.3a illustrates one of the different proposed designs. The gear consists of an outer rotor and an inner rotor which consist of ferromagnetic teeth. Between the rotors is a set of pole pieces that must be magnetized either by a winding or permanent magnets. Neuland's method marks a new leap towards the establishment of useful magnetic gearing.

Martin [Mar68] improved Neuland's concept by separating the permanent magnets and the pole pieces. Several designs and different topologies were proposed. A brief description of the basic principle of operation was provided in which the selection of the number of pole pieces was explained and the gear ratio was expressed in terms of speeds and the numbers of poles. Martin's best design is shown in Fig.1.3b. There are two rotors made up of alternating magnetic poles, and there is a set of pole pieces. Martin's design seems to be the best, but it was not realized industrially because the transmitted torques were low due to the use of ceramic magnets which have low remanence. Neuland's and Martin's techniques will be compared in terms of torque density in Chapter 3.

1.3   Academic investigations

The magnetic gear was first academically investigated in 1969 [AS69]. The details of their method is not known and only a brief description about it is found in another publication by Hesmondalgh and Tipping [HT80] of Manchester University in the UK. Their method appears in Fig.(1.4) where three elements of the same topology operate as a single gear. Each element seems to be based on Neuland's design. The method was investigated theoretically and verified experimentally.

A different approach was contributed by Tsurumoto and Kikuchi [TK87] in Japan at Tohoku Gakuin University. Their method was the analogy with mechanical pinion and gear, and they employed SmCo5 magnets (Fig.1.5).

In 2001, a research was published by Atallah and Howe [AH01] of Sheffield University in the UK in which Martin's design was improved by using NdFeB SPM, and by redesigning the the cross section of a pole piece as sector- shaped. A torque density of 100 kNm/m^3 was reported. The operating principle was developed by deriving the gear ratio from the expressions of the air-gap flux density. The analysis was general and the design parameters were not considered.
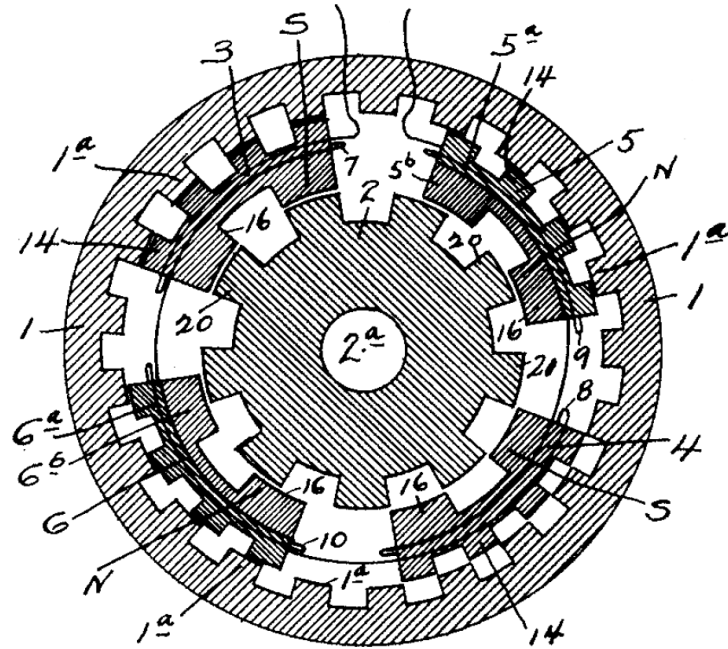
(a)
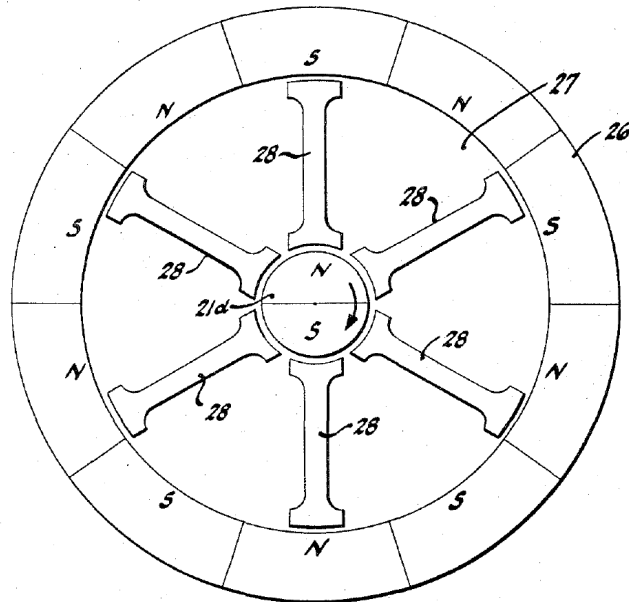
(b)

Figure 1.3: Magnetic gears of concentric design (a) Neuland's design [Neu16] (b) Martin's design [Mar68]
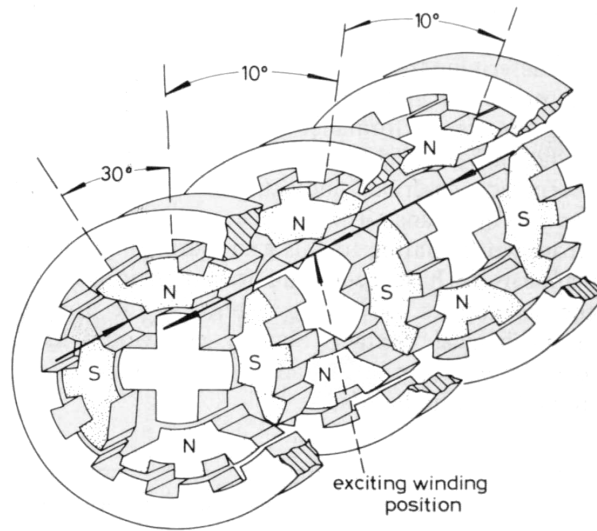
Figure 1.4: Multi-element magnetic gear [HT80]
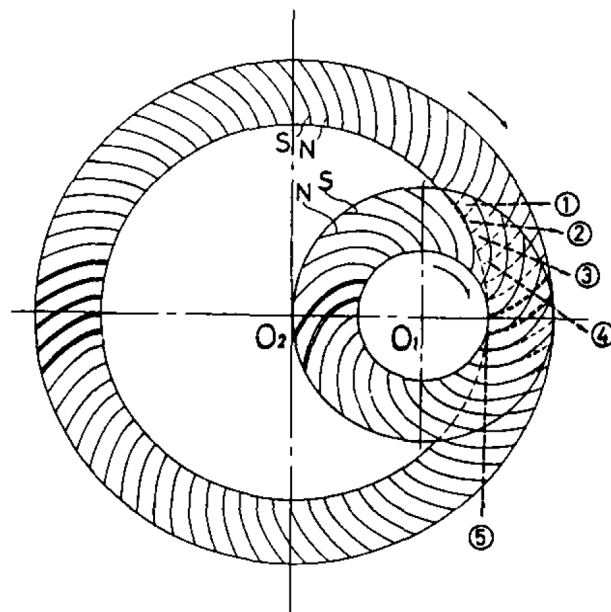
Figure 1.5: Magnetic pinion and gear [TK87]

In addition, design and optimization guidelines were not provided.

Many publications appeared based on this gear with different designs and performance improvements but the basic operating principle remains the same. Rasmussen et al [RAJN03] used interior permanent magnets (IPM) of spoke-type for the high-speed rotor and Liu et al [LCJY09] applied IPM to the low-speed rotor. Frank and Toliyat [FT10] investigated the IPM design theoretically and experimentally. Jian and Chau [JC10] proved that Halbach array magnets would elevate the torque density and reduce the cogging torques in comparison with a similar gear that employed SPM.

1.4   Simulation methods

There are numerous methods for simulating electromagnetic devices. The most commonly used method is the finite element analysis (FEA). There are many FEA software packages capable of 2D/3D static and transient analysis. The new magnetic gear was simulated with FEA [AH01] [RAJN03].

Some researchers employed the reluctance network analysis (RNA) [FNI11]. RNA and FEA were compared in terms of accuracy and simulation speed using the same model of a magnetic gear. The results are close but RNA is faster with a total simulation time of seven minutes compared to six hours with FEA.

The winding function theory (WFT) [FT10] was applied to simulate the magnetic gear. Their results were close to FEA results but there was no comparison in terms of the simulation speed.

Although RNA and WFT are faster than FEA, the development process of an accurate model is long because there is no available commercial software. Hence, the FEA was employed in this study. The JMAG Designer [Cor12]was used in this study to validate all the proposed methods and to obtain the simulation data for comparison with experimental measurements. JMAG is capable of 2D/3D static and transient analysis. The FEMM 4.2 software [Mee12] was used for 2D static analyses and for quick design purposes. The results were re-validated with JMAG.

1.4.1   Finite element analysis

The main quantities of rotating machines that are calculated by any FEA software are flux density, inductance, speed and electromagnetic torques. The flux density B is calculated from the magnetic vector potential A which is calculated from the current density taking core saturation into account.

$$B = \Delta \times A \tag{1.1}$$
$$\Delta \times (\frac{B}{\mu(B)}) = J$$

where $\mu(B)$ is the permeability of a material as a function of flux density and J is current density.

Inductance is calculated as the ratio of magnetic flux linkage to applied current

$$L = \frac{\lambda}{i} \tag{1.2}$$

Speed is calculated as the time derivative of displacement

$$\omega = \frac{d\theta}{dt} \tag{1.3}$$

Torque in the ith and j^{th} direction is calculated with Maxwell stress tensor defined by

$$
\begin{aligned}
T_{ij} &= \frac{1}{\mu_o}(B_i B_j - \frac{1}{2}B^2 \delta_{ij}) \\
B^2 &= B_i^2 + B_j^2
\end{aligned}
\tag{1.4}
$$

where δ_{ij} is Kronecker's delta.

1.5   Study objectives

The objective of this study is to develop concepts and methods that realize magnetic variable transmission which is useful in applications that require variable torque and/or speed such as auto-motives, electric hoists, wind power generation

systems, and so on.

In this work, several techniques have been developed based on Atallah's magnetic gear. Two techniques adopt the method of pole changing to change the gear ratio. Another technique uses a multi-element design of several magnetic gears of different topologies. Using any technique, the torque of an input shaft can be transmitted to an output shaft at a different speed. The output torque can be adjusted to match the load torque by controlling the winding current while keeping the load speed constant.

The developed techniques were designed and optimized using finite element analysis (FEA), and one method of pole changing was verified experimentally. Design and optimization guidelines have been set for magnetic gears. This would shorten the time of the design process, reduce the volume and weight of the gearbox, and it would elevate the torque density. The guidelines have been deduced from the analytical equations of the magnetic flux and from the transmitted torques expressed in terms of design parameters.

1.6   Outline of thesis

The thesis focuses on describing the concepts and operating principles of the developed methods. It consists of eight chapters. The first chapter mainly documents the evolution of magnetic gearing. A summary of the recent publications on magnetic gearing is included.

Chapter 2 is a literature review of the published researches and patents in the area of non-mechanical variable transmission; electrical variable transmission (EVT) and magnetic variable transmission (MVT). The literature dates back to the year 1891. Most of the concepts and techniques are found in patents, and improvements and analyses of those methods are reported in academic publications.

Chapter 3 compares three techniques of magnetic gearing: singly-excited method, doubly-excited method and multi-element method. The doubly-excited method is selected as the candidate for the realization of MVT for its merit of high torque density.

Chapter 4 clarifies the concept behind magnetic gearing, and it explains the

theory of modulated flux with the aid of Fourier analysis. Design and optimization guidelines are developed based on the derived equations.

The purpose of Chapter 5 is to set design guidelines of the electromagnetic gear which was used to design and optimize the developed methods of MVT.

Chapter 6 explains the concept of pole changing as a technique to realize magnetic variable transmission. A salient-pole electromagnetic gear is employed, and a 5-step variable transmission is achieved. The method is validated by FEA and experimentally.

Chapter 7 explains another method of magnetic variable transmission by incorporating several magnetic gears of different topologies. The method is validated by only FEA.

Chapter 8 concludes the thesis and presents suggestions for improvements and further research.

Chapter 2

Literature Review

2.1 Introduction

The literature dates back to the year 1891. All the basic concepts and techniques of contactless variable transmission are found in patents, and the academic publications provide analyses and improvements. The contactless variable transmission is possible by two techniques:

1. Electrical variable transmission
2. Magnetic variable transmission

2.2 Electrical variable transmission (EVT)

There are many patents and researches on electrical variable transmission (EVT). The main concept is coupling an electric motor with an electric generator, and the speed and/or torque can be varied by controlling the excitation of both machines.

The first and most well known EVT technique is the Ward-Leonard system [Leo91]. Direct-current motor-generator sets were employed (Fig.2.1). The stators of the machines are connected in parallel but the field windings are separate. By controlling the field currents, the output torque and/or speed can be varied. The restriction is that the two machines must be the same. The large volume of the whole system and the power losses appear as the main drawbacks.

Ward-Leonard's concept was adopted [BC04] by using an alternating-current
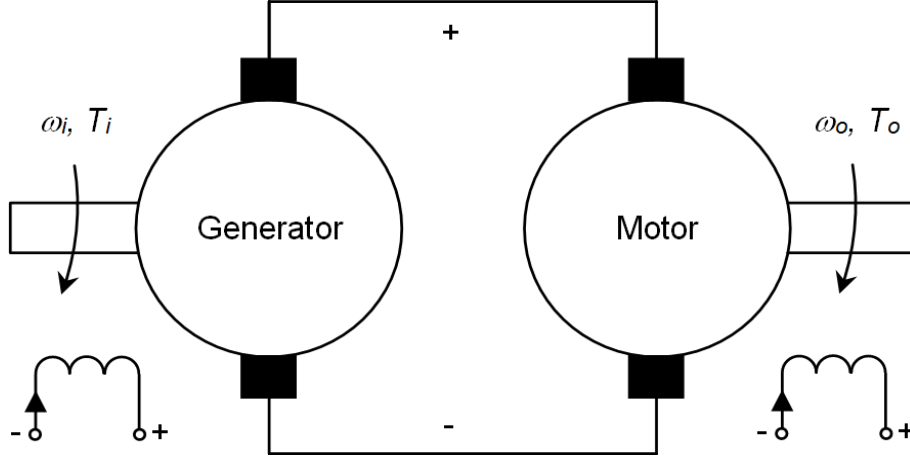
Figure 2.1: Ward-Leonard system

motor-generator set. An induction motor and a synchronous generator having different numbers of poles were coupled, and variable torque or speed was achievable.

Hefel [Hef40] also employed a direct-current motor-generator set. His improvement to the previous patents was the concentric design in which the motor and generator were one single machine.

Utilizing Ward-Leonard's concept and Hefel's design, an advanced design was proposed [HR04] for a city bus using induction machines.

2.3 Magnetic variable transmission (MVT)

At the beginning of this study in October 2009, most of the published researches and patents proposed magnetic gears with fixed gear ratios. There were only two patents by Magnomatics Limited ([RA09] and [CRA09]) but no academic publications. Their approach uses a doubly-excited magnetic gear and a 3-phase brushless motor concentric to each other forming a single machine.

This approach was studied theoretically [JC10] and torque equations were derived. The method was verified experimentally [SCW11]. Further theoretical investigation was described in a recent publication [WAC11] and realization and experimental validation were described in another work [AWCD12]. However, optimization was not covered and the derived equations were general and may

not be useful for design purposes.

2.4   Comparison between EVT and MVT

Due to the accumulation of research and due to the progress of power electronics and control, the EVT technology is considered mature nowadays. The required components and machines are available off the shelf and thus it can be easily realized for various applications. However, it is complex, bulky and costly. Moreover, it is not immune to overloading.

The MVT technology is still under continuous research and development but it has many advantages: simpler design and control algorithms, cheaper if mass produced and immune to overloading. This study is considered as the second contribution to the development of MVT.

Chapter 3

Comparative Study of Magnetic Gears

3.1 Introduction

Before the development of magnetic variable transmission, the methods of magnetic gearing need to be compared. A comparative study is essential before the adoption of any method for the realization of MVT.

The techniques patented by Neuland and Atallah will be compared in terms of torque density, cost and simplicity of design. Discussions will be made about the multi-element method investigated by Hesmondhalgh et al for any possibility of achieving higher torque density than the previous methods.

3.2 Singly-excited magnetic gear

An improved design of Neuland's magnetic gear is illustrated in Fig.3.1a where the pole pieces are symmetrically distributed in the air-gap between the rotors. It consists of three parts:

1. Inner rotor composed of ferromagnetic teeth
2. Outer rotor composed of ferromagnetic teeth
3. Stationary pole pieces composed of ferromagnetic teeth and permanent magnets

There is a single source of excitation and so it will be referred to as singly-excited. The number of poles of the inner rotor, P_i, is equal to the number of inner teeth of the pole pieces. The number of teeth of the outer rotor, P_o, is the same as the number of the outer teeth of the pole pieces. The number of pole pieces, P_s, is the same as the number of the teeth of the inner rotor. The gear ratio is

$$G_r = \frac{P_o}{P_i} = \frac{T_o}{T_i} = \frac{\omega_i}{\omega_o} \qquad (3.1)$$

where T_o and T_i are the torques of the outer and inner rotors, respectively. ω_o and ω_i are the respective angular speeds.

The torque equations provided by [HT80] were derived on the assumption of an excitation by a winding. The torque exerted on the outer rotor can be modified and expressed for an excitation by permanent magnets as

$$T_o = \frac{1}{8\mu_o} \frac{r_o l_a}{g_o} \frac{P_o}{P_s^2} \frac{\theta_o}{|\theta_o|} \left[\frac{B_{rem} l_m}{1 + \frac{(g_i + l_m) N_o t_o (1-\alpha_o)}{g_o N_i t_i (1-\alpha_i)}} \right]^2 \qquad (3.2)$$

where μ_o is the permeability of air, l_a is the axial length and B_{rem} is the remanence of the permanent magnet. The other design parameters are shown on Fig.3.1a. $\alpha_o = \frac{R_o |\theta_o|}{t_o}$ and $\alpha_i = \frac{R_i |\theta_i|}{t_i}$. A similar expression is obtained for the torque of the inner rotor by interchanging the subscripts i and o.

To obtain the highest torque density, the air gaps should be as short as possible. The selection of the number of teeth of the rotors is decided by the desired gear ratio and the torque equations suggest having the minimum number of pole pieces. Permanent magnets of high remanence would raise the torque density. If the last term of the equation is expanded, the radial thickness of the magnets can be expressed more appropriately as a ratio of the circumferential thickness of an inner teeth or $\frac{l_m}{t_i}$.

3.3 Doubly-excited magnetic gear

Atallah's magnetic gear looks similar to Neuland's. Unlike Neuland's design, the pole pieces of Atallah's design (Fig.3.1b) do not consist of permanent magnets or
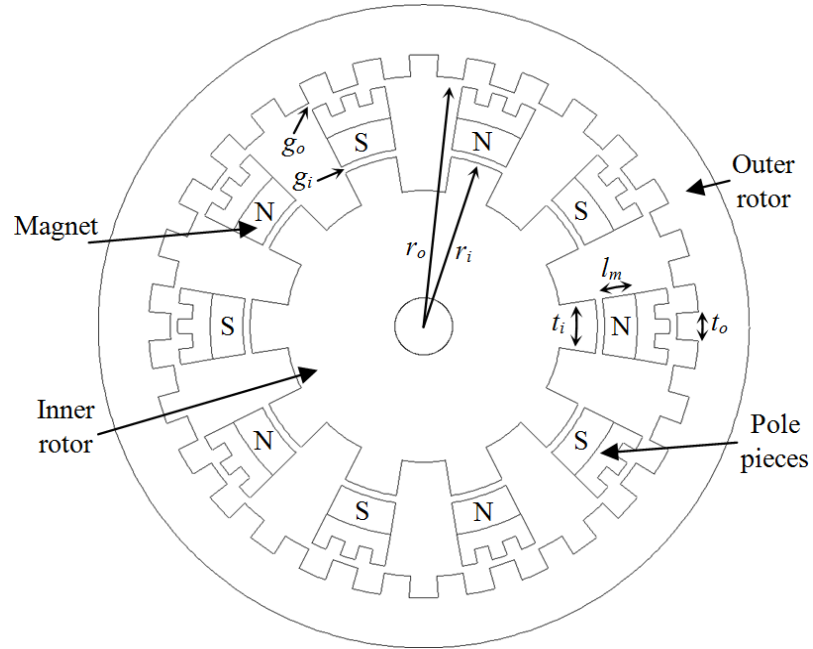
(a)
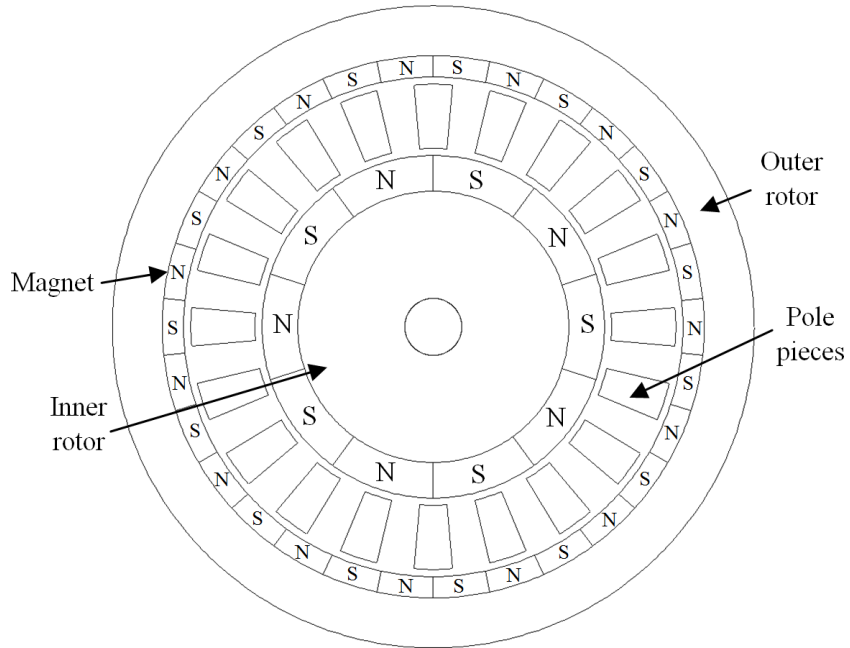
(b)

Figure 3.1: Magnetic gears (a) single-excited design (b) doubly-excited design

coils; they are simply made of a ferromagnetic material like iron or silicon steel. In addition, Atallah's magnetic gear employs permanent magnets on the outer and inner rotors instead of teeth. This is a doubly-excited gear because there are two sources of excitation. The number of the pole pieces is set as the sum of the pole pairs of the permanent magnets of both rotors.

$$P_s = P_o \pm P_i \qquad (3.3)$$

Here, P_o and P_i denote the number of pole pairs of the outer and inner rotors, respectively. The gear ratio is determined from Eq.(3.1). The rotors turn in the same/opposite direction when the sign is minus/plus, respectively. For the topology in Fig.3.1b, the rotors turn in opposite directions.

3.4   Comparison between singly-excited and doubly-excited methods

Three gears of different topologies were considered, and their design parameters are listed in Table 3.1. All the gears have NdFeB magnets of remanence 1.25 T. The air-gap length is 1mm.

The singly-excited gears were optimized according to Eq.(3.2) but the doubly-excited gears were not optimized. The dimensions of a member of a singly-excited gear are similar to the dimensions of a member of a corresponding doubly-excited gear.

Static FEA simulations were conducted to calculate the maximum torque densities. For the purpose of ease of comparison, the results are shown in bar graphs in Fig.3.2.

Despite being unoptimized, the doubly-excited design is superior to the singly-excited design in terms of torque density. On average, the doubly-excited design produces a density of 38 kNm/m^3 and the singly-excited design produces around 13.5 kNm/m^3 which is nearly a third of the former result.

In terms of weight, the singly-excited gear would weigh less by 20% but the doubly-excited gear is also superior in terms of torque/weight. It produces an av-

Gear 1				
Design	P_o	P_i	P_s	Volume (cm^3)
Neuland	20	10	10	1.65
Atallah	10	5	15	1.65
Gear 2				
Design	P_o	P_i	P_s	Volume (cm^3)
Neuland	24	8	8	1.34
Atallah	12	4	16	1.34
Gear 3				
Design	P_o	P_i	P_s	Volume (cm^3)
Neuland	30	10	10	1.65
Atallah	15	5	20	1.65

Table 3.1: Design parameters of compared gears

erage density of 5.9 Nm/kg wheras the singly-excited design produces 2.2 Nm/kg.

In terms of cost, the singly-excited gear would be less costly due to the fewer number of magnets and pole pieces. Overall, the doubly-excited gear produces a higher performance and it is favored for this study.

3.5   Multi-element design

The singly-excited magnetic gear was utilized and improved by Hesmondalgh et al. Several identical magnetic gears were used and each magnetic gear was referred to as *element*. Two designs were proposed: double-slotted element (Fig.3.3a) and shunt-type element (Fig.3.3b).

The inner rotors are aligned on the input shaft and rotate at the same speed. The poles of the inner rotor of an element are offset from those of an adjacent element by an angle:

$$\gamma_i = \frac{1}{N} \times \frac{360°}{P_i} \tag{3.4}$$

where N is the number of elements. The outer rotors are connected by the output
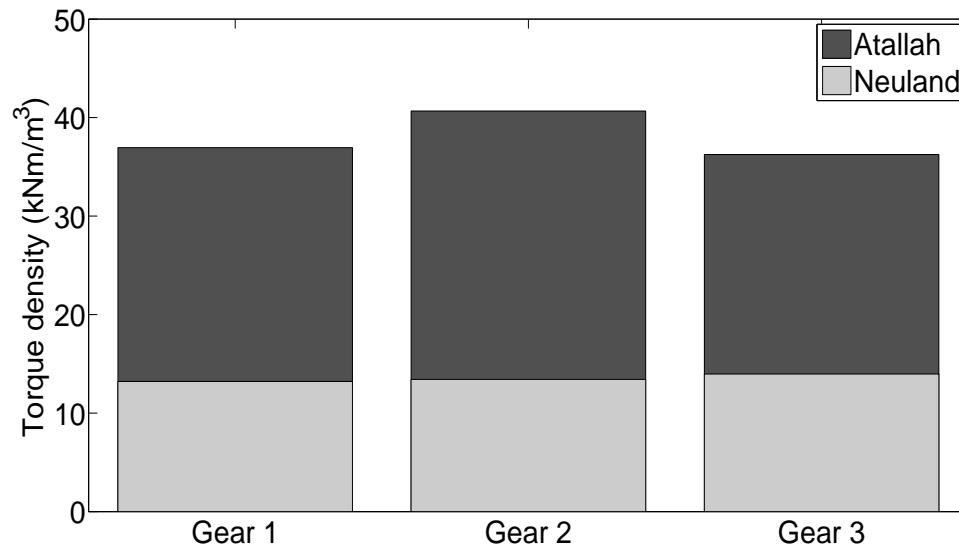
(a)
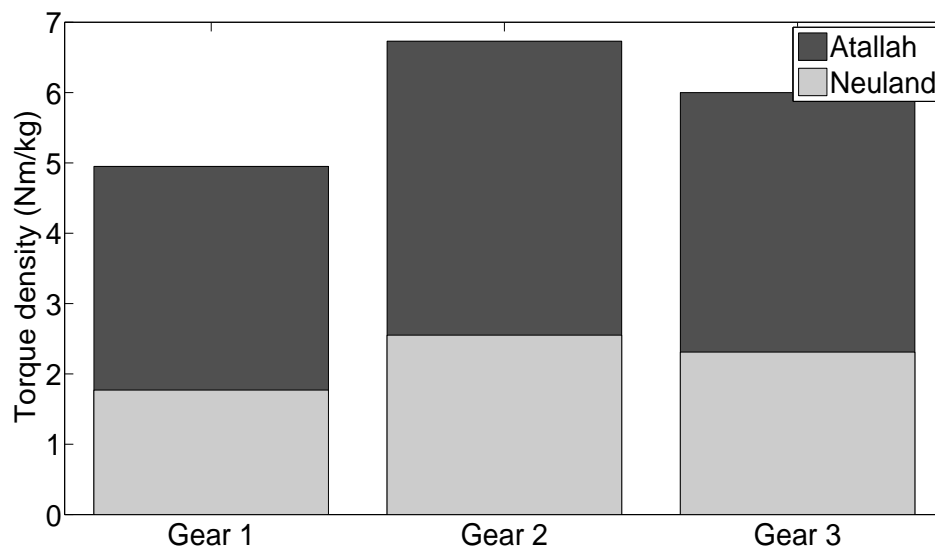
(b)

Figure 3.2: Comparison between singly-excited and doubly-excited gears (a) Torque/volume ratio (b) Torque/weight ratio

shaft and are also offset from each other by an angle:

$$\gamma_o = \frac{1}{N} \times \frac{360°}{P_o} \tag{3.5}$$

The stationary blocks are kept unchanged. The gear ratio is calculated from Eq.(3.1).

Magnetic permeance, inductance and torque were derived for both designs. In addition, extensive optimization of the two designs was theoretically explained using analytical equations, and design and optimization guidelines were provided. Although the principle of operation was explained, the concept behind magnetic gearing was not comprehended.

Although this approach would elevate the torque density, the theoretical torque density was below 1 kNm/m^3. It cannot compete with the doubly-excited gear due to the single excitation method and the increased stack length.

3.6   Conclusion

Different designs and topologies of magnetic gears have been compared. It is concluded that the doubly-excited magnetic gear is the best candidate for the development of magnetic variable transmission mainly because of its high torque density and simple manufacturability.

(a)

(b)
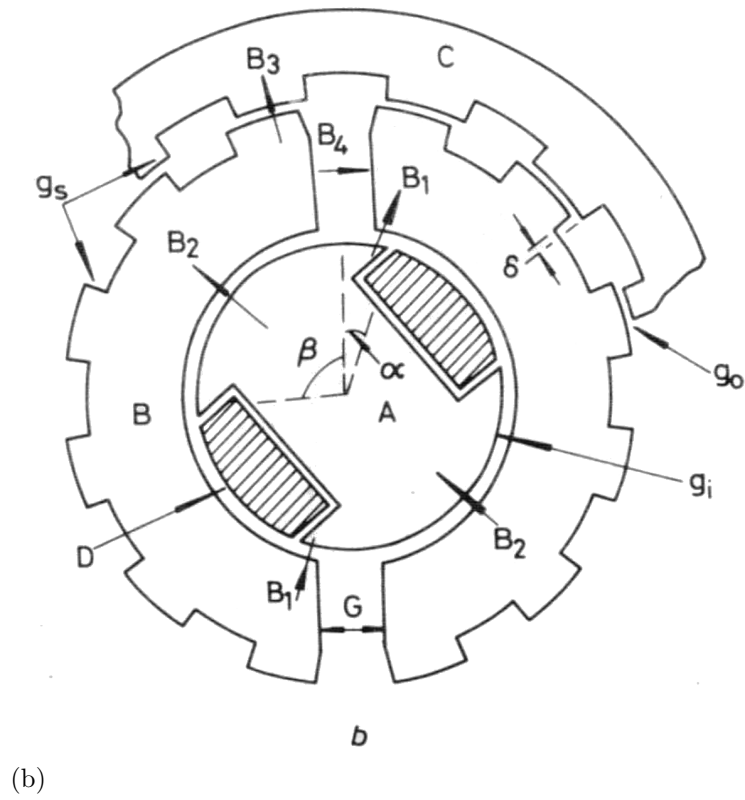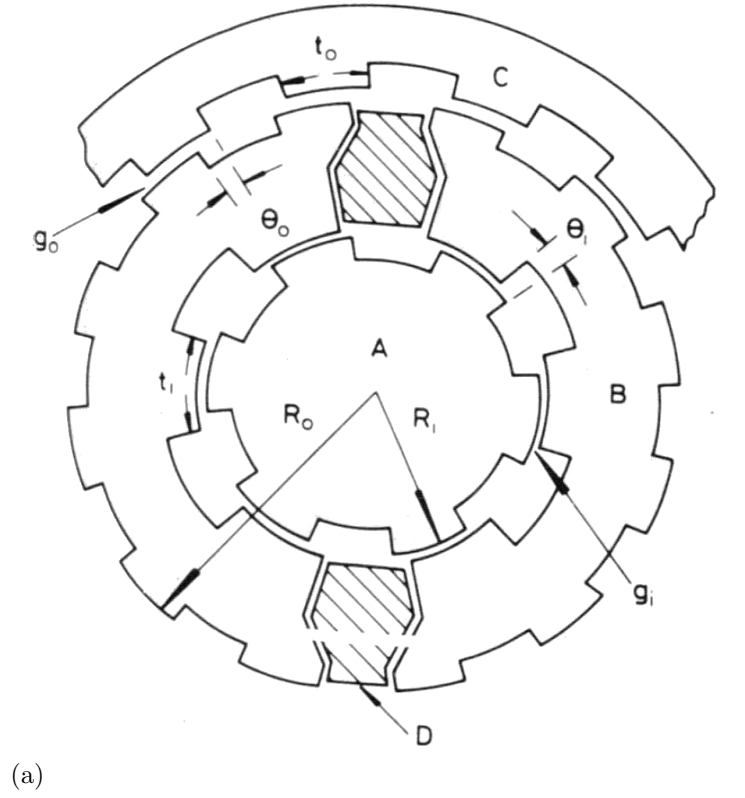
Figure 3.3: Designs of multi-element magnetic gear (a) Double-slotted design (b) Shunt-type design [HT80]

Chapter 4

Theoretical Analysis of Doubly-excited Gear

4.1 Aim of analysis

The theory of magnetic gearing is not well explained in the literature, and no useful expressions of flux and transmitted torques have been derived.

This chapter aims to improve the understanding of the theory of magnetic gearing. Design guidelines are set and expressions in terms of design parameters of torques and flux are presented.

4.2 Principle of operation

For the theoretical analysis, a 15-5-20 topology of an optimized design of the doubly-excited gear (Fig.3.1b) is assumed. There are fifteen pole pairs in the outer rotor, twenty pole pieces and five pole pairs in the inner rotor.

The outer rotor usually has more poles than the inner rotor. They are often known as low-speed and high-speed rotors, respectively. At standstill, the permanent magnets are aligned. While the pole pieces are kept stationary, the movement of any rotor forces the other rotor to turn because the magnets always tend to align to each other. The same operation occurs if one of the rotors is kept fixed while the other rotor and pole pieces are free to rotate. Without the

pole pieces, the air gap permeance is constant. The presence of pole pieces chops the permeance waveform which creates air-gap pole harmonics other than those produced by the magneto-motive forces. The movement of pole pieces causes the cutting of magnetic flux between the magnets and thus the rotors turn in order to get aligned with each other but at different speeds.

To transmit torque having the minimum number of harmonics from one rotor to the other, the number of pole pieces should be the sum of pole pairs of the permanent magnets.

For this topology, the ideal gear ratio is 3:1 in terms of torque, or 1:3 in terms of speed. In other words, the torque of the outer rotor is 300% bigger than that of the inner rotor, or the inner rotor is 300% faster than the outer rotor.

4.3   Equivalent magnetic circuit

Before the advent of computers, electric machines were designed with the aid of equivalent magnetic and electric circuits. More accurate magnetic circuits were developed with analogue computers [Atk58]. Nowadays, even more accurate circuits can be developed with powerful digital computers using RNA.

Part of the equivalent magnetic circuit of the magnetic gear developed using RNA is shown in Fig.4.1 where the magnetic gear is laid out flat. The reluctances are considered in the radial and circumferential directions. The shaded rectangles indicate low reluctances such as those of the iron cores.

To have an insight on the factors that affect the performance of the magnetic gear, the reluctance network seems complex and so a simpler yet adequate circuit can be derived from it. To achieve that, the following assumptions are made:

1. The most useful magnetic flux crosses the air gaps radially
2. No flux leakage or fringing
3. The permeability of iron is infinite
4. Saturation, eddy currents and hysteresis are ignored

With these assumption, the most useful reluctances are those of the air gaps and in the radial direction. The other reluctances are ignored. The resultant reluctance of the air gap, R_g, maybe determined from the air-gap function which
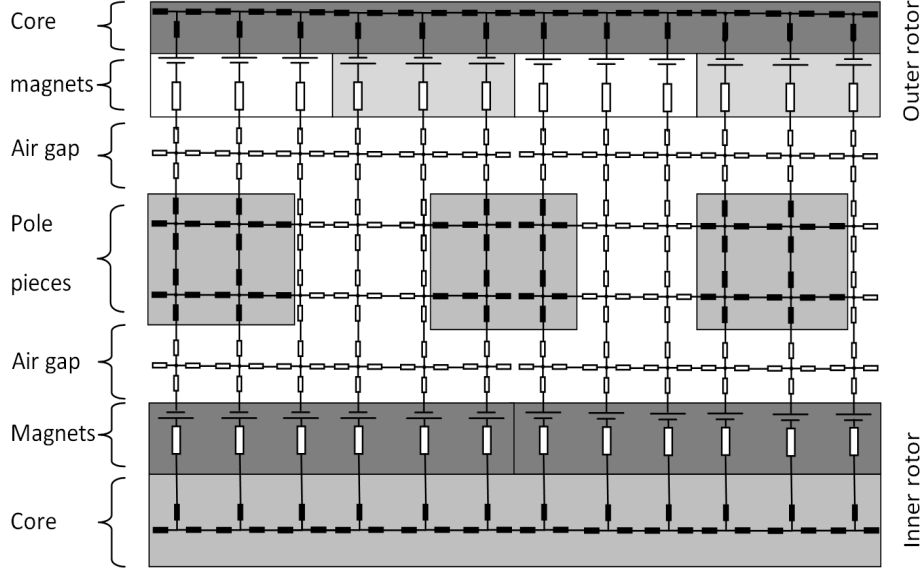
Figure 4.1: Part of reluctance network of magnetic gear

depends on the position of the pole pieces.

$$R_g(\theta) = \frac{g(\theta)}{\mu_o A_g(\theta)} \tag{4.1}$$

The resultant reluctance is important for calculating magnetic flux. A simpler approach is to use the air-gap permeance as the next section explains.

4.4 Electromagnetic gear

To simplify the analysis, the magnetic gear can be thought of as current-carrying loops separated by a set of pole pieces and air gaps as illustrated in Fig.4.2. This is referred to as *electromagnetic gear*. The loops are equivalent to magnetic poles. The parts are named differently because the pole pieces are free to rotate. For the convenience of analysis, the electromagnetic gear is laid out flat in Fig.4.3.

Each pole occupies a portion of its full pitch. The pitches of the inner rotor,

outer rotor and pole pieces are, respectively,

$$
\begin{aligned}
\lambda_i &= \frac{\pi}{P_i} \\
\lambda_o &= \frac{\pi}{P_o} \\
\lambda_s &= \frac{2\pi}{P_s}
\end{aligned}
\tag{4.2}
$$

Thus, the circumferential widths of each loop and pole piece maybe expressed as

$$
\begin{aligned}
l_{i\theta} &= \alpha_i \lambda_i r_1 \\
l_{s\theta} &= \alpha_s \lambda_s r_2 \\
l_{o\theta} &= \alpha_o \lambda_o r_3
\end{aligned}
\tag{4.3}
$$

where α_i, α_s and α_o are the arc-to-pitch ratios of the inner rotor loop, pole pieces, and outer rotor, respectively. r_1, r_2 and r_3 are the radii of the inner rotor, pole pieces and outer rotor, respectively.

For an axial length l_a, the areas occupied by each loop and pole piece are

$$
\begin{aligned}
A_i &= l_{i\theta} l_a = \alpha_i \frac{\pi r_i}{P_i} l_a \\
A_s &= l_{s\theta} l_a = 2\alpha_s \frac{\pi r_s}{P_s} l_a \\
A_o &= l_{o\theta} l_a = \alpha_o \frac{\pi r_o}{P_o} l_a
\end{aligned}
\tag{4.4}
$$

4.5 Harmonic analyses

The loops produce magneto-motive forces (mmf). Without the pole pieces, the air-gap permeance is constant (Fig.4.4a) regardless of the motion of any rotor; the gear would operate as a coupling. The flux is proportional to the mmf and the air-gap permeance. Consequently, the flux waveform is similar in shape to that of the resultant mmf. The introduction of the pole pieces produces a chopped waveform which is drawn in Fig.4.4b.
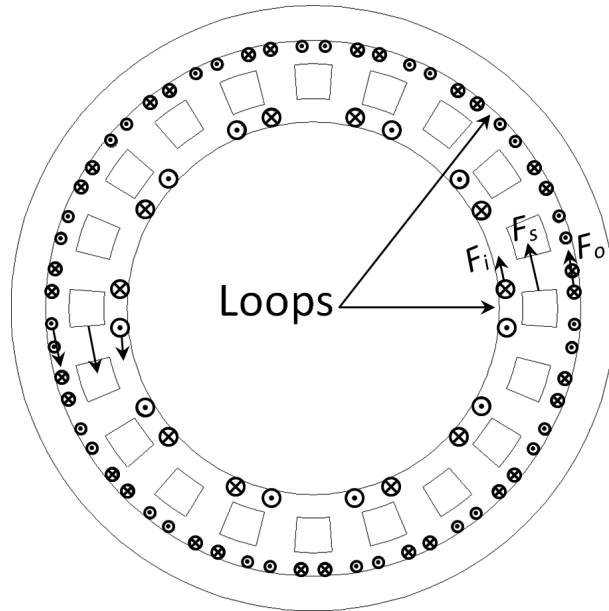
Figure 4.2: Loop magnetic gear
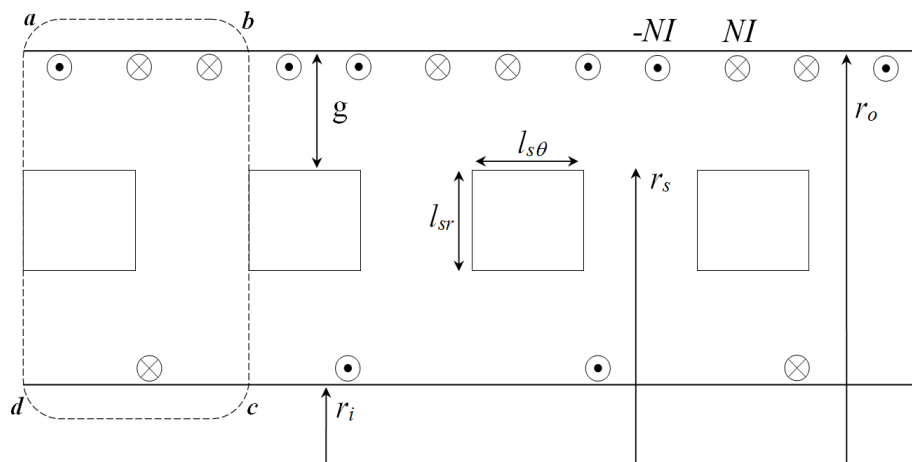
Figure 4.3: Loop gear laid out flat

26
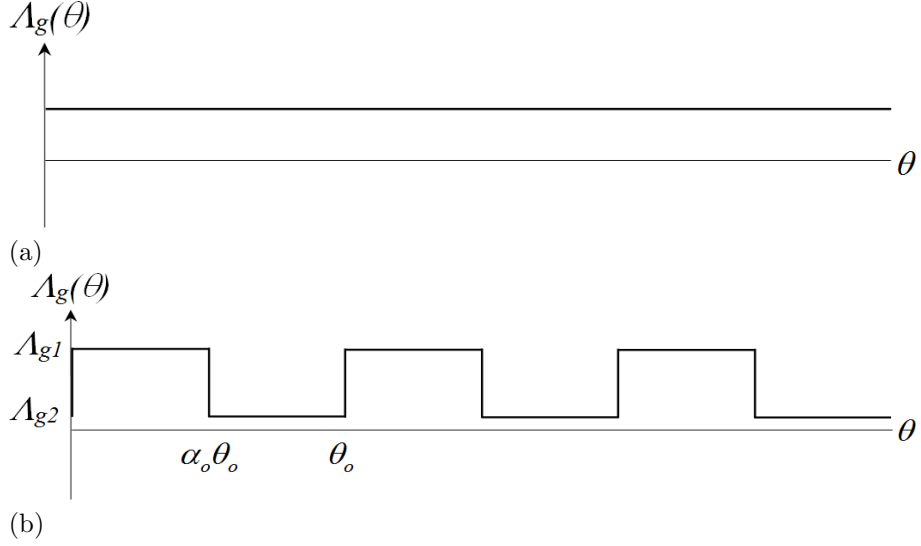
Figure 4.4: Air-gap permeance (a) without pole pieces (b) with pole pieces

The permeance depends on the position of the pole pieces and it varies between two values A_{g1} and A_{g2}. A_{g1} is the permeance of the minimum air gaps which exist between the stator and pole pieces and between the inner rotor and pole pieces. A_{g2} is the permeance of the air gap between the stator and inner rotor and it is too small compared to A_{g1}. The flux waveform is now modulated and it differs in shape from that of the mmf. This was Neuland's and Martin's approach to realize magnetic gearing although they did not investigate it theoretically.

4.5.1 mmf harmonics

The mmf waveforms are obtained by applying Ampere's law around the path *abcd*.

$$\oint_{abcd} \overrightarrow{H}.\overrightarrow{dl} = I_{enclosed} \tag{4.5}$$

This path is θ_s wide and is moved in steps of one slot length of a loop on the outer rotor ($0.5\theta_o$) until two pitches of inner rotor loop ($2\theta_i$). Then, the total current enclosed by the path equals the resultant mmf. The mmf waveforms are shown in Fig.4.5. F_{m1} is the mmf of the outer rotor, F_{m2} is the mmf of the inner
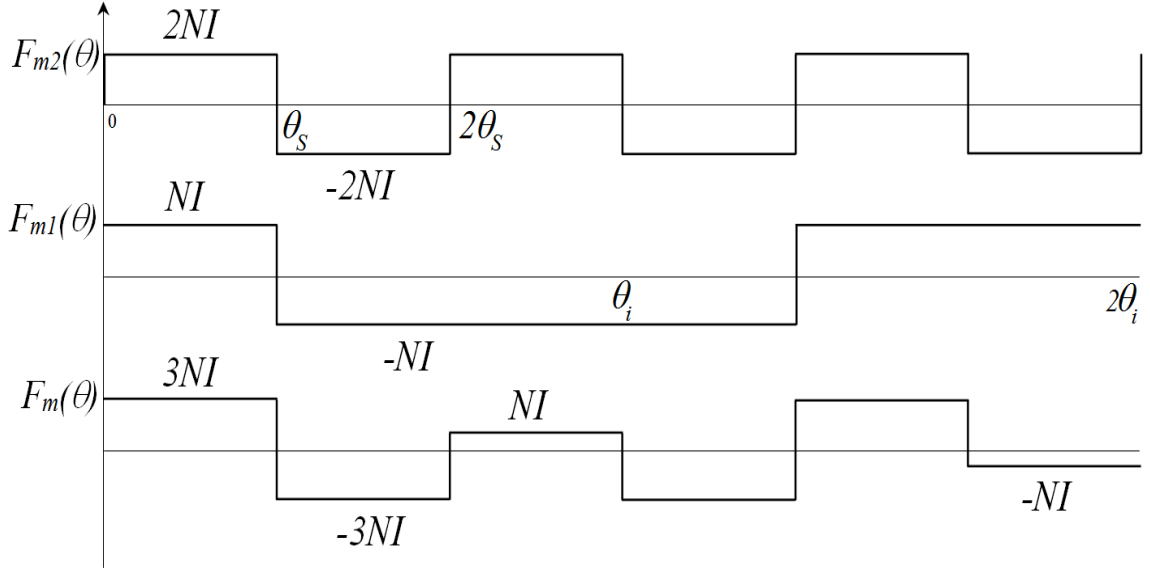
Figure 4.5: mmf waveforms

rotor and F_m is the resultant mmf.

Applying Fourier series to the waveforms in Fig.4.5 yields

$$F_m(\theta) = \sum_{m=1,3,..}^{\infty} \frac{2NI}{m\pi}[\sin(mP_i(\theta - \theta_i)) + 2\sin(mP_o(\theta - \theta_o))] \qquad (4.6)$$

where θ_i and θ_o are the angular displacements of the inner and outer rotors, respectively. The harmonics of the fundamental component of the resultant mmf are plotted in Fig.4.6. In the absence of the pole pieces, only the resultant mmf creates kP_i and kP_o poles in the air gaps between the stator and inner rotor as concluded from Eq.(4.13). When $k=1$, $P_i=5$ and $P_o=15$, there will be two significant components of pole pairs: 5 pairs and 15 pairs.

4.5.2 Permeance harmonics

If there are no pole pieces, the air-gap permeance in the radial direction is constant and it is independent of the position of any rotor. It has a an average value

$$\Lambda_g = \pi\mu_o l_a \frac{r_o + r_i}{r_o - r_i} \qquad (4.7)$$
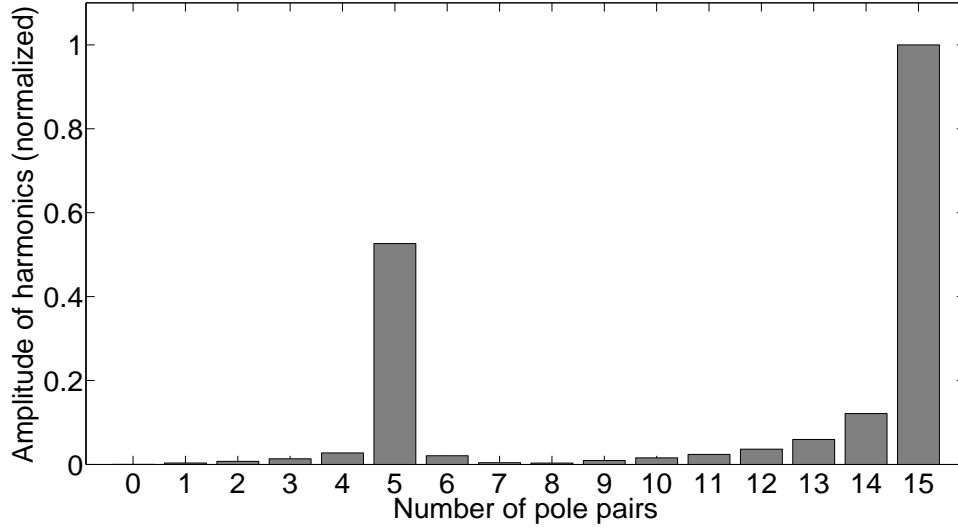
Figure 4.6: mmf harmonics

With pole pieces, the air-gap permeance varies between two values depending on the rotation angle θ:

$$\Lambda_{g1} = \frac{2\pi\mu_o l_a}{gP_s}\alpha_s \tag{4.8}$$

$$\Lambda_{g2} = \frac{2\pi\mu_o l_a}{(g+l_{or})P_s}(1-\alpha_s) \tag{4.9}$$

Applying Fourier analysis to the waveform in Fig.4.4b yields

$$\Lambda_g(\theta) = a_o + \sum_{n=1}^{\infty} a_n \cos(nP_s(\theta-\theta_s)) + b_n \sin(nP_s(\theta-\theta_s)) \tag{4.10}$$

where θ_s is the angular displacement of the pole pieces and

$$
\begin{aligned}
a_o &= \frac{2\pi\mu_o l_a}{gP_s}\frac{1+\alpha_s^2\frac{l_{or}}{g}}{1+\frac{l_{or}}{g}} \\
a_n &= \frac{2\pi\mu_o l_a}{gP_s}\frac{1+\alpha_s(2+\frac{l_{or}}{g})}{1+\frac{l_{or}}{g}}\frac{\sin(2n\pi\alpha_s)}{n\pi} \\
b_n &= \frac{2\pi\mu_o l_a}{gP_s}\frac{1+\alpha_s(2+\frac{l_{or}}{g})}{1+\frac{l_{or}}{g}}\frac{(1-\cos(2n\pi\alpha_s))}{n\pi}
\end{aligned}
\tag{4.11}
$$

This air gap permeance creates nP_s+1 harmonic components. For $\alpha_s=1$ and $n=1$, there is only one component which is due to a_o (Fig.4.7a). Fig.4.7b shows the harmonics for different values of α_s. There are many harmonics but the significant ones are due to $P_s=20$ and the highest amplitude is when $\alpha_s=0.5$.

4.5.3 Flux harmonics

The magnetic flux that links both windings and that crosses the air gaps is the most important flux that produces electromagnetic torques. It is proportional to the mmf and air-gap permeance. In the absence of the pole pieces, the flux is the product of Eq.(4.6) and Eq.(4.7)

$$
\begin{aligned}
\phi_g(\theta) &= F_m(\theta) \times A_g(\theta) \\
&= 2\mu_o l_a NI \frac{r_o+r_i}{r_o-r_i} \sum_{m=1,3,..}^{\infty} \frac{1}{m} [\sin(mP_i(\theta-\theta_i)) + 2\sin(mP_o(\theta-\theta_o))]
\end{aligned}
\tag{4.12}
$$

The air-gap flux has the same number of harmonics as the resultant mmf, and no change occurs to the displacement of the space harmonics. The gear would work as a coupling.

Before calculating the flux in the case of the presence of the pole pieces, it is insightful to see this effect on the waveform of the flux. The flux waveform is obtained by multiplying the waveforms of the mmf and air-gap permeance. The waveforms in Fig.4.8 are at two different positions of the pole pieces: at $\theta=0$ and at some angle $\theta=\gamma$. The average value of flux depends on the position of the pole pieces. The flux harmonics are due to the contribution of mmf and permeance harmonics. These harmonics are revealed in the following derivation

$$
\begin{aligned}
\phi_g(\theta) = \phi_g| \sum_{m=1,3,..}^{\infty} \sin(mP_i(\theta-\theta_i)) + 2\sin(mP_o(\theta-\theta_o)) \\
\times [a_o + \sum_{n=1}^{\infty} a_n \cos(nP_s(\theta-\theta_s)) + b_n \sin(nP_s(\theta-\theta_s))]
\end{aligned}
\tag{4.13}
$$

where $|\phi_g|$ is the amplitude of the flux.
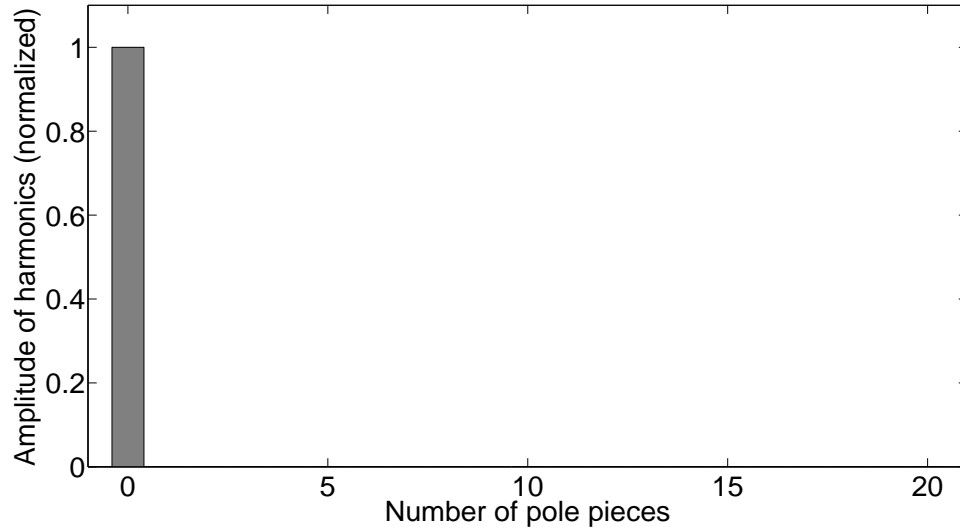
(a)
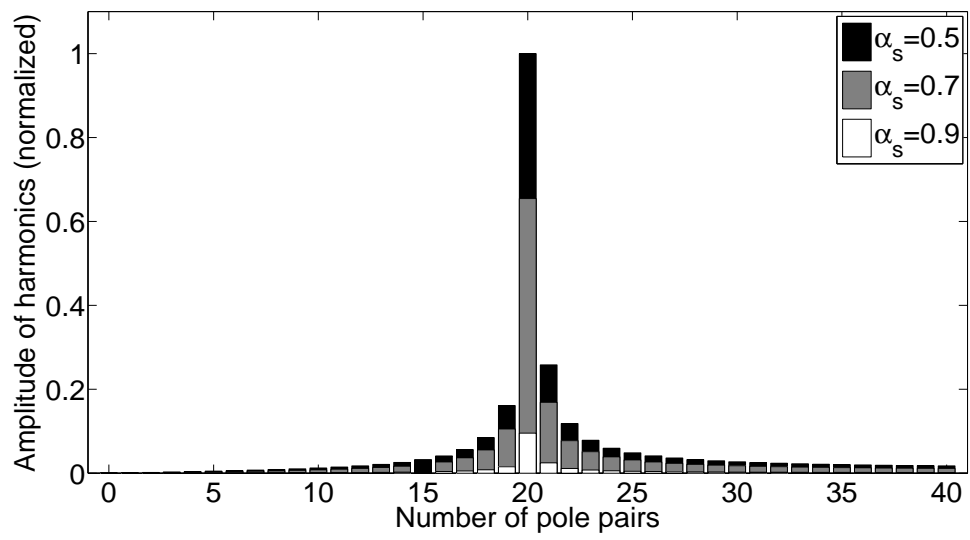
(b)

Figure 4.7: Pole harmonics of air-gap permeance (a) at α_s=1 (b) at different α_s

The fundamental component of flux found from Eq.(4.13) is expressed as follows:

$$
\begin{aligned}
\phi_{g1}(\theta) &= a_o \sin(P_i(\theta - \theta_i)) + 2a_o \sin(P_o(\theta - \theta_o)) \\
&+ a_1 \sin(P_i(\theta - \theta_i)) \cos(P_s(\theta - \theta_s)) \\
&+ 2a_1 \sin(P_o(\theta - \theta_o)) \cos(P_s(\theta - \theta_s)) \qquad (4.14) \\
&+ b_1 \sin(P_i(\theta - \theta_i)) \cos(P_s(\theta - \theta_s)) \\
&+ 2b_1 \sin(P_o(\theta - \theta_i)) \cos(P_s(\theta - \theta_s))
\end{aligned}
$$

The second and third term of the above equation can be expressed as

$$
\frac{a_1}{2}[sin((P_s + P_i)(\theta - \frac{P_i\theta_i + P_s\theta_s}{P_s + P_i})) - sin((P_s - P_i)(\theta - \frac{P_i\theta_i - P_s\theta_s}{P_s - P_i}))] \ (4.15)
$$
$$
+a_1[sin((P_s + P_o)(\theta - \frac{P_o\theta_o + P_s\theta_s}{P_s + P_o})) - sin((P_s - P_o)(\theta - \frac{P_o\theta_o - P_s\theta_s}{P_s - P_o}))]
$$

A similar expression can be obtained for the fourth and fifth terms of Eq.(4.14).

In addition to P_o and P_i harmonics resultant mmf, it is learned from Eq.(4.15) that the magnetic flux contains $P_s \pm P_i$ and $P_s \pm P_o$ harmonics as a result of the interaction of the resultant mmf and the chopped air-gap permeance. Applying the superposition principle, the displacement of the outer rotor is the same as that of the space harmonics created by the mmf of the inner rotor and the air-gap permeance

$$
\theta_o = \frac{P_i}{P_s \pm P_i}\theta_i \pm \frac{P_s}{P_s \pm P_i}\theta_s \qquad (4.16)
$$

This equation assumes that all the gear members are rotating. There are two gear ratios one of which is between the inner and outer rotors $(\frac{P_i}{P_s \pm P_i})$ and the other between the pole pieces and the outer rotor $(\frac{P_s}{P_s \pm P_i})$. The number of pole pairs of the outer rotor is

$$
P_o = P_s \pm P_i \qquad (4.17)
$$

It maybe chosen as $P_s + P_i$ or $P_s - P_i$. It is customary to first set the number of
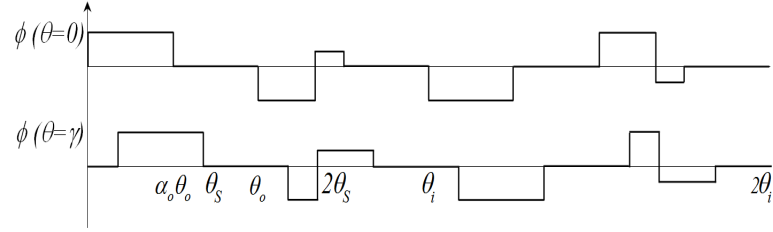
Figure 4.8: Flux waveform at two positions of the pole pieces

pole pairs of the permanent magnets and choose the number of pole pieces from

$$P_s = P_o \pm P_i \tag{4.18}$$

The amplitude of the fundamental flux maybe expressed as

$$|\phi_g| \propto \frac{l_a N I}{(g + l_{or}) P_s} (1 - \cos(2\pi\alpha_s)) \tag{4.19}$$

The harmonic spectrum of the fundamental component of flux for different values of α_s is plotted in Fig.4.9. As predicted previously, the ratio of 0.5 gives the highest amplitude of flux. In addition, the following pole pair harmonics appear with significant amplitude in the air gap due to the flow of fundamental component of modulated flux: P_i=5, P_o=15, P_i+P_s=25 and P_o+P_s=35.
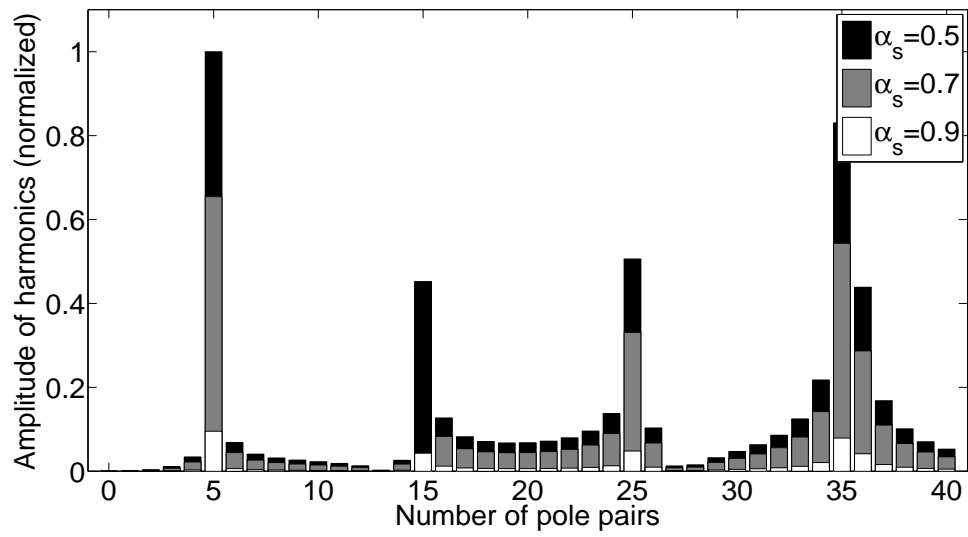
Figure 4.9: Flux pole harmonics

4.6 Derivation of torques

For design and optimization purposes, only the amplitudes of transmitted torques will be derived and there is no need to include harmonics. All derivations are based on the loop magnetic gear of Fig.4.3.

4.6.1 Torques exerted on inner and outer rotors

For a flux density B_i in the air gap near a loop face on the inner rotor, each conductor experiences a Lorentz force:

$$F_i = IB_il_a \sin \beta \tag{4.20}$$

where β is the angle between the current and flux density vectors.

$$B_i = \frac{\phi}{A_i} \tag{4.21}$$

For $2P_i$ poles with N turns on the inner rotor and for $\beta = \pi/2$, the total torque can be derived from Eq.(4.4) and Eqs.(4.19)-(4.21):

$$T_i = 2P_iF_ir_1 = \frac{2(P_i)^2r_1NI}{\pi\alpha_i}|\phi_g| \tag{4.22}$$

Substituting Eq.(4.19) in Eq.(4.22) yields

$$T_i(\theta) = k_i\frac{\alpha_o}{\alpha_i}\frac{P_i^2}{P_s}\frac{l_ar_1N^2I^2}{g + l_{or}} \tag{4.23}$$

The torque T_o exerted on the outer rotor is derived in the same fashion:

$$T_o(\theta) = k_o\frac{\alpha_o}{\alpha_o}\frac{P_o^2}{P_s}\frac{l_ar_3N^2I^2}{g + l_{or}} \tag{4.24}$$

where k_i and k_o are constants.
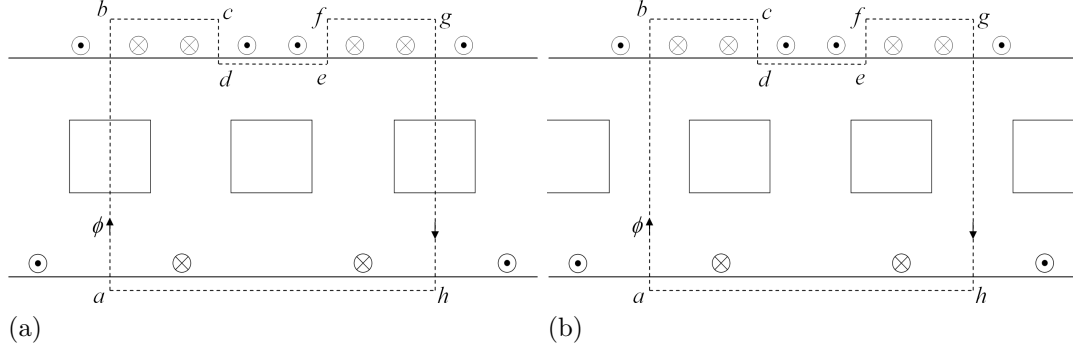
Figure 4.10: Generation of torque of pole pieces (a) fully aligned position (b) fully unaligned position

4.6.2 Torque exerted on pole pieces

The pole pieces experience a reluctance torque T_s that, along with T_i, tends to align the poles of the rotors. Fig.4.10a is the case when the poles of the rotors are fully aligned with the pole pieces, and Fig.4.10b shows the case when the pole pieces are fully unaligned with the electromagnetic poles. The dotted path *abcdefgh* is the ideal flux. It is assumed that there is no leakage flux outside the gear.

From Eq.(4.10), Λ_g has a high value at the aligned position at $\theta = \pi/2P_s$ and a low value at the unaligned position at $\theta = 2\pi/P_s$.

One method to derive the maximum torque exerted on the outer rotor is via the rate of change of magnetic field energy, W_F, from a high-permeance position to a low-permeance position.

The energy density inside the pole pieces is too small compared to the energy density in the air gaps. Hence, the torque is calculated from the energy density in the air gaps.

The air gaps between the stator and inner rotor vary with the variation of the position of the pole pieces, being minimum in the aligned position and maximum in the unaligned position.

The field energy stored in the air gaps is

$$ W_F \;=\; \frac{1}{2}\mu_o H^2 \int dv \qquad (4.25) $$

H can be found by applying Eq.(4.5) to the flux path.

In the aligned position at $\theta = \pi/2P_s$,

$$
\begin{aligned}
H_1 &= \frac{NI}{g} \\
W_{F1} &= 2\alpha_o \frac{\pi \mu_o r_2 l_a N^2 I^2}{g P_s}
\end{aligned}
\tag{4.26}
$$

In the unaligned position at $\theta = 2\pi/P_s$,

$$
\begin{aligned}
H_2 &= \frac{NI}{(g + l_{or})} \\
W_{F2} &= 2(1 - \alpha_s) \frac{\pi \mu_o r_2 l_a N^2 I^2}{(g + l_{sr}) P_s}
\end{aligned}
\tag{4.27}
$$

The total torque exerted on the outer rotor can now be expressed as

$$
\begin{aligned}
T_s &= k_s P_s \frac{\Delta W_F}{\Delta \theta} \\
&= k_s P_s r_2 l_a N^2 I^2 \left[\frac{\alpha_s}{g} - \frac{1 - \alpha_s}{g + l_{sr}} \right]
\end{aligned}
\tag{4.28}
$$

where k_s is a constant that depends on the topology of the electromagnetic gear.

T_s is a reaction torque and, according to Newton's third law of motion, it is equal to the sum of T_i and T_o

$$
T_s = T_i + T_o
\tag{4.29}
$$

T_i and T_o represent the action. Eq.(4.29) is useful for judging simulation results.

Chapter 5

Design and Optimization of Electromagnetic Gear

5.1 Introduction

The electromagnetic gear analyzed in Chapter 4 would have a low torque density compared to the one with permanent magnets. However, the electromagnetic gear offers several advantages such as the possibility of torque control, field control, frequency control and the possibility of pole changing. To keep these advantages and raise the torque density, the electromagnetic poles need to be of salient poles. The basic equations derived in Chapter 4 were utilized with the aid of FEA to design and optimize the electromagnetic gear.

The schematic diagram of a salient-pole electromagnetic gear is shown in Fig.5.1 having the same topology as the loop gear presented in Chapter 4.

Different designs of the electromagnetic gear were made to developing several techniques of magnetic variable transmission. Thus, it is necessary to set approximate guidelines and hints for the design and optimization of electromagnetic gears. Some of these guidelines maybe applicable to magnetic gears. No integrated design guidelines are found in the literature nor is an adequate optimization approach.

The initial design stage of the doubly-excited magnetic gear is briefly illustrated by the flow chart of Fig.5.2. The design parameters are the dimensions
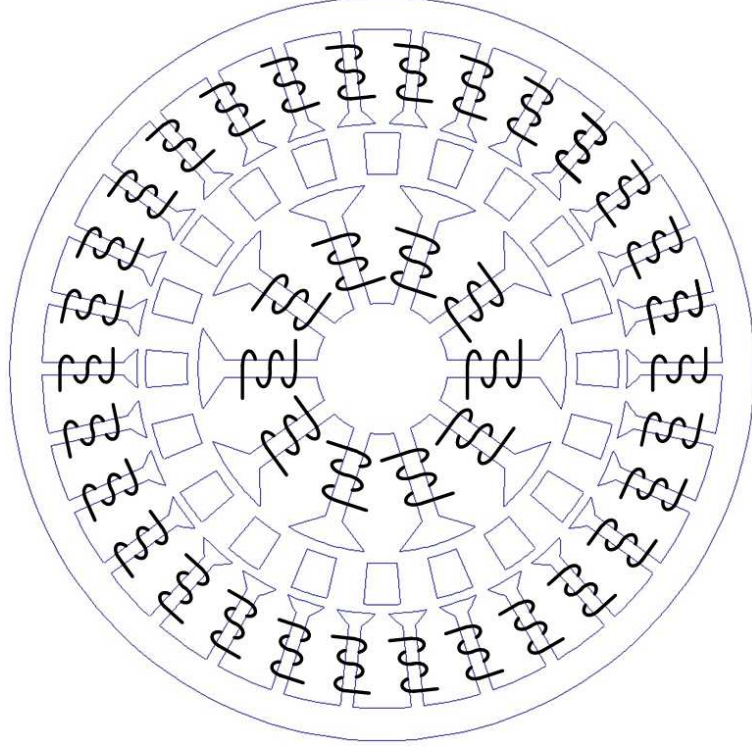
Figure 5.1: Electromagnetic Gear

of the parts of the magnetic gear, and optimization is the process of finding the optimum dimensions that would produce the highest possible torque density.

Eqs.(4.23)-(4.24) and Eq.(4.28) are approximate but adequate for design and optimization purposes. They offer several useful design hints and they provide an insight into the factors that affect the transmitted torques.

The transmitted torques increase with the number of poles. Eq.(4.23) says that the torque of the inner rotor would increase four folds if the number of its poles were doubled.

The transmitted torques vary linearly with the axial length l_a, and they are inversely proportional with the air gap and the radial length of the pole pieces. Another factor is the mmf which highly influences the torques. If the mmf was doubled, the torque would be four folds. The arc-to-pitch ratios of the poles are important design parameters, and there are optimum values at which the torques are maximum. These optimum values would elevate the transmitted torques by 10-40%.
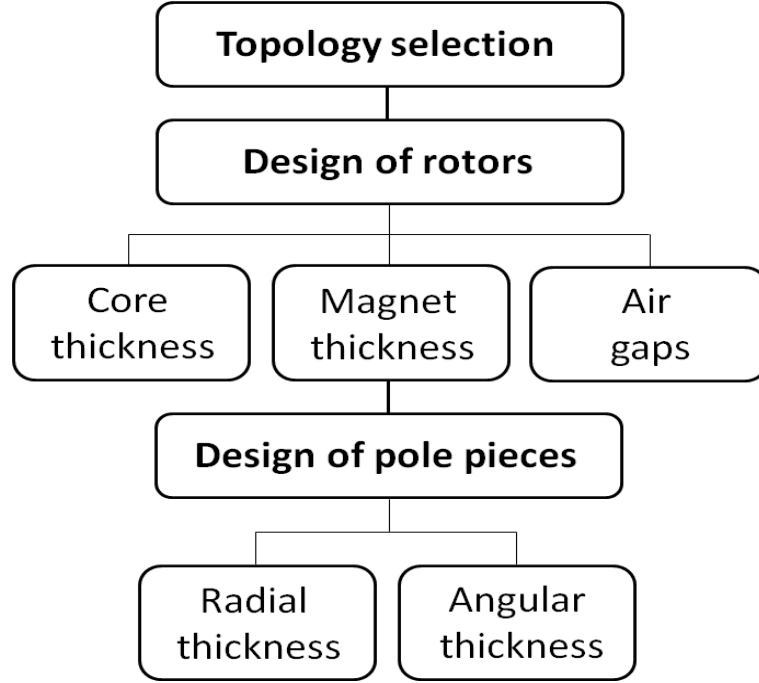
Figure 5.2: Flow chart of design of doubly-excited magnetic gear

5.2   Topology selection

It is learned from Eqs.(4.23)-(4.24) that the torque density is proportional to the square of the number of pole pairs of the stator and inner rotor. A gear ratio is decided according to the intended application of the magnetic gear. The gear ratio is determined from the selected topology. A high gear ratio is possible with a few poles in the inner rotor relative to the number of poles in the outer rotor.

5.3   Selection of air gap length

All torques are inversely proportional to the length of the air gaps. Hence, the air gaps should be selected to be as short as practically possible.
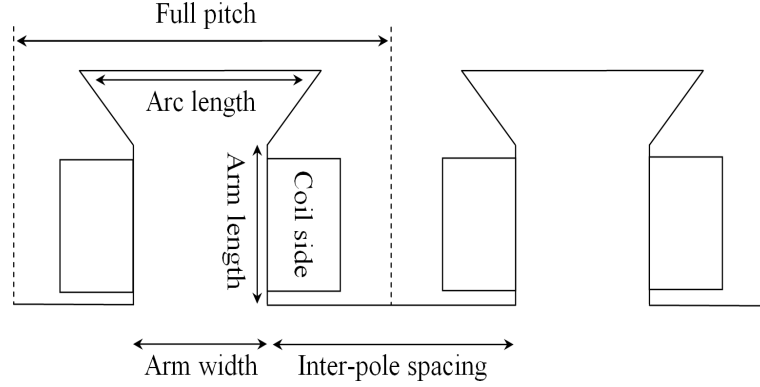
Figure 5.3: Salient pole

5.4 Pole and coil design

The salient pole with its design parameters is presented in Fig.5.3. A coil is wound around each pole. The arc length is a portion of the full pitch, and its optimum value is accurately determined by FEA. The arm width is a portion of the arc length, and the arm length is decided by the number of coil turns.

Each side of a coil occupies part of the spacing between poles, and the ratio of this segment to the spacing is the packing factor (k_{pf}) which should not exceed 75% in order to allow some air ventilation and to limit temperature rise.

The number of turns is approximately determined from

$$N = \frac{k_{pf}(\frac{2\pi r}{P} - l_{aw})}{4\pi d^2} \tag{5.1}$$

where r is the radius of the pole, P is the number of poles, l_{aw} is the arm width, and d is the diameter of the conductor.

If the conductor is rated at a current value of I_{rated}, the maximum current density is

$$J_{max} = \frac{I_{rated}}{4\pi d^2} \tag{5.2}$$

To prolong the conductor insulation and to limit the temperature rise, the applied current density is reduced to a half of the maximum value.

5.4.1 Design of pole pieces

Eq.(4.9), Eqs.(4.23)-(4.24) and Eq.(4.28) provide hints for an optimum design of the pole pieces. First, there is a ratio between the circumferential and radial thickness of a pole piece. The radial thickness should be less than the circumferential thickness so that the magnetic flux and consequently the torques become higher. The optimum ratio depends on the selected topology and can be accurately determined by FEA. Second, the circumferential thickness of the pole piece should be a portion of the full pitch. It has been deduced that the optimum ratio is 0.5.

The best shape of the pole piece cannot be decided from the torque equations. There are three possible shapes of the cross section of a pole piece: sector-shaped, rectangular and circular.

The permeance of a sector-shaped cross section is [Per02]

$$
\begin{aligned}
\Lambda_{or} &= \mu \frac{l_\theta l_a}{ln(\frac{r_{out}}{r_{in}})} \\
\Lambda_{o\theta} &= \mu \frac{ln(\frac{r_{out}}{r_{in}})l_a}{l_\theta}
\end{aligned}
\tag{5.3}
$$

And the permeance of a rectangular cross section is

$$
\begin{aligned}
\Lambda_{or} &= \mu \frac{wl_a}{h} \\
\Lambda_{o\theta} &= \mu \frac{hl_a}{w}
\end{aligned}
\tag{5.4}
$$

The permeance of a circular cross section can be approximated by a square of sides r tangent to the circle

$$
\Lambda_{or} = \Lambda_{o\theta} = \mu l_a
\tag{5.5}
$$

(a)

(b)

(c)
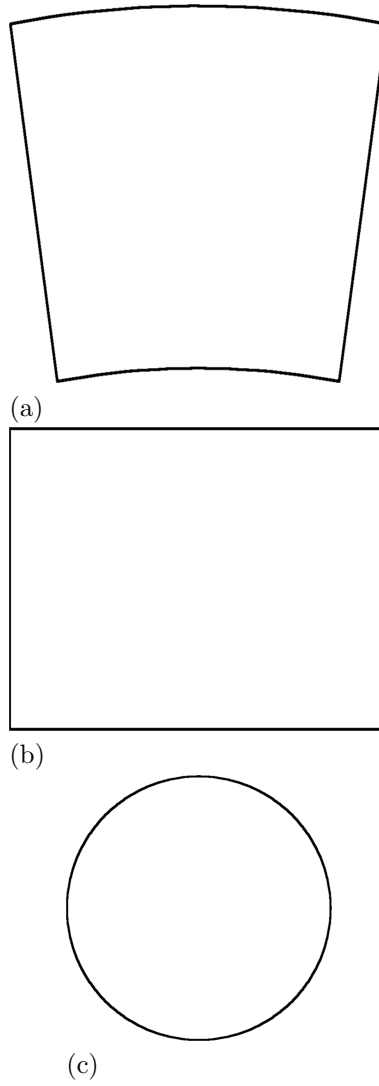
Figure 5.4: Possible shapes of cross section of pole piece (a) sector (b) rectangular (c) circular

5.5 Simulation results and discussions

2D static simulations were conducted on different models and topologies of the electromagnetic gear. The FEMM software was used. The maximum torque of each rotor was calculated for one pole pitch. The results are expressed in normalized values in order to draw useful conclusions.

The effect of a single design parameter was simulated at a time. The discretization data of a simulation session is presented in Table 5.1.

In the analysis, the rotor windings are connected in series. The windings have the same number of turns/slot.

5.5.1 Variable mmf

The amplitude of the mmf is NI. By increasing the current or number of turns of any winding, all the transmitted torques are proportional to N^2I^2. By doubling either I or N, the torques are increased four folds. In Fig.5.5, for an mmf of 0.2 p.u the torque is around 0.06 p.u; for an mmf of 0.4 p.u, the torque is around 0.23 p.u which is close to four times its previous value. This agrees with Eqs.(4.23)-(4.24) and Eq.(4.28). This is a very useful characteristic of the electromagnetic gear in case of load changes. The current can be increased when the load increases to avoid overloading the gear.

5.5.2 Variable air gap

In all electric machines, torque is inversely proportional to the air-gap length. For any topology and for the same radial length of the pole pieces, the torque of the outer rotor is inversely proportional to the variation of the air gap length. Fig.5.6 shows the results which agree with Eq.(4.28). Increasing the air-gap length ten folds from 0.1 p.u to 1.0 p.u results in a torque reduction of nearly 65% from 1.0 p.u to around 0.35 p.u. In small machines, typical air-gap lengths range from 0.5 mm to 1.5 mm.

Table 5.1: Discretization data of simulation.

Number of elements	62546
Number of nodes	32145
Number of steps	300
Total simulation time (h)	2
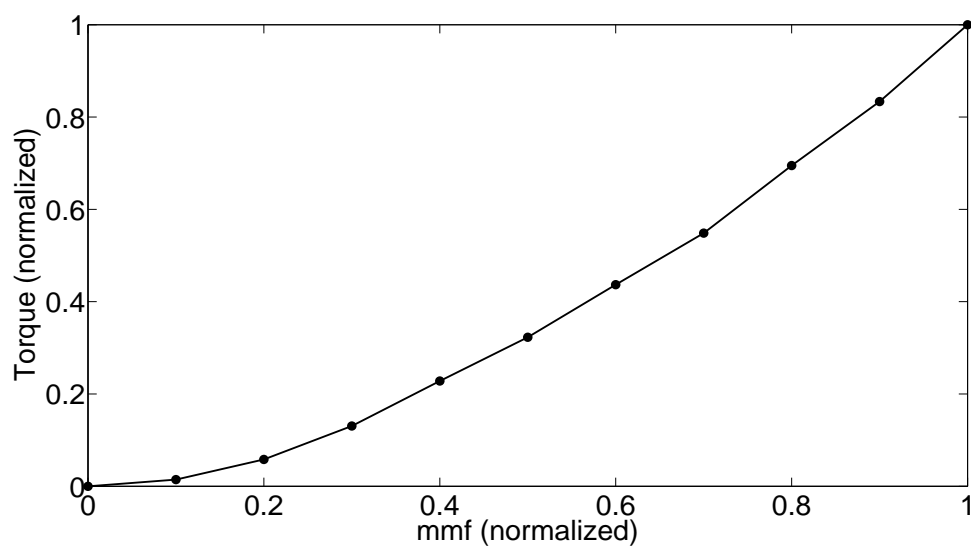
Figure 5.5: Variation of torque with mmf
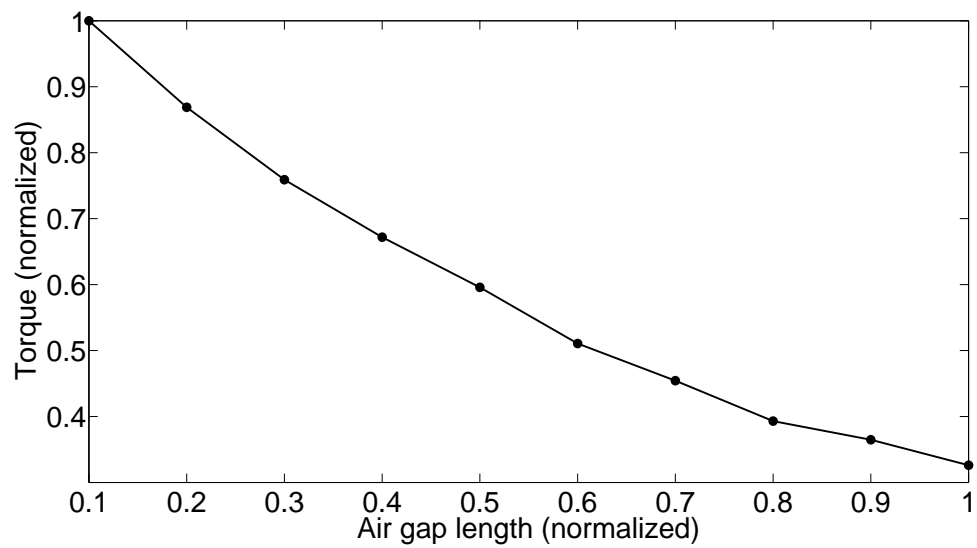
Figure 5.6: Variation of torque with air gap length
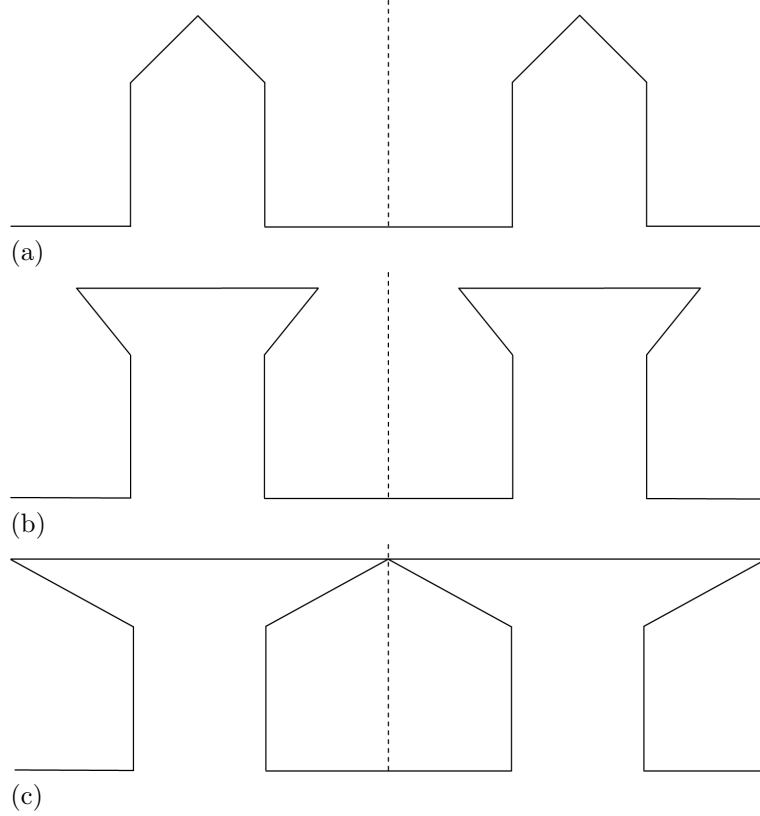
Figure 5.7: Arc-to-pitch ratio of salient pole (a) 0 (b) 0.7 (c) 1.0

5.5.3 Variable arc-to-pitch ratio

To investigate the influence of the arc-to-pitch ratios of the poles on the transmitted torques, the arc-to-pitch ratios of the poles of the outer rotor were varied from 0 to 1 for different ratios of the poles of the inner rotor. The shapes of salient poles at different ratios are illustrated in Fig.5.7. Likewise, the arc-to-pitch ratios of the poles of the inner rotor and the pole pieces were varied. The arm width of each salient pole was kept constant.

When α_i is varied from 0 to 1, the torque of the outer rotor reaches its highest possible value when $\alpha_o = 0.7$ and at $\alpha_i = 0.5\text{-}0.8$. The curves are presented in Fig.5.8a. By varying α_o from 0 to 1 for different values of α_i, the torque of the outer rotor is high at $\alpha_o = 0.6\text{-}0.8$ and at $\alpha_i = 0.5$ (Fig.5.8b).

In Fig.5.9a, the torque of the inner rotor is maximum at $\alpha_i = 0.6\text{-}0.8$ and at both $\alpha_o = 0.5$ and $\alpha_o = 0.7$. In Fig.5.9b, the torque is maximum at ratios of $\alpha_i =$

47

0.5 and α_o=0.5-0.7.

In Fig.5.10a, the torque of the pole pieces is maximum at α_o=0.7 and at α_i=0.5-0.7. In Fig.5.10b, this torque is maximum at α_o=0.5-0.7 and α_i=0.5.
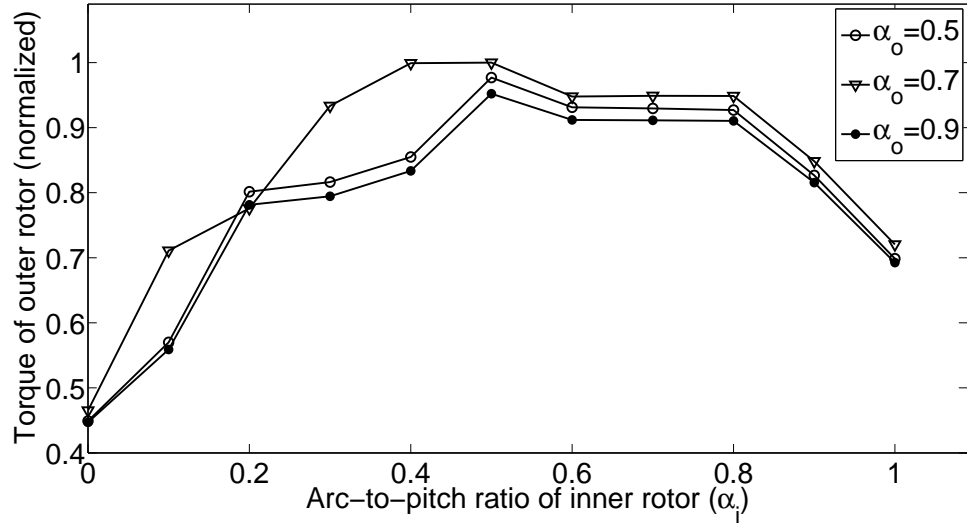
(a)
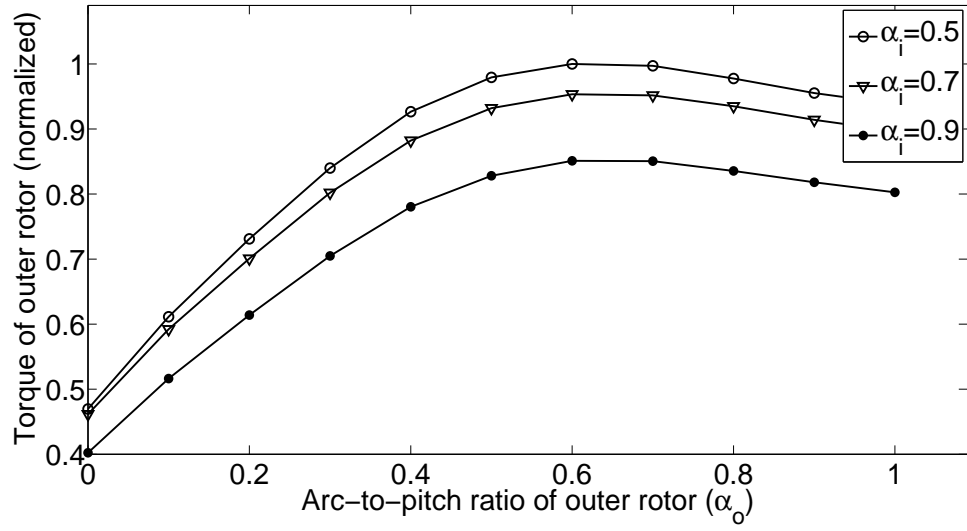
(b)

Figure 5.8: Influence of pole arc-to-pitch ratio on torque of outer rotor (a) α_i varied (b) α_o varied

49
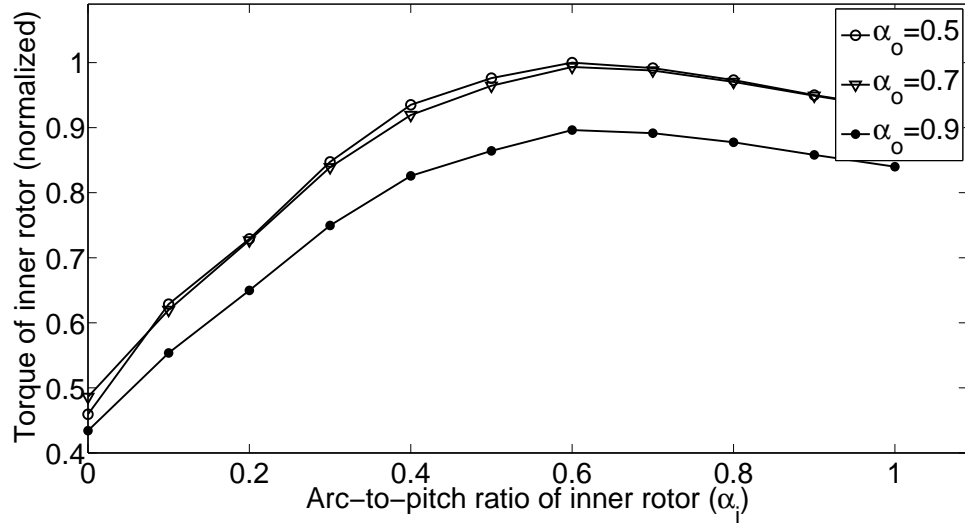
(a)
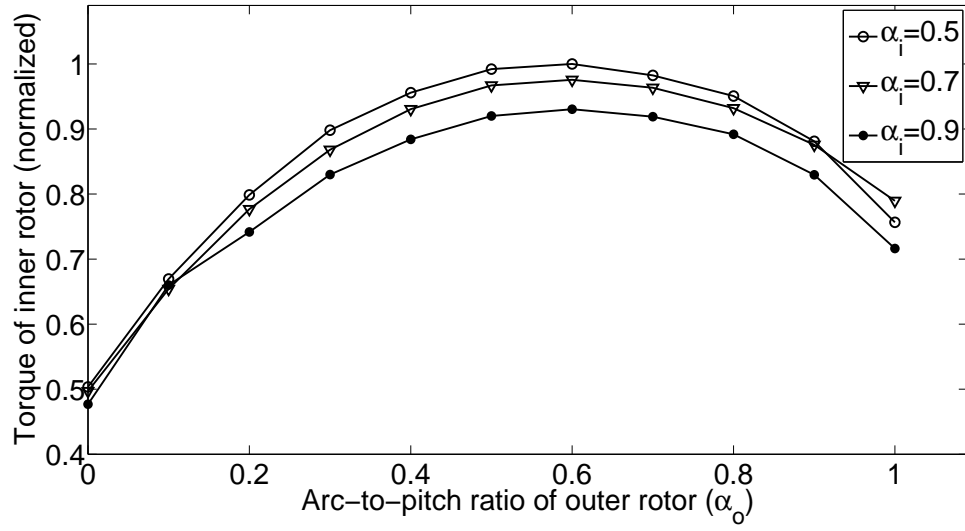
(b)

Figure 5.9: Influence of pole arc-to-pitch ratio on torque of inner rotor (a) α_i varied (b) α_o varied
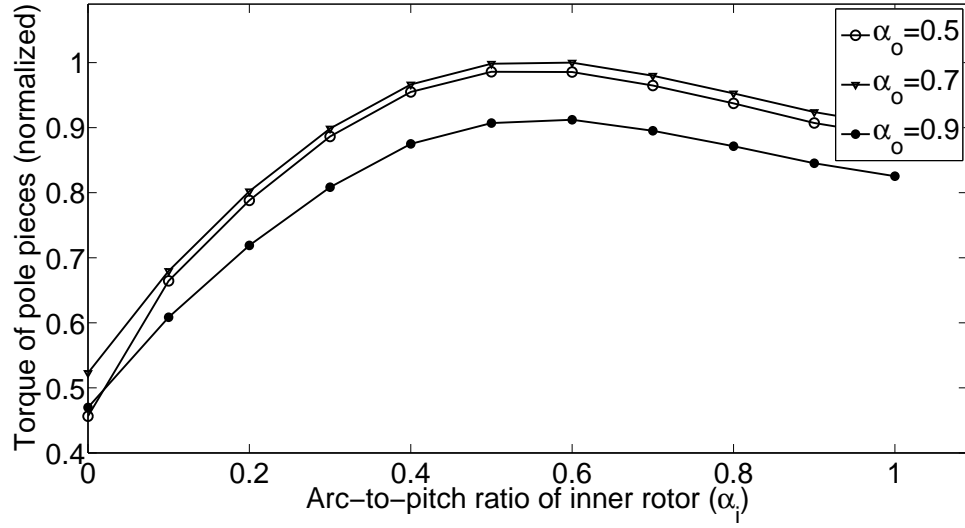
(a)
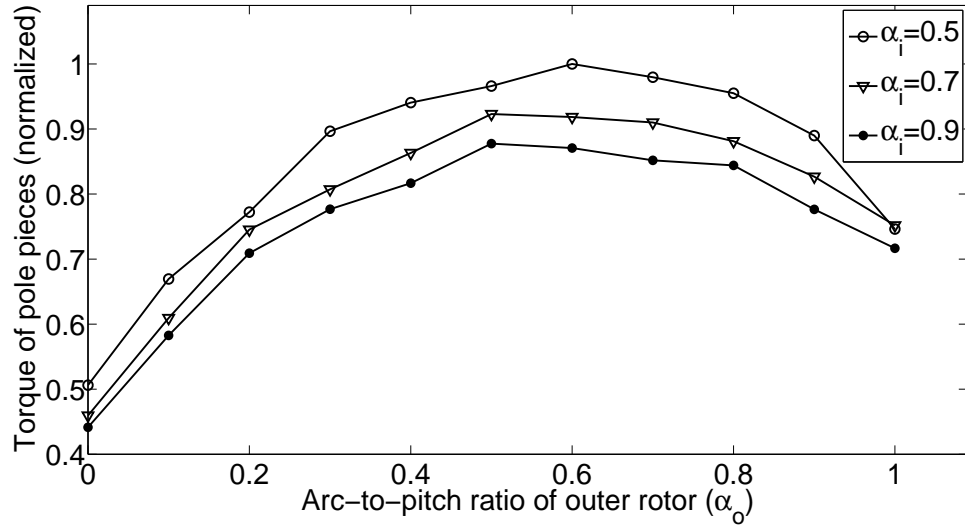
(b)

Figure 5.10: Influence of pole arc-to-pitch ratio on torque of pole pieces (a) α_i varied (b) α_o varied

5.6   Design of pole pieces

5.6.1   Shape

Three models were constructed using different sizes and topologies in order to make a correct conclusion rather than basing conclusions on one topology which might not apply to other topologies. Three shapes were applied: sector, rectangular and circular. The results are presented in Fig.5.11. In all topologies, the sector-shaped pole pieces develop the highest torques whereas the rectangular-shaped pole pieces develop the lowest torques. The difference in torque between the different shapes decrease with the increase of the number of pole pieces. In the 31-3-34 topology, the circular-shaped pole pieces develop a torque that is 90% of that developed by the sector-shaped pieces. With less pole pieces, this difference increases. In the 10-4-14 topology, the circular-shaped and rectangular-shaped pole pieces develop torques around 70% of that developed by the sector-shaped pole pieces.

5.6.2   Circumferential length

When the arc-to-pitch ratio of the pole pieces is varied, the transmitted torques vary in a similar trend. Maximum torque occurs at a ratio α_o=0.5 (Fig.5.12). A ratio of 1 means that all the pole pieces are connected altogether with no space in between; no useful torques are transmitted as predicted by Fig.4.7a. A ratio of 0.5 was selected for the optimized design.

5.6.3   Radial length

Eqs.(4.10)-(4.11) offer a hint for the design of the pole pieces; there is a ratio between its radial and circumferential length. The radial length increases the reluctance of the pole piece. If α_o and the air gap length are constant, the torque of the outer rotor varies slightly when the radial length of the pole pieces is varied as Fig.5.13 shows. The radial length should be between 50-100% of the circumferential length. This also would reduce the weight of the pole piece.
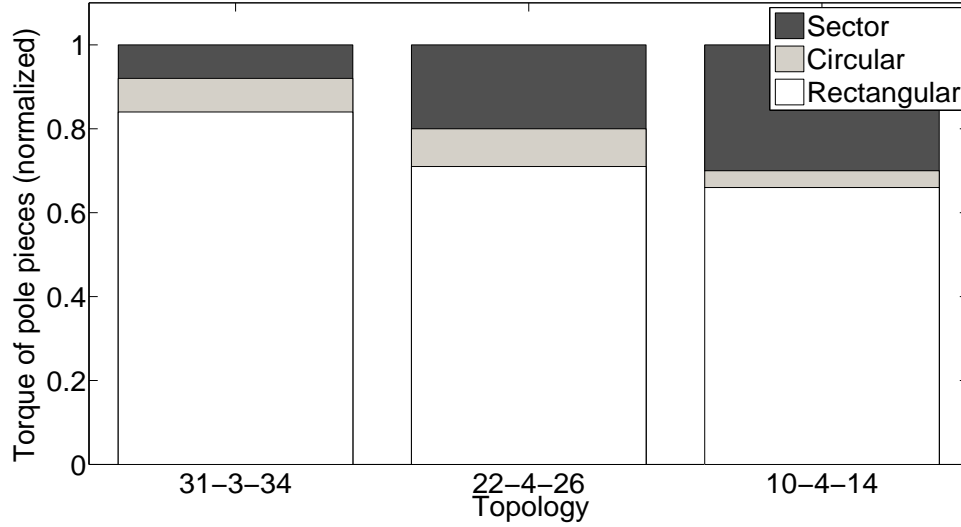
Figure 5.11: Influence of shape of pole pieces

5.6.4 Thickness of bridge connecting pole pieces

In practice, the pole pieces are connected together by a bridge to simplify the mechanical design and the assembly of the prototype and to provide a mechanical support. This bridge provides a path for flux to flow tangentially and so part of the mutual flux is lost which reduces the transmitted torques. Fig.5.14 shows the influence of the thickness of the bridge on the torque exerted on the pole pieces. If the thickness of the bridge is 10% of the radial thickness of the pole pieces, the torque is reduced by around 15%. If the ratio is 50%, the torque is reduced by 80%.
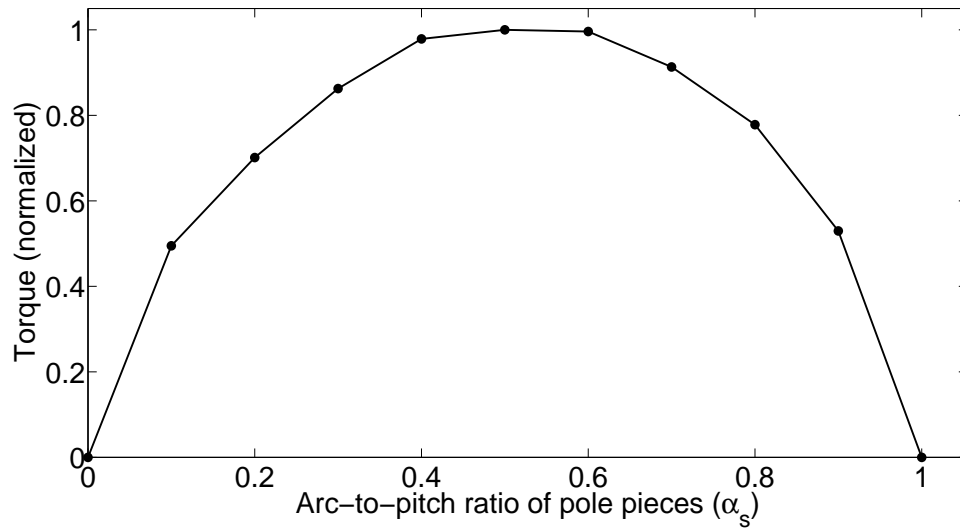
Figure 5.12: Influence of pole arc-to-pitch ratio of pole pieces on transmitted torques
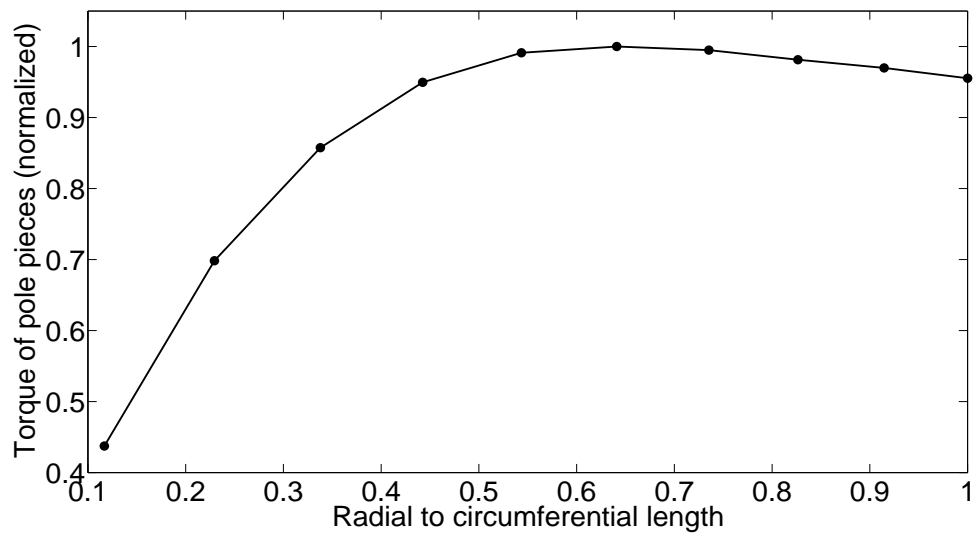
Figure 5.13: Variation of torque with radial length of pole pieces

54
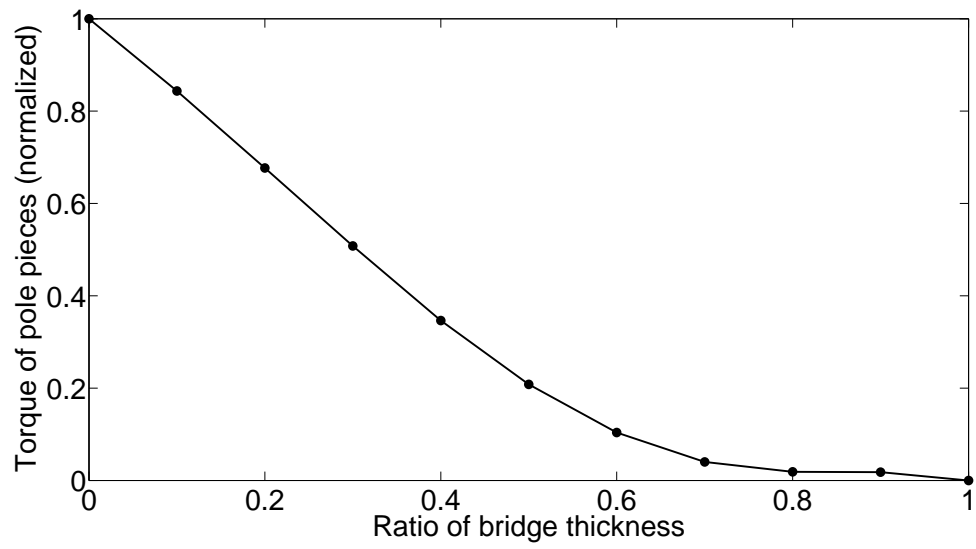
Figure 5.14: Variation of torque with thickness of bridge connecting pole pieces

Chapter 6

Magnetic Variable Transmission by Pole Changing

6.1 Introduction

The gear ratio of the magnetic gear can be changed by changing the number of poles. This can be achieved by changing the number of poles of the outer rotor, inner rotor and/or pole pieces if Eq.(4.18) is satisfied. Hence, variable transmission is possible if a technique to achieve pole changing is realized. Two techniques are proposed:

1. Electromagnetic gear

The permanent magnets on both rotors are replaced with windings. The gear ratio is changed by changing the number of poles of the windings while keeping the number of pole pieces unchanged.

2. Hybrid magnetic gear

The word *hybrid* refers to the use of a winding and permanent magnets. The gear ratio is changed by changing the number of pole pieces and the poles of the winding.
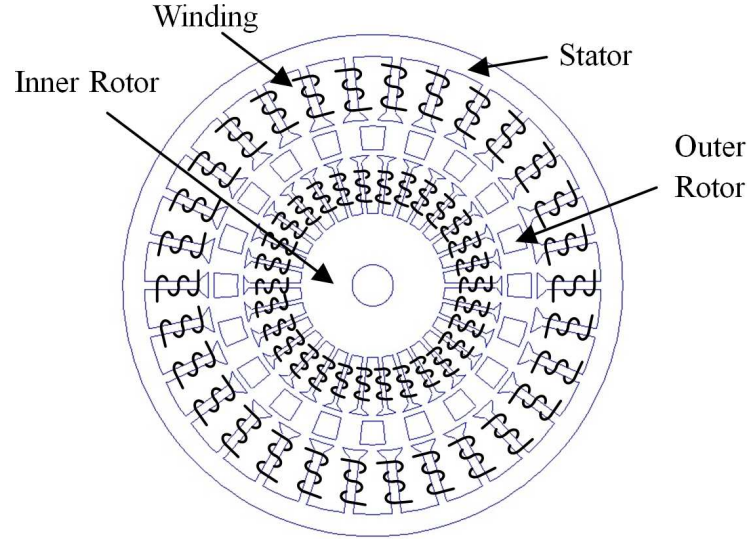
Figure 6.1

6.2 Method 1: Electromagnetic gear

6.2.1 Construction

Fig.6.1 shows the optimized electromagnetic gear and Table 6.1 lists the design parameters. The members of the gear are named differently because the function of each member is different. The pole pieces are not stationary but act as the outer rotor. The outer rotor is stationary here to avoid using slip rings; it acts as a stator. The stator and inner rotor contain concentrated windings which are wound around salient poles and which are excited with direct current. The inner rotor is provided with slip rings. The stator and inner rotor have 30 poles each and there are 20 pole pieces. The gear was designed and optimized based on the guidelines explained in Chapter 4. The concentrated winding was selected because of its simplicity, shorter length of end winding and lower copper losses. Moreover, more coil turns can be applied.

The arc-to-pitch ratio of each pole is 0.75 which produces the maximum possible torques. The length of the arm of each pole allows many coil turns to be wound. The transmitted torques are proportional to the width of each pole and so the width was selected to be as big as practically possible without altering the shape of saliency. This width is around 25% of the length of the full pitch.

57

Table 6.1: Design parameters of electromagnetic gear.

Diameter of stator	170 mm
Diameter of inner rotor	88 mm
Air-gap length	0.5 mm
Stack length	100 mm
Number of poles of stator	30
Number of poles of outer rotor	20
Number of poles of inner rotor	30
Pole arc-to-pitch ratio of stator	0.75
Pole arc-to-pitch ratio of outer rotor	0.5
Pole arc-to-pitch ratio of inner rotor	0.75
Number of turns per slot of stator winding	600
Resistance per slot of stator winding	78.3 ohm
Number of turns per slot of inner rotor winding	200
Resistance per slot of inner winding	24.6 ohm
Rated winding current per slot	0.5A
wire diameter	0.2 mm

Table 6.2: Possible topologies of electromagnetic gear.

P_s	15	5	10	12	8
P_i	5	15	10	8	12
P_o	20	20	20	20	20
G_r	4.00	1.33	2.0	2.5	1.67

The cross section of each pole piece is sector-shaped and each pole piece occupies 50% of its full pitch. The length of each air gap is 0.5mm which is small but practically realizable.

6.2.2 Principle of operation

The gear ratio can be changed by exciting the correct number of poles of both windings so that Eq.(4.18) is satisfied. The number of pole pieces is fixed and it is the sum of the pole pairs of the stator poles and the inner rotor poles. The gear ratio can be re-expressed from Eq.(4.16) as

$$G_r = \frac{P_o}{P_i} = \frac{\theta_i}{\theta_o} \tag{6.1}$$

Here, P_o denotes the number of pole pieces.

Table 6.2 lists some of the possible topologies in which the excited poles are the most symmetric. The process of pole changing is illustrated in Fig.6.2 with the most symmetric combination of poles.

It is possible to vary the gear ratio from 1.33 to 4.00 over five steps by exciting more poles in the stator and less poles in the inner rotor. The switching from one ratio to the other is performed by a switching circuit that receives a signal from a speed sensor which measures the speed of the outer rotor of the gear. The details of the switching circuit are provided in Appendix A. The block diagram of the system is depicted in Fig.6.3. The prime mover may be a wind turbine, a motor or a gasoline engine. The load may be a generator, a centrifugal pump, an electric hoist or any type of load that requires variable torque and/or speed.

The coils are connected in parallel (Fig.6.4) so that the supply voltages are small. Each coil is rated at 0.5A. The stator resistance per slot is 78.3 ohms on average, and that of the inner rotor is 24.6 ohms. The stator winding is rated at 40V/15A and the rotor winding at 12V/15A.

To demonstrate this technique, the 15-5-20 and 5-15-20 topologies will be used. When switching from the 15-5-20 topology to the 5-15-20 topology, the output speed can be varied between $\frac{1}{4}\omega_i$ and $\frac{3}{4}\omega_i$ for a constant input speed ω_i.

Ideally, the output torque would be reduced from $\frac{3}{4}T_i$ to $\frac{1}{4}T_i$. Generally,

$$T_o = \frac{\omega_i}{\omega_o}T_{in} \tag{6.2}$$

The load torque must be below the output torque in both topologies. The winding current can be increased in case the load torque exceeds the output torque. Fig.6.5 shows the ideal torque-speed curve along with two types of load.

For a constant input speed, the output torque would be roughly constant over a wide range of output speed. For different values of current, there are different torque-speed characteristics. The rated output torque is obtained by the rated current. In the case of a fan or a pump as a load, the load torque varies to the square of the speed or $T_{fan}=k\omega_o^2$ where k is a constant. An electric hoist has a constant load at a constant or variable speed. An example is the overhead crane which often employs a two-speed hoist.

At the rated current I_{rated}, the rated output torque exceeds the load torques at all speeds. For the fan load, the current maybe decreased to I_1 at ω_{o1} and I_2 at ω_{o2}. For the hoist load, the current maybe decreased to I_3 at ω_{o1} and I_4 at ω_{o2}. The operating points P_1-P_4 are the most efficient at which the torque-speed curve of the electromagnetic gear crosses the load curve. In practice, the electric current is slightly increased so that the output torque exceeds the load and inertial torques according to the motion equation

$$T_o = T_L + J_o\frac{d\omega_o}{dt} \tag{6.3}$$

where J_o is the inertia of the load and the outer rotor.
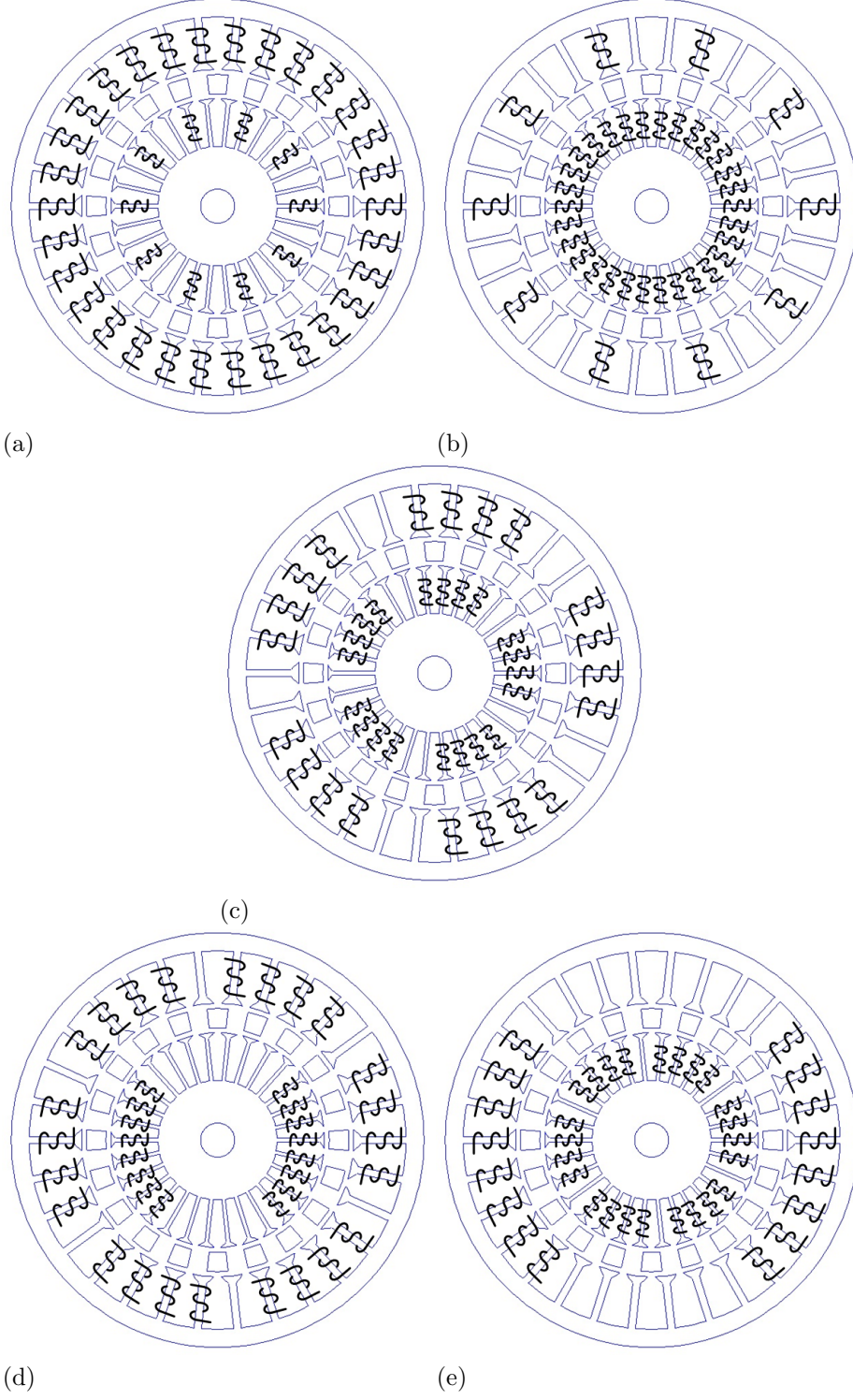
Figure 6.2: Process of pole changing (a) 15-5-20 topology (b) 5-15-20 topology
(c) 10-10-20 topology (d) 12-8-20 topology (e) 8-12-20 topology
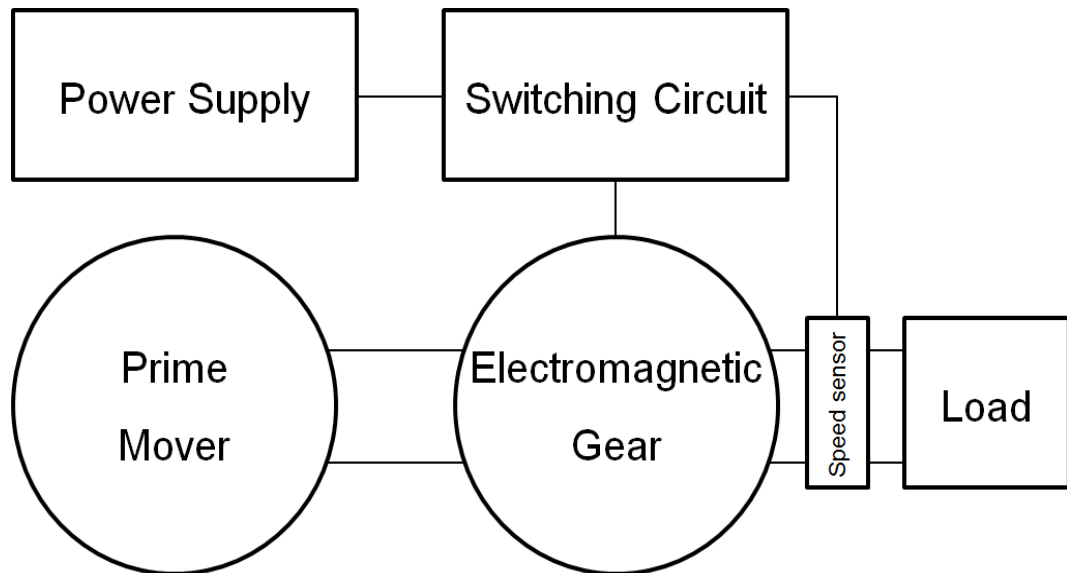
Figure 6.3: Block diagram of electromagnetic gear system
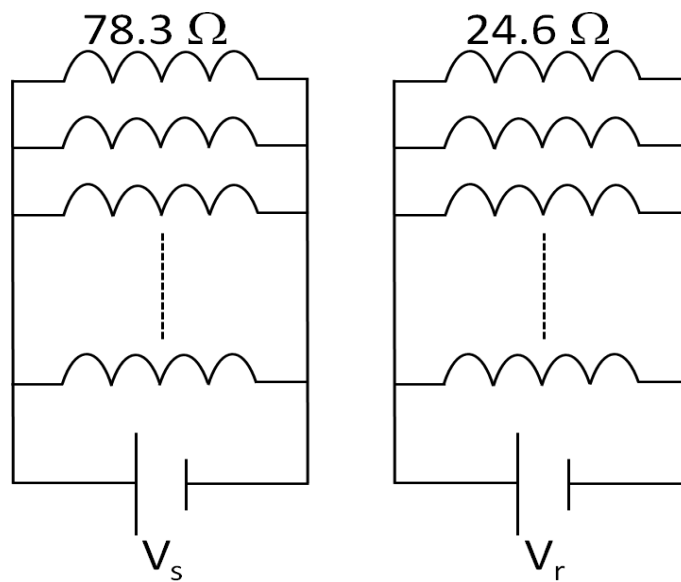
Figure 6.4: Electric circuit
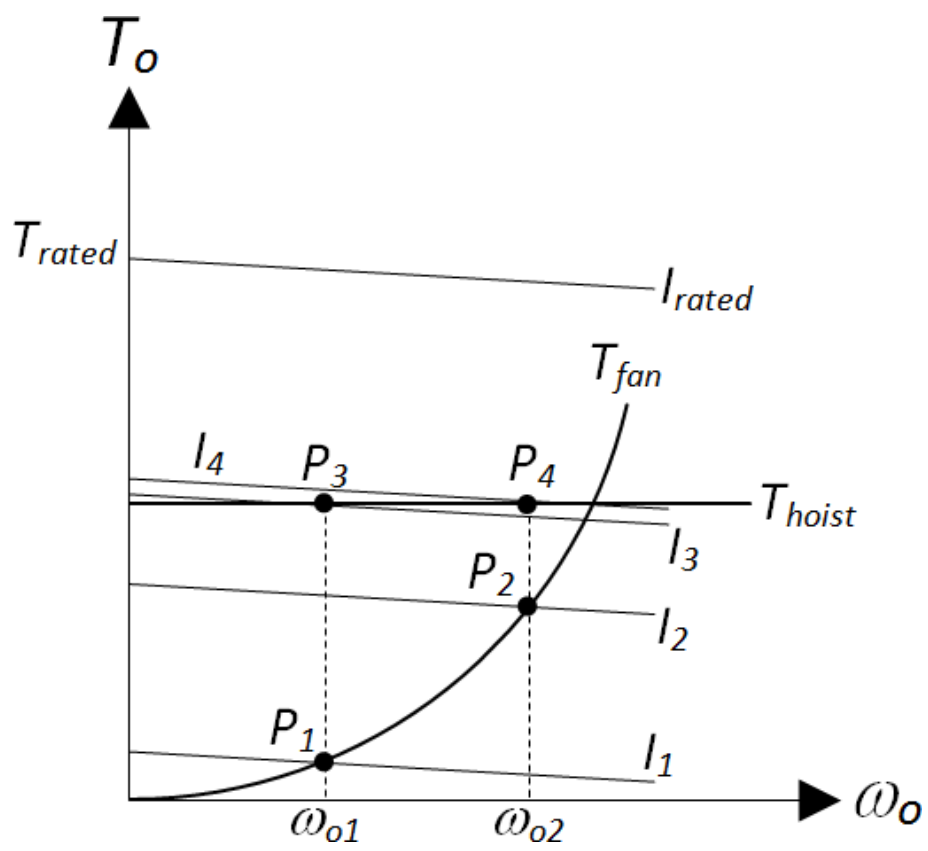
Figure 6.5: Torque-speed characteristics with a constant load and a variable load
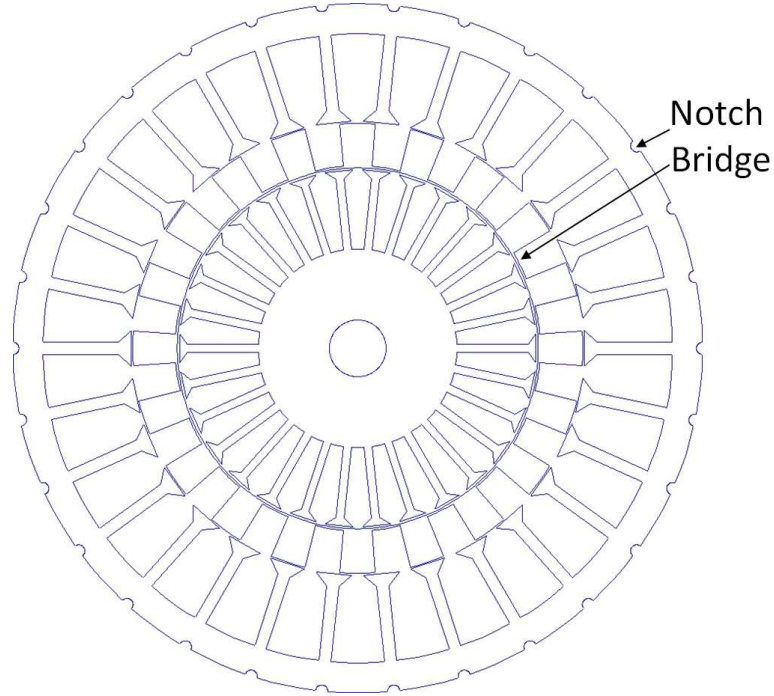
Figure 6.6: Introducing notches and bridge for prototyping

6.2.3 Prototyping

For prototyping purposes, the schematic diagram in Fig.6.1 is modified in Fig.6.6. A prototype was constructed having the same parameters listed in Table 6.1. The stator core has notches that keep the casing fixed and prevent it from slipping. The pole pieces are connected by a thin bridge to provide a mechanical support.

Two views of the actual prototype are shown shown in Fig.6.7. The hermetically sealed slip rings are maintenance free, and they connect the winding of the inner rotor with a power supply.

(a)

Stator terminals

Input shaft

Slip rings

Output shaft
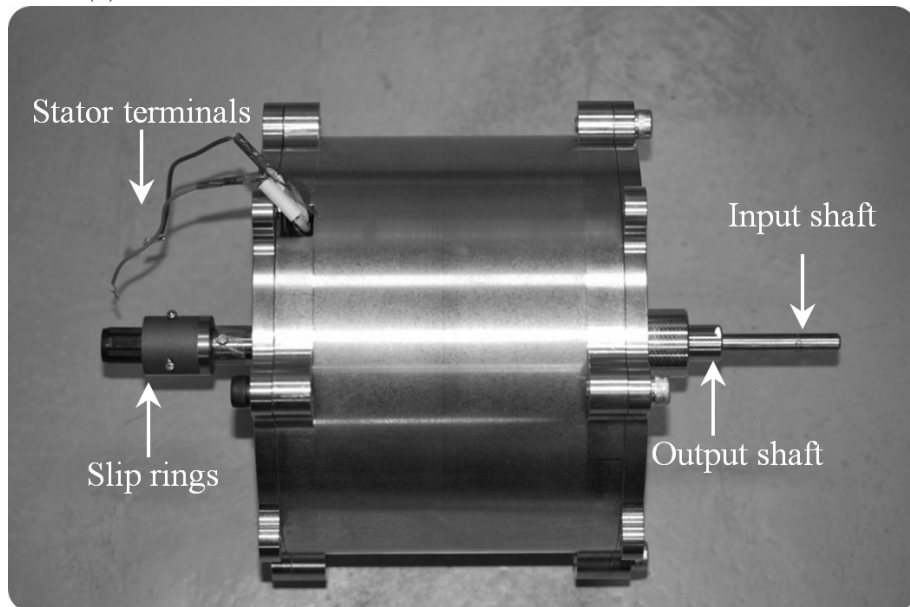
(b)

Figure 6.7: Constructed prototype (a) front view (b) side view

Table 6.3: Discretization data of simulation.

Static simulation	
Number of elements	40567
Number of nodes	21406
Step time (ms)	50
Number of steps	241
Total simulation time (h)	1
Dynamic simulation	
Number of elements	40567
Number of nodes	21406
Step time (ms)	0.5
Number of steps	6001
Total simulation time (h)	7

6.2.4   Simulation results

To confirm the validity of the operation of the electromagnetic gear, extensive simulations were carried out. The static simulations provide basic information such as maximum transmitted torques and flux density. The dynamic simulations were conducted to calculate the variable gear ratio and efficiency. Moreover, the effects of switching and loading conditions could be investigated. Table.6.3 contains the discretization data of the static and dynamic simulations.

To reduce the simulation time, a fifth model was constructed and a periodic rotation boundary was set to 72° (Fig.6.8).

6.2.4.1   Validation of variable gear ratio from speed response

The process of pole changing was performed with the 15-5-20 and 5-15-20 topologies. A step speed of ω_i=333 rpm was applied to the inner rotor of the simulation model. The output speed was calculated from the motion equation.

Two cases were simulated. In the first case, a load of 0.1 Nm and a current of 0.25A/slot were applied. In the second case, the load was increased four folds to 0.4 Nm and the applied current had to be doubled to 0.5A/slot so that the output torque exceeds the load and inertial torques. In both cases, the average
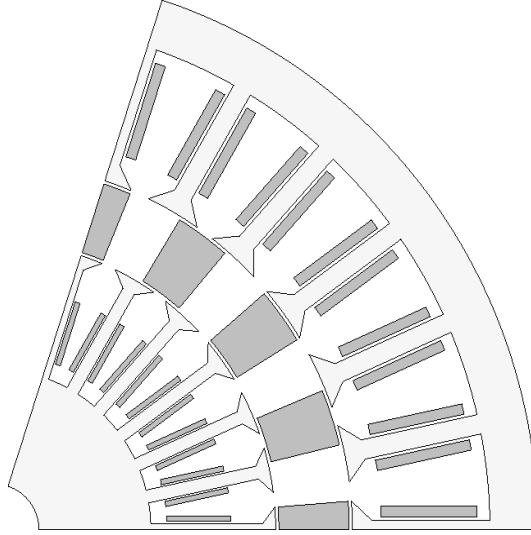
Figure 6.8: JMAG 2D simulation model

output speed should be close to 83 rpm for the 15-5-20 topology and 250 rpm for the 5-15-20 topology.

The speed and torque responses are shown in Fig.6.9. The 15-5-20 topology has a faster response because the resultant mmf and, consequently, the magnetic flux are bigger. Pole changing takes place at t=1.5s. At a load of 0.1 Nm and a current of 0.25A/slot, the output speed increases gradually until it settles down at an average value of nearly 83 rpm after 0.2 seconds in the 15-5-20 topology. In the 5-15-20 topology, the output speed settles down at 250 rpm after 1.3 seconds. At a load of 0.4 Nm and current of 0.5/slot, the output speed settles down at 83 rpm after 0.2s in the 15-5-20 topology, and it settles down at 250 rpm in the 5-15-20 after 0.7s which is quicker than the first case because the mmf was increased. The speed ripples occur due to the saliency of the electromagnetic poles. The response time differs from one topology to the other because of the responses of the electric currents which depend on the inductances of the equivalent electric circuit.

The effect of pole changing on the angular displacement of the outer rotor is presented in Fig.6.10. The slope of the displacement changes after pole changing, and the corresponding speed can be calculated as the slope of the displacement.

The corresponding waveforms of the output torque are presented in Fig.6.11.

It is observed that the output torque exceeds the load torque. These results confirm the validity of the method.

The effect of pole changing on the current waveforms is plotted in Fig.6.12 for both loads where I_s is the total stator current and I_r is the total rotor current. In the 15-5-20 topology and at a load of 0.1 Nm, the rotor current climbs to to nearly 7.5A for 11 ms and then it gradually decrease until it settles down at roughly 2.5A after 0.2s. The stator current settles down at 7.5A. In the 5-15-20 topology and at a load of 0.1 Nm, the rotor current settles down at an average value of 7.5A after over 1s whereas the stator current settles down at 2.5A.

When the load is increased to 0.4 Nm and the current to 0.5A/slot, the steady-state average value of rotor current is 7.5A in the 15-5-20 topology and 15A in the 5-15-20 topology. The stator current is 15A in the 15-5-20 topology and 7.5A in the 5-15-20 topology. The transient period of the currents is shorter in this case.
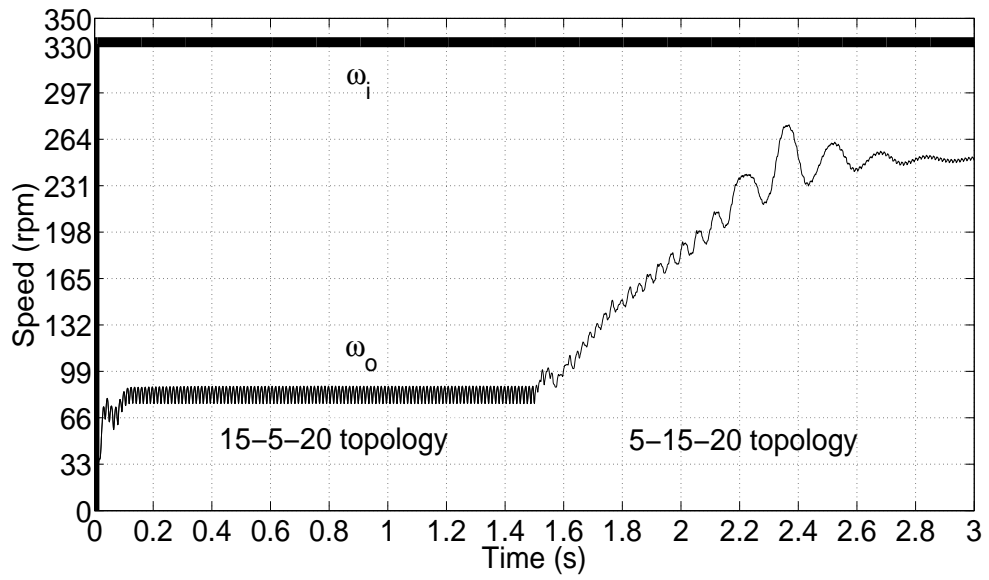
(a)
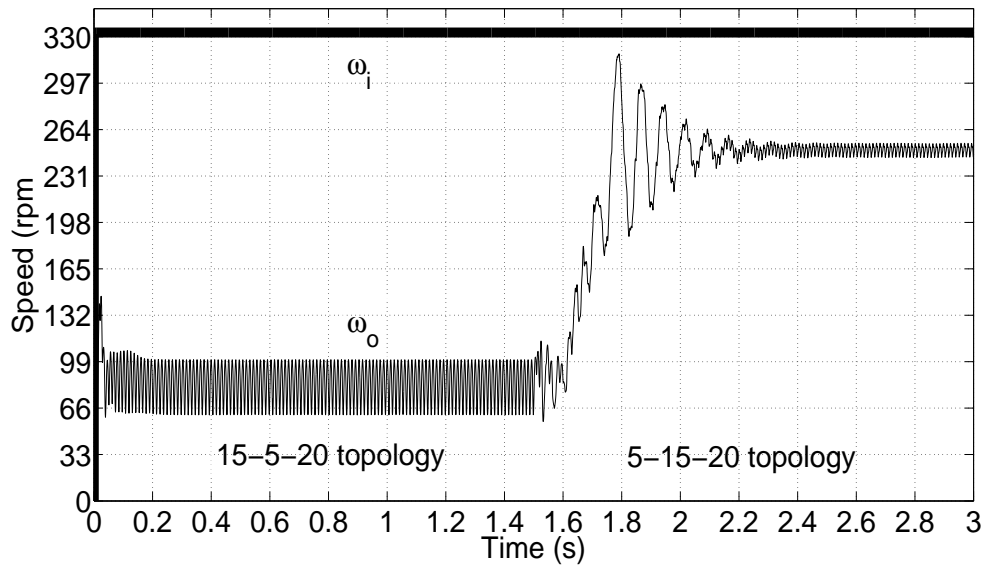
(b)

Figure 6.9: Response of output speed at (a) 0.1 Nm (b) 0.4 Nm

(a)

(b)

Figure 6.10: Angular displacement at (a) 0.1 Nm (b) 0.4 Nm

(a)

(b)

Figure 6.11: Current waveforms at (a) 0.1 Nm (b) 0.4 Nm

71
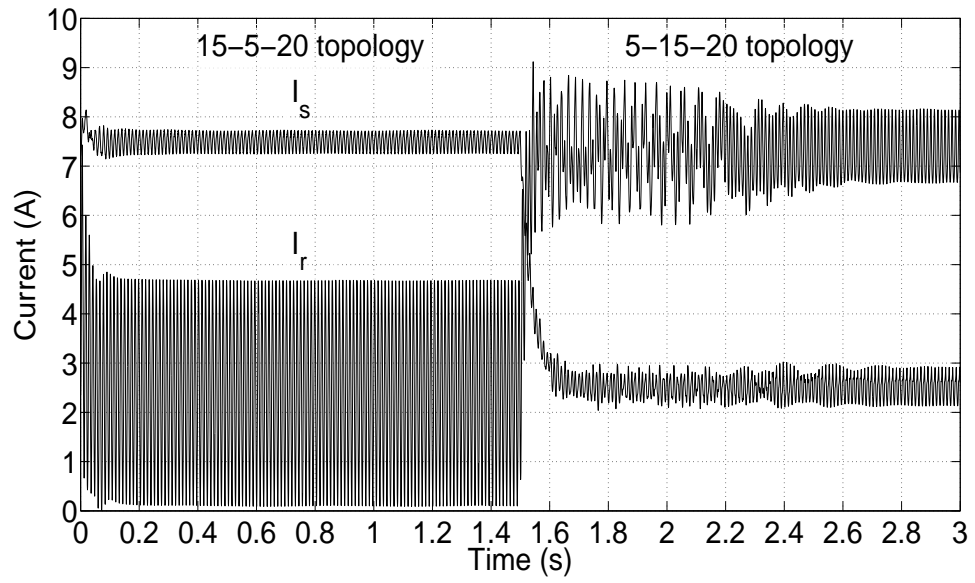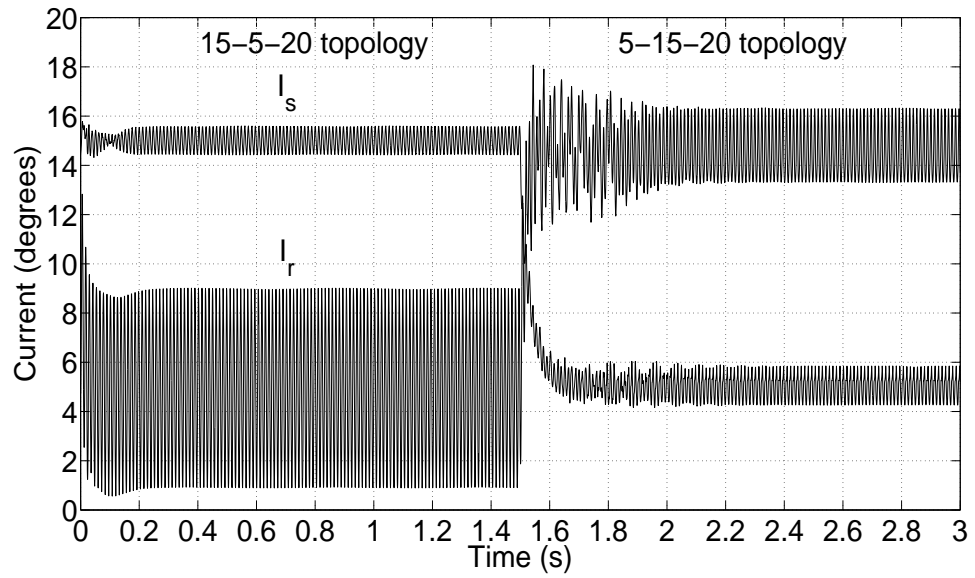
Figure 6.12: Current waveforms at (a) 0.1 Nm (b) 0.4 Nm

6.2.4.2 Flux density

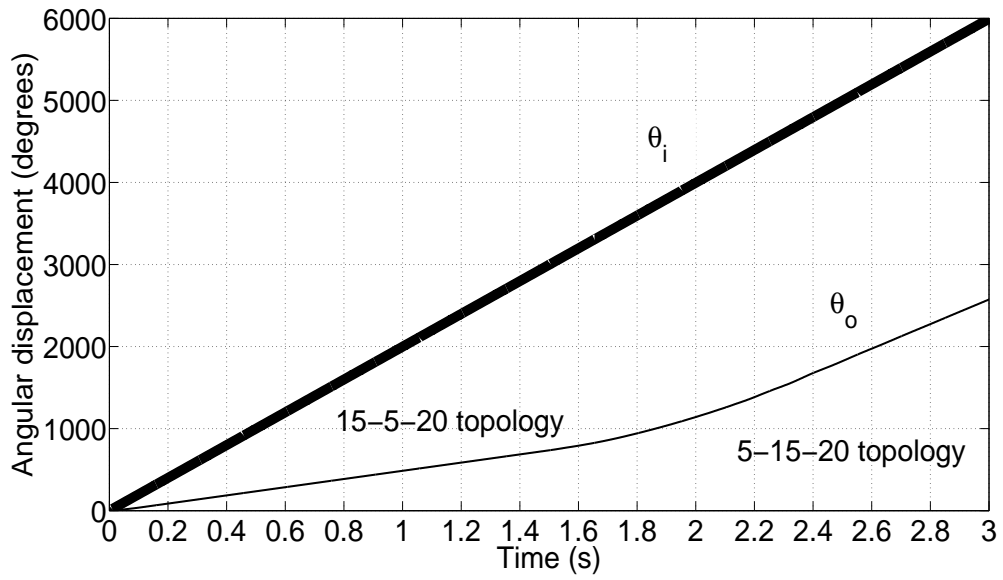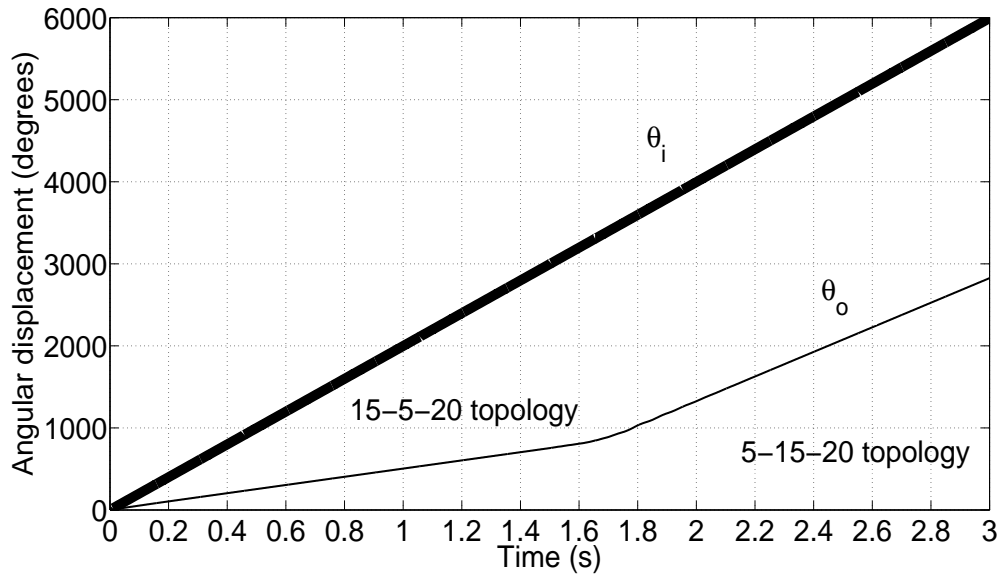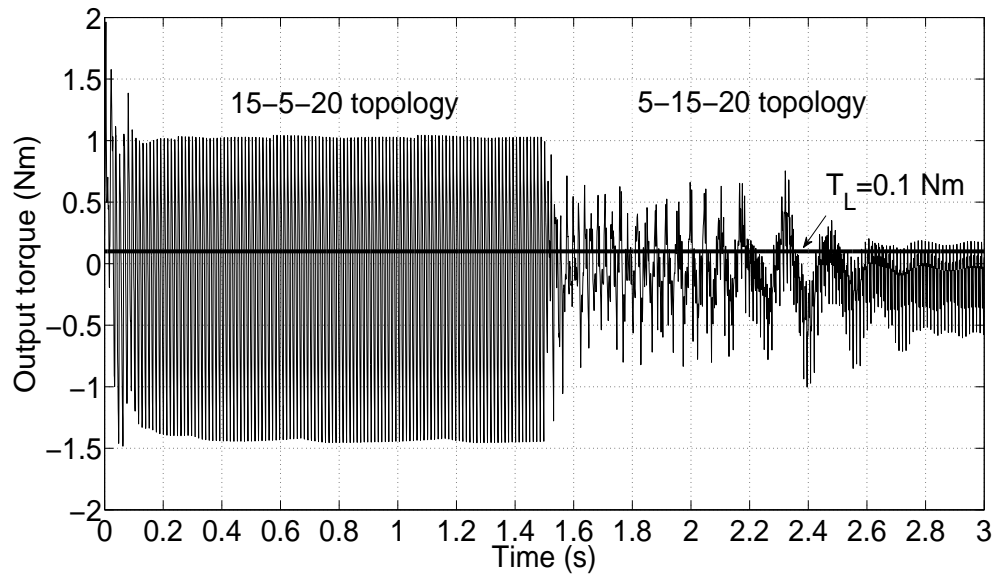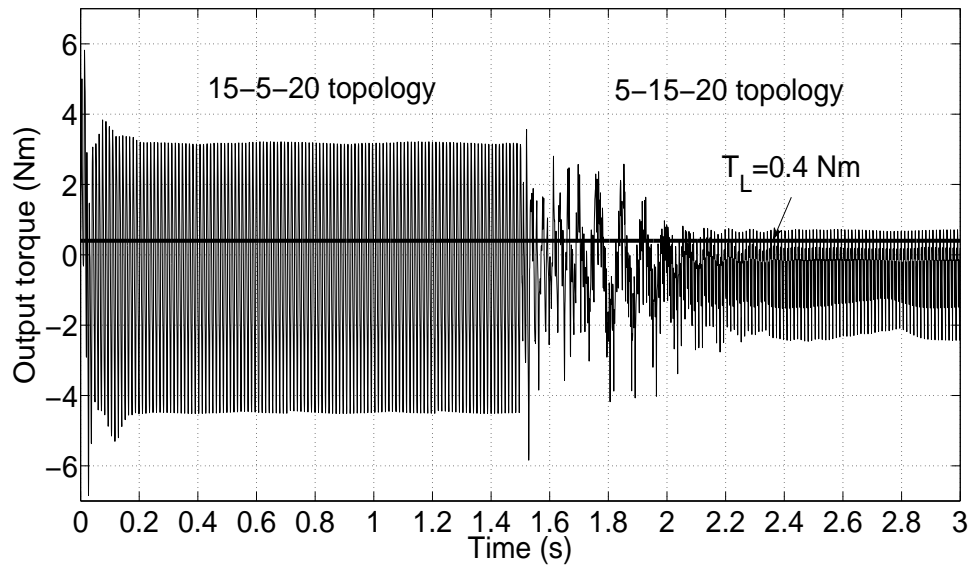Pole changing can be observed by viewing magnetic flux lines. Presented in Fig.6.13 are the flux lines of both topologies when the poles are fully aligned. The excited poles carry most of the flux. There is a small leakage flux between the poles due to the symmetry of the design.

The distribution of the flux density (Fig.6.14) exhibits a more clear picture of pole changing. The flux density is high in the regions of the excited poles.

The variations of the flux density in the air gaps is shown in Fig.6.15. In either topology and near either air gap, the flux density was calculated for one period of the minimum number of poles which is 10 poles; the period is 36°.

In the 5-15-20 topology, the period of the flux density in the air gap between the pole pieces and the inner rotor is 36°, and its average value is 0.28 T. The period of flux density in the air gap between the pole pieces and the stator is 12°, and its average value is 0.17 T.

In the 15-5-20 topology, the two periods change to 12° and 36°, respectively, and the average values change to 0.24T and 0.36 T, respectively. The flux density rises to its peak whenever the poles get aligned.

The flux density rises higher if more poles are excited. In Fig.6.15a, the flux density in the air gap near the inner rotor is higher in the 5-15-20 topology than in the 15-5-20 topology because there are more poles in the inner rotor. The same behavior is observed in the air gap near the stator when there are more stator poles (Fig.6.15b).
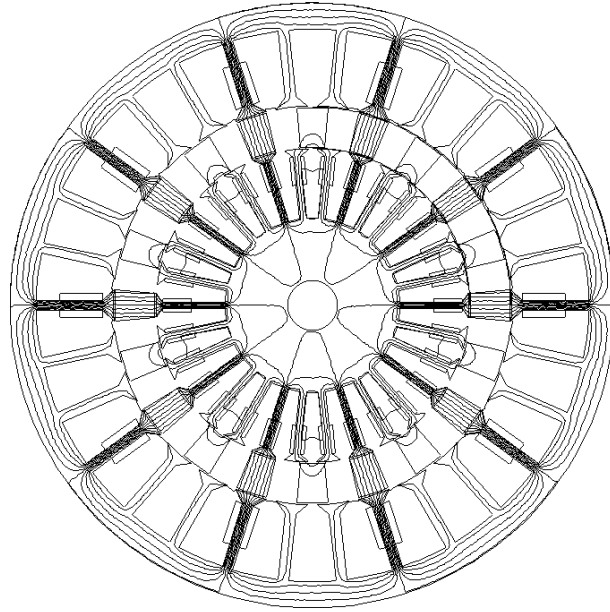
(a)
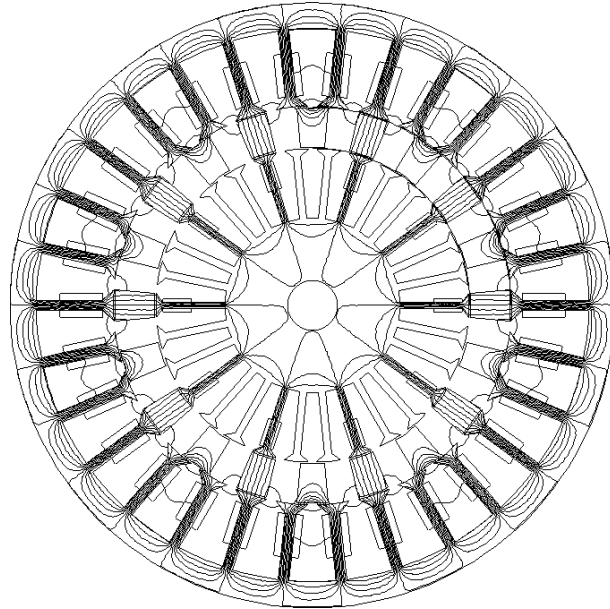
(b)

Figure 6.13: Flux lines (a) 5-15-20 topology (b) 15-5-20 topology

(a)

(b)
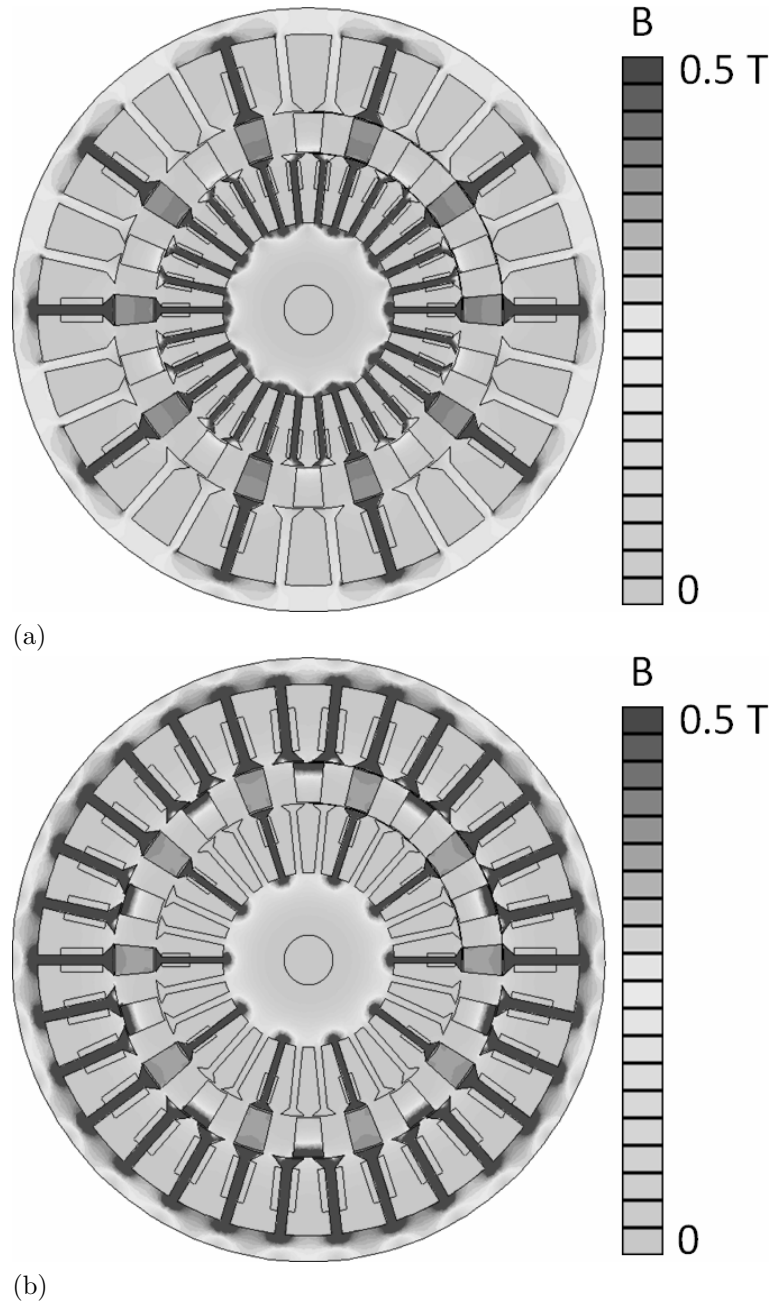
Figure 6.14: Flux density plot (a) 5-15-20 topology (b) 15-5-20 topology
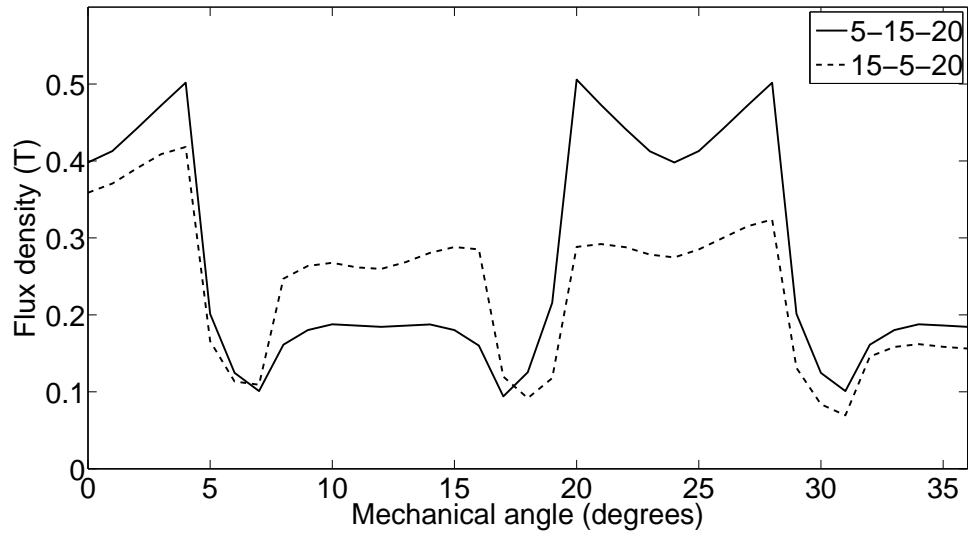
(a)
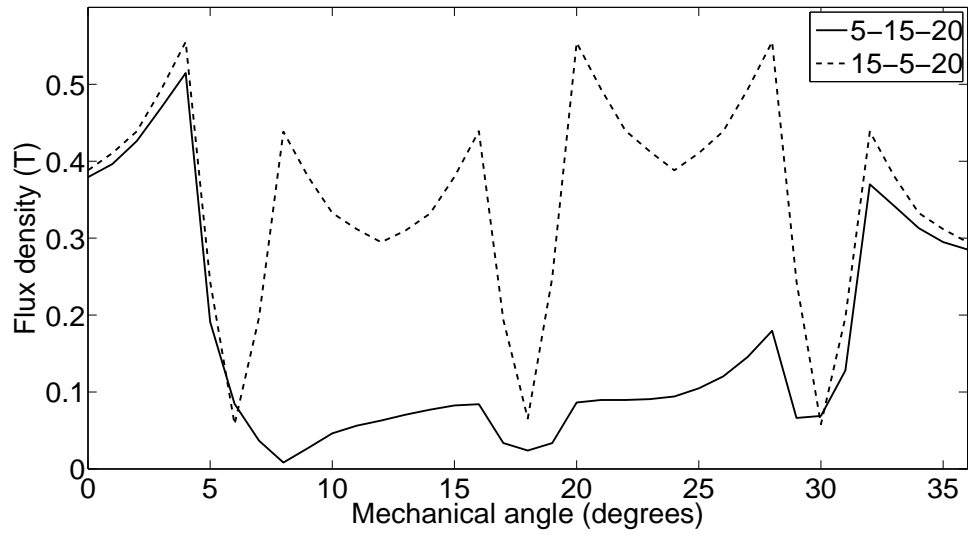
(b)

Figure 6.15: Flux density in air gap between pole pieces and (a) inner rotor (b) stator

Table 6.4: Simulated maximum torques.

Original Design		
Topology	Outer rotor (Nm)	Inner rotor (Nm)
5-15-20 topology	3.1	2.1
15-5-20topology	1.6	0.8
Prototype Design		
Topology	Outer rotor (Nm)	Inner rotor (Nm)
5-15-20 topology	2.8	1.3
15-5-20topology	1.4	0.5

6.2.4.3 Transmitted torques

The maximum transmitted torques were obtained by rotating one of the rotors while the other was stationary. The effective values are listed in Table 6.4.

The prototype design reduces the torques of the outer and inner rotors. The reason is that some of the flux does not reach the inner rotor but it flows through the bridge connecting the pole pieces. Fig.6.16 shows part of the simulated flux of the prototype model. The torque is produced by the flux that crosses the air gap radially. The flux flowing through the bridge does not contribute to torque production and so it is regarded as lost flux.

By switching from one topology to the other, the torques are changed. For instance, the torque of the outer rotor changes from 3.1 Nm in the 5-15-20 topology to 1.6 Nm in the 15-5-20 topology. The gear ratio cannot be calculated from these values because they represent fundamental and other harmonic components.

The torque waveforms are shown in Fig.6.17-6.18. Variable transmission is evident in the waveforms. The outer rotor generates nearly 3.1 N.m in the 5-15-20 topology, and this value reduces to 1.6 Nm in the 15-5-20 topology. The period is 72° in both topologies because the number of pole pieces is not changed.

The period and amplitude of the torque waveform of the inner rotor change during pole changing. In the 5-15-20 topology, the period is 24° and the the torque is 2.1 Nm. The period increases to 72° and the torque drops to 0.8 Nm in the 15-5-20 topology.

The bridge does not alter the shapes of the waveforms. It reduces the am-
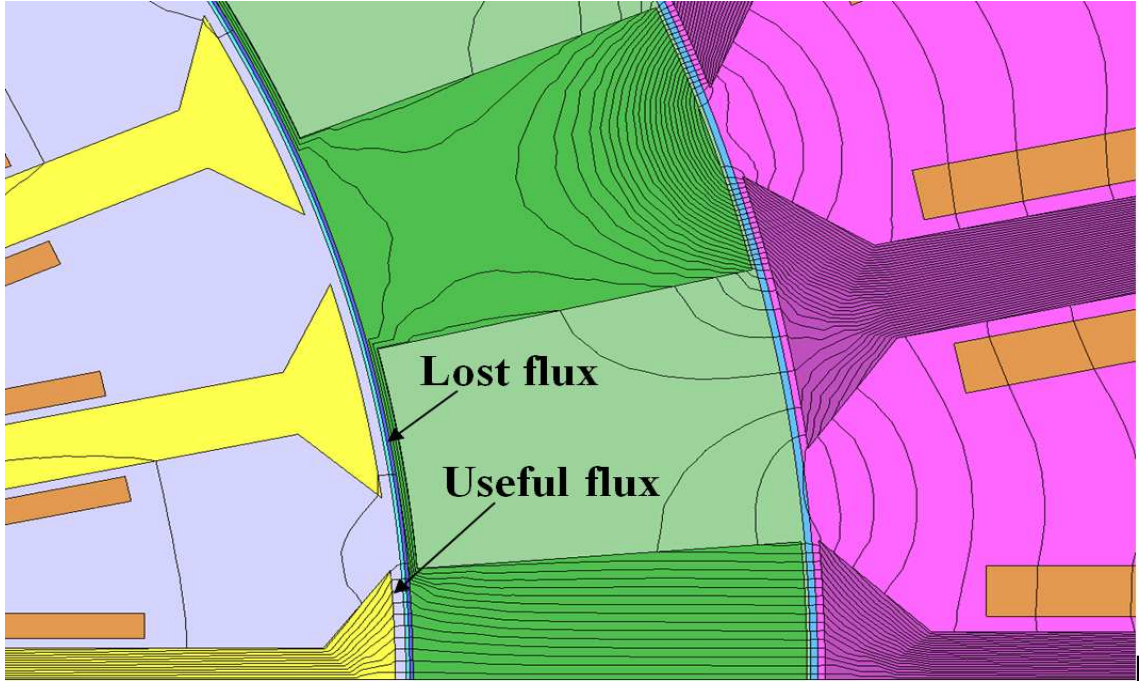
Figure 6.16: Simulated flux lines of prototype model

plitudes of the torques. In the 5-15-20 topology, the outer torque is reduced by roughly 10% to 2.8 Nm and the inner torque is reduced by 38% to 1.3 Nm. In the 15-5-20 topology, the outer torque is reduced by 55% to 1.4 Nm and the inner torque by 76% to 0.5 Nm. The periods of the torque waveforms are not altered.
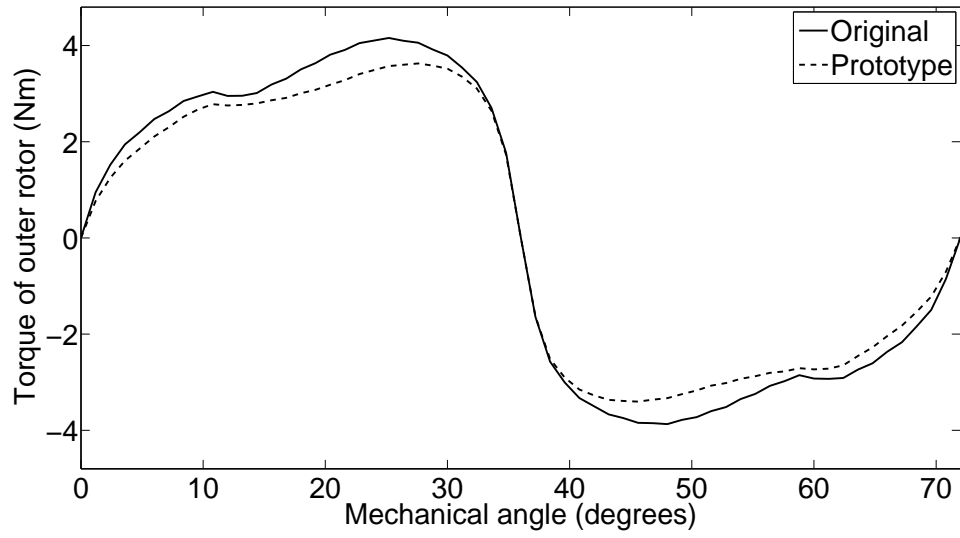
(a)
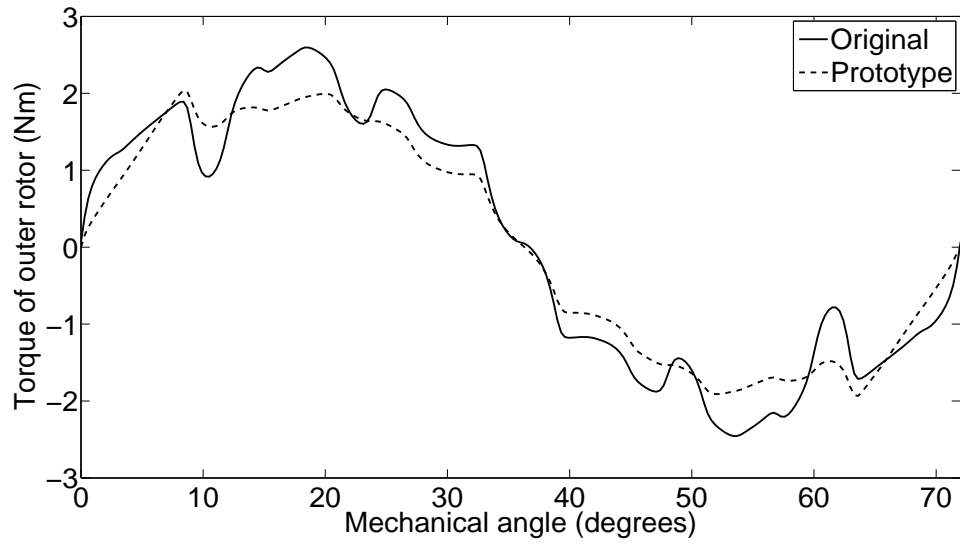
(b)

Figure 6.17: Simulated torques of outer rotor (a) 5-15-20 topology (b) 15-5-20 topology
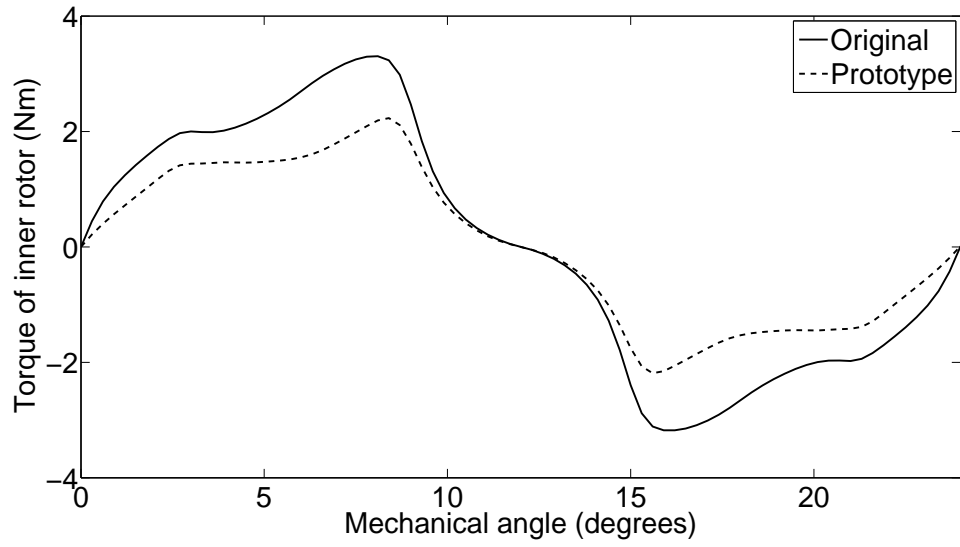
(a)
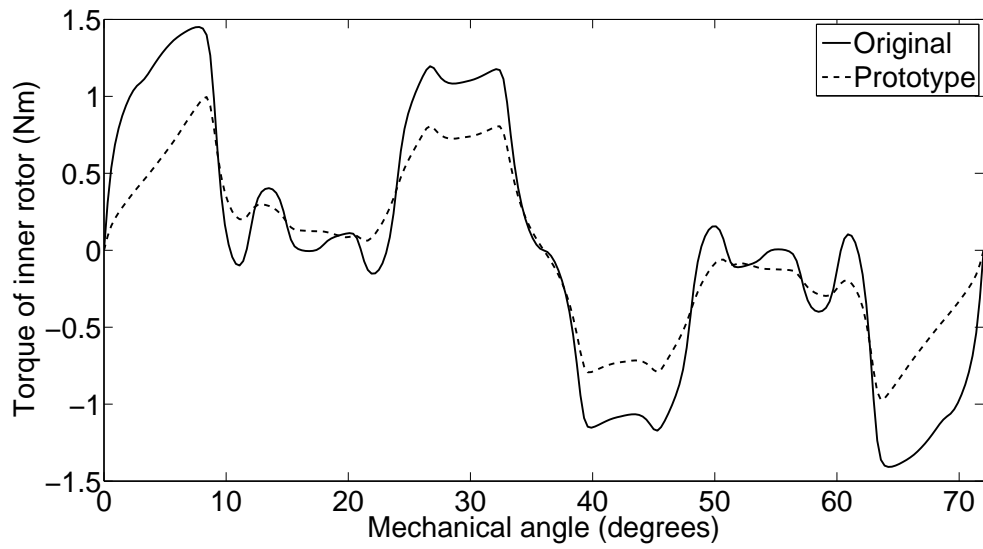
(b)

Figure 6.18: Simulated torques of inner rotor (a) 5-15-20 topology (b) 15-5-20 topology

Table 6.5: Cogging torques.

Topology	Inner rotor (Nm)	Outer rotor (Nm)
5-15-20 topology	0.168	0.164
15-5-20topology	0.17	0.194

6.2.4.4 Cogging torques

Cogging torque is a very crucial quantity that must be taken into account during the design stage, and it should be very small. The cogging torques of both rotors were calculated with the stator winding de-energized. The effective values of these torques are listed in Table 6.5. The inner rotor produces nearly 0.17 Nm while the outer rotor produces 0.16 Nm and 0.19 Nm in both topologies.

The cogging torques complete one cycle during one cycle of one excited pole of the inner rotor. In other words, the period of the cogging torques is a quarter of the period of the electromagnetic torque of the inner rotor which is evident from the waveforms presented in Fig.6.18 and Fig.6.19. When switching from one topology to another, the period of the cogging torques changes according to the ratio of the change of the number of poles in the inner rotor; the amplitude of the cogging torque is very slightly different. In the 15-5-20 topology, the period of the cogging torques is 18°. Increasing the number of poles three folds to 30 in the 5-15-20 topology results in a period of 6° which is a third of that in the 15-5-20 topology.

6.2.4.5 Inductances

The self inductances per pole of the rotor and stator windings are presented in Fig.6.20. The inductances are maximum when the stator and inner rotor are fully aligned, and they are minimum when they are fully unaligned.

In the 15-5-20 topology, the self inductance of the inner rotor, L_{rr}, has a peak of 53 mH per pole and a trough of 32 mH per pole. The self inductance of the stator winding, L_{ss}, has a peak of 537 mH per pole and a trough of 512 mH per pole. L_{ss} is bigger because the stator winding has more turns and more poles than the rotor winding. In the 5-15-20 topology, L_{rr} has a peak of 59 mH and a
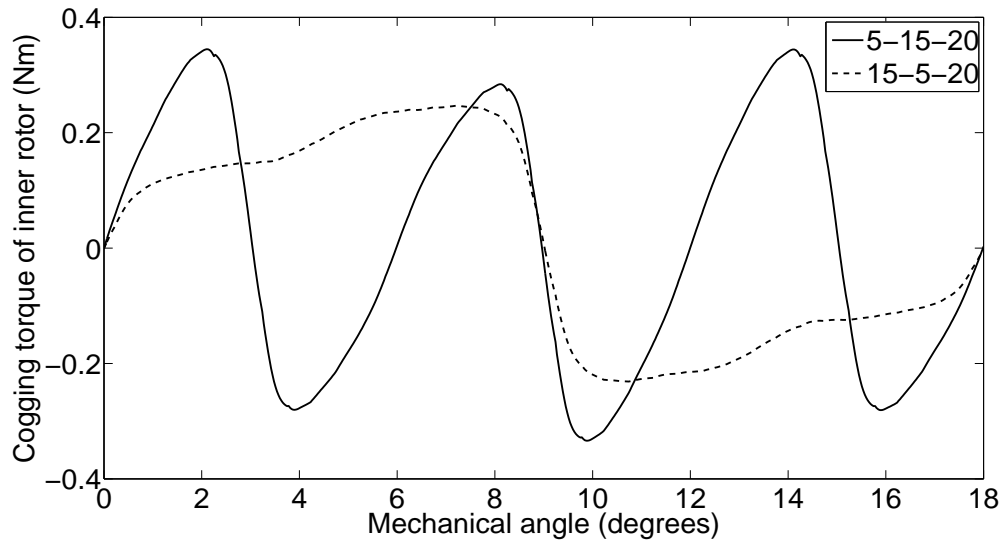
(a)
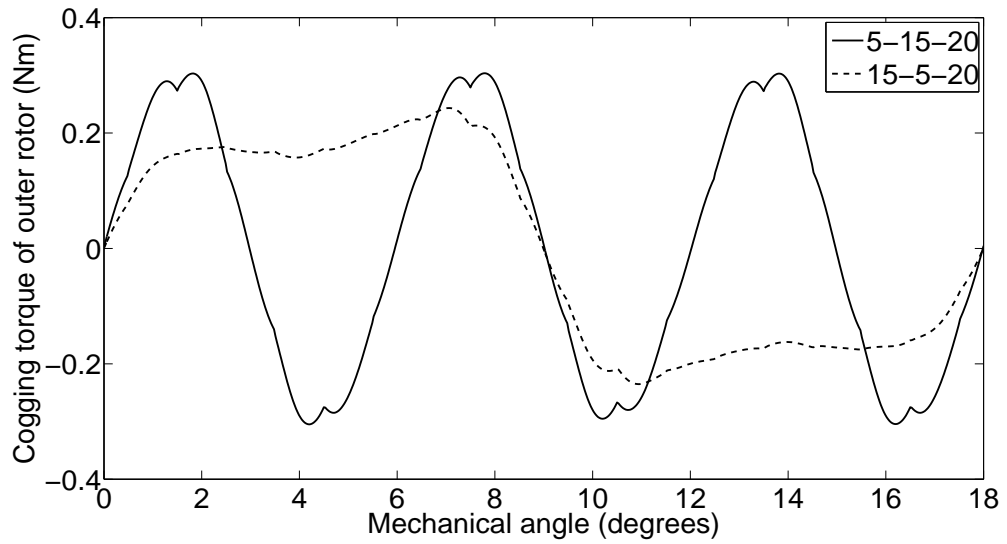
(b)

Figure 6.19: Simulated cogging torques (a) Inner rotor (b) Outer rotor

trough of 56 mH, and L_{ss} has a peak of 499 mH and a trough of 313 mH.

The mutual inductances are much smaller than the self inductances, and they are presented in Fig.6.21. In the 15-5-20 topology, the mutual inductance between the inner rotor and the stator when only the stator winding is excited, L_{rs}, has a peak of around 8 mH. When only the winding of the inner rotor is excited, the mutual inductance, L_{sr}, has a peak of 1 mH. In the 5-15-20 topology, L_{rs} has a peak of 1 mH and L_{sr} has a peak of nearly 9 mH.

6.2.4.6 Efficiency of transmission

The function of the electromagnetic gear is to step up or step down torque. The efficiency of power transmission was determined from the dynamic simulations for some speeds and loads. The efficiency is calculated from this equation:

$$\eta = \frac{P_{out}}{P_{in}} \times 100 = \frac{T_o\omega_o}{T_{in}\omega_i} \times 100 \qquad (6.4)$$

There is always an optimum operating point of high efficiency at which the gear generates enough torque to overcome load torque at a certain speed. A range of 0-360rpm input speed was applied to the inner rotor for two values of load torque, and the corresponding speed and torque of the outer rotor were calculated. The efficiency is plotted in Fig.6.22 where the inner rotor is the input and the outer rotor is the output.

For a load of 1 Nm, the efficiency is approaching 90% over the whole speed range. Below 200 rpm of input speed and 0.1 Nm of load, the efficiency is also high but it drops to 70% beyond 250 rpm of input speed. Consequently, the electromagnetic gear can be operated to transmit power efficiently if the speed/load range is known.
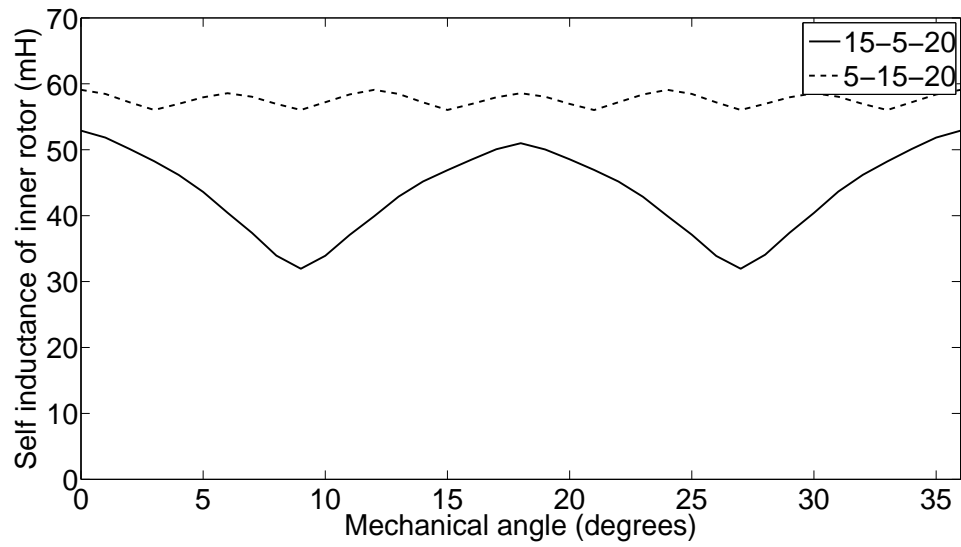
(a)
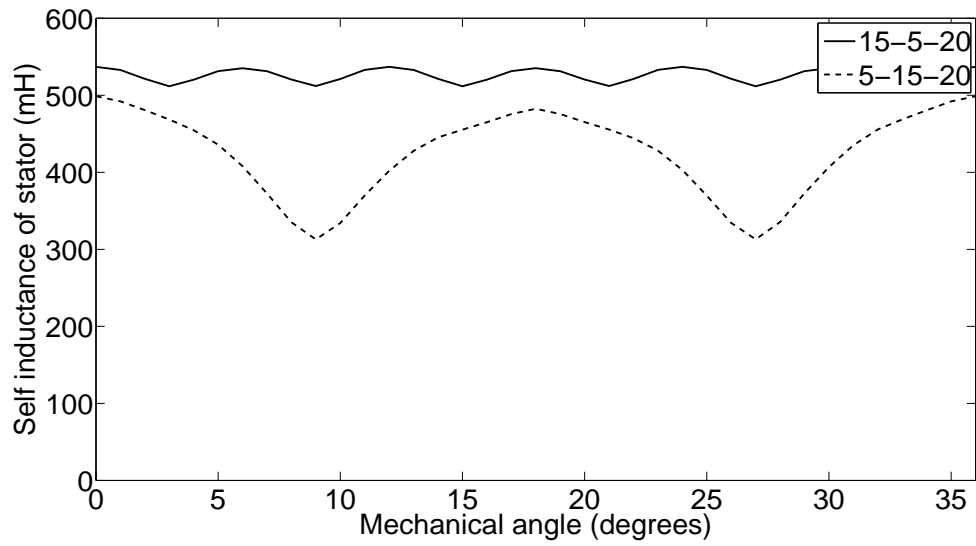
(b)

Figure 6.20: Self inductance of (a) inner rotor pole (b) stator pole
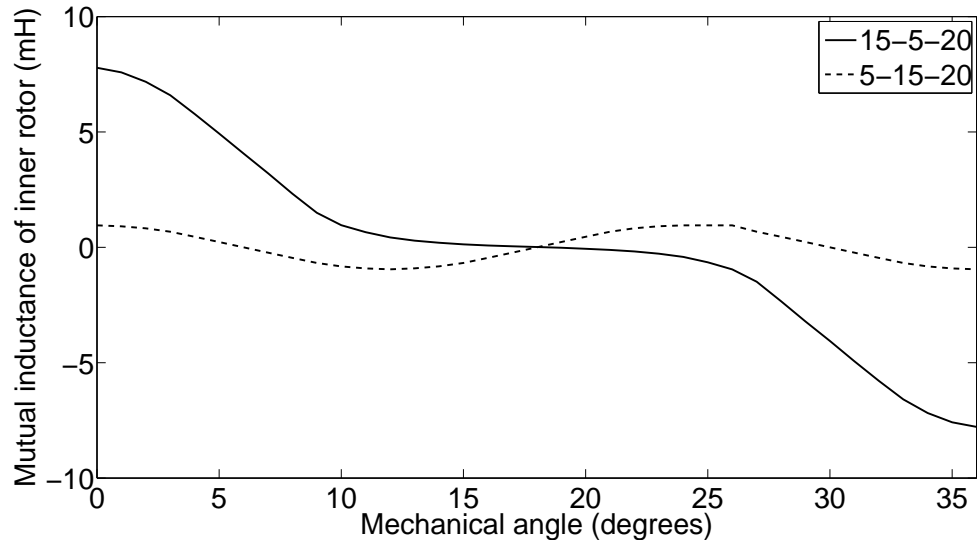
(a)
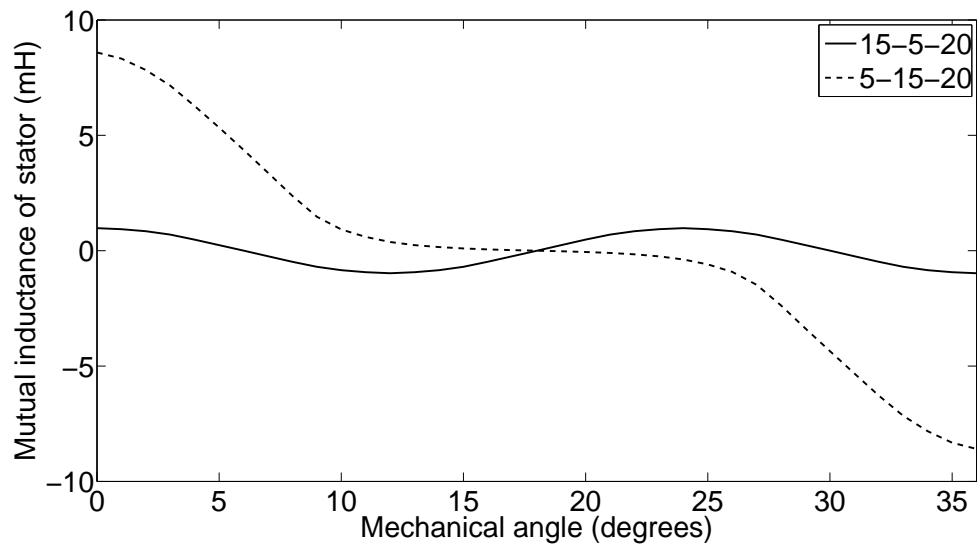
(b)

Figure 6.21: Mutual inductance between inner rotor and stator when (a) stator winding excited (b) inner rotor winding excited
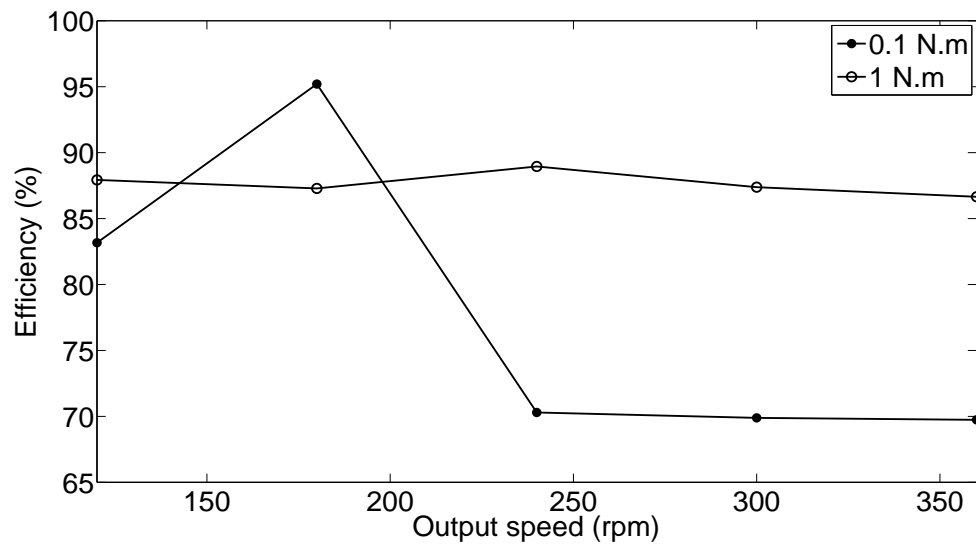
Figure 6.22: Efficiency variation with output speed

6.2.5 Experimental results

The same conditions applied during the simulations were applied in the experiments using the 15-5-20 and 5-15-20 topologies to verify the proposed concept of electromagnetic variable transmission.

The experimental setup is shown in Fig.6.23. Because the electric current is supplied to the inner rotor via slip rings, the torque of the outer rotor could not be measured directly and belts and pulleys were necessary to transmit the torque to the torque transducer II for measurement.

The torque measurement system is presented in Fig.6.24. A maximum of 50 revolutions per second can be set from dedicated software on a personal computer (PC) that is connected to a servo controller. The servo controller supplies the signal received from the PC to two ac servomotors via drivers. Each servomotor is coupled with a mechanical gearbox and a torque transducer. The torque transducer sends the measured torque as a signal to the PC through a data acquisition system. One gearbox has a gear ratio of 1:80 and the other 1:9. Hence, the maximum speed that can be applied to the input shaft is 333.3 rpm.

#### 6.2.5.1 Variable gear ratio

The inner rotor was driven at different speeds, and the corresponding speeds of the outer rotor were measured with an optical tachometer. The measured gear ratios are shown in Fig.6.25. The speed ratio is 4 in the 15-5-20 topology, and it is 1.33 in the 5-15-20 topology as predicted by Eq.(3.1).

6.2.5.2 Transmitted torques

To measure the torques, one rotor was turned at 1 rpm by the servomotor and its torque was measured simultaneously while the other rotor was locked. The same condition was applied in the simulations. The measured maximum torques are listed in Table 6.6 and their waveforms are presented in Fig.6.26-6.27.

The outer rotor is rated at 2.4 Nm and the inner rotor at 1.0 Nm in the 5-15-20 topology. These values drop to 1.2 Nm and 0.4 N.m, respectively, in the 15-5-20 topology.
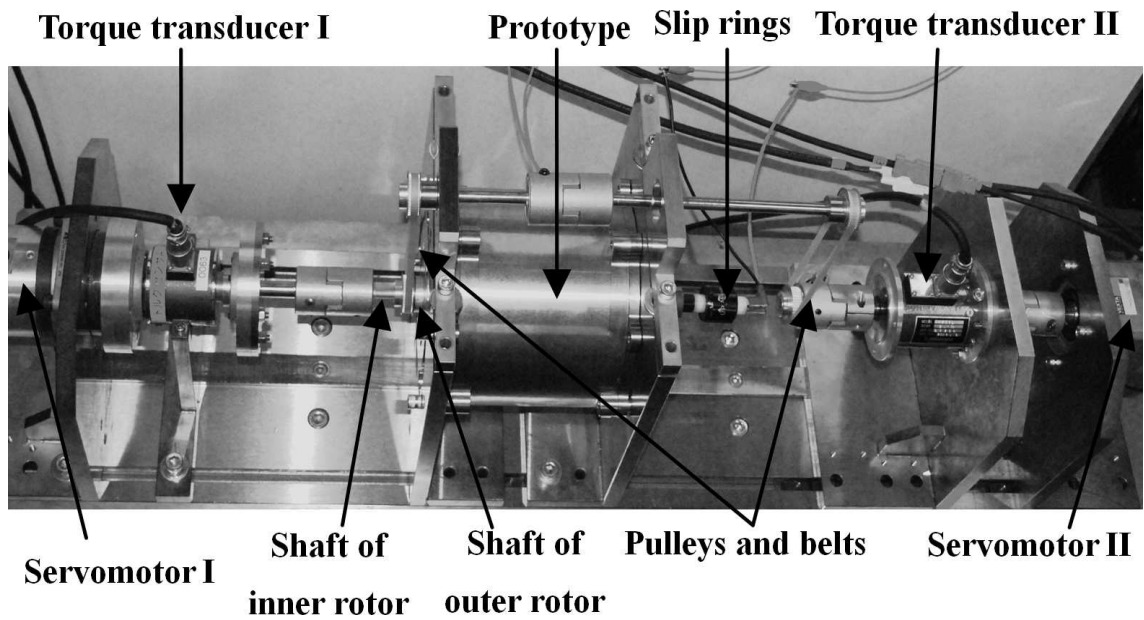
Figure 6.23: Experimental setup of electromagnetic gear
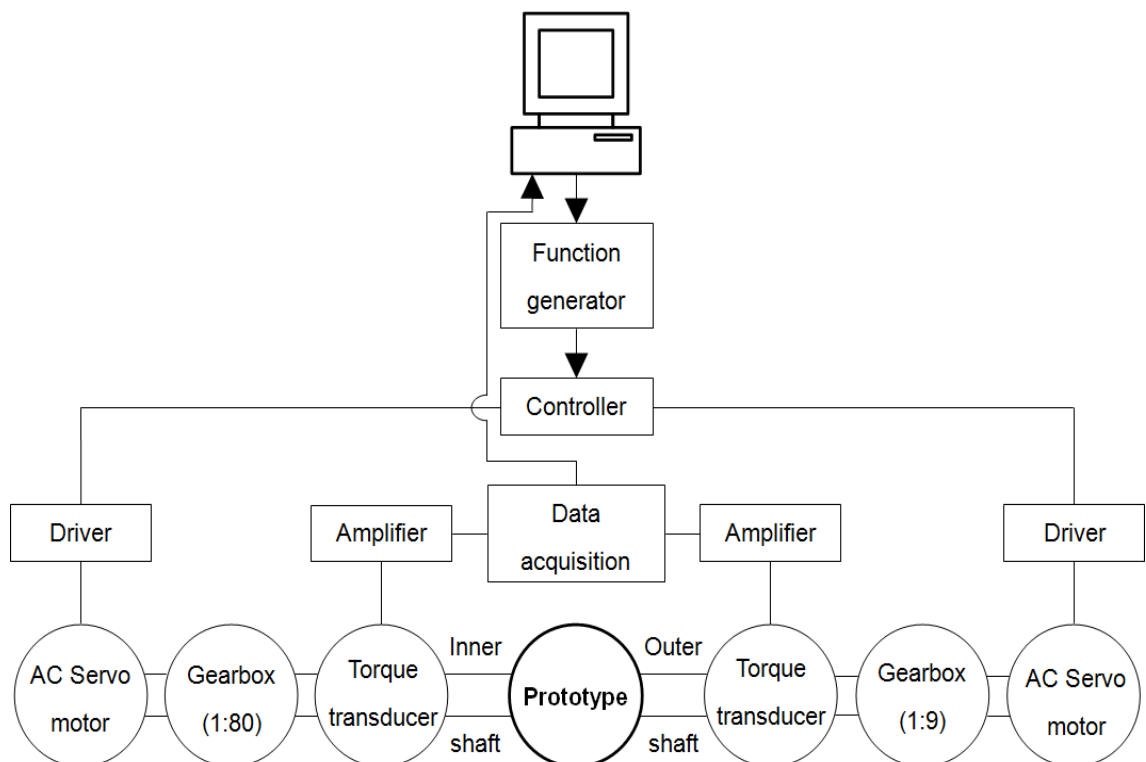
Figure 6.24: Torque measurement system
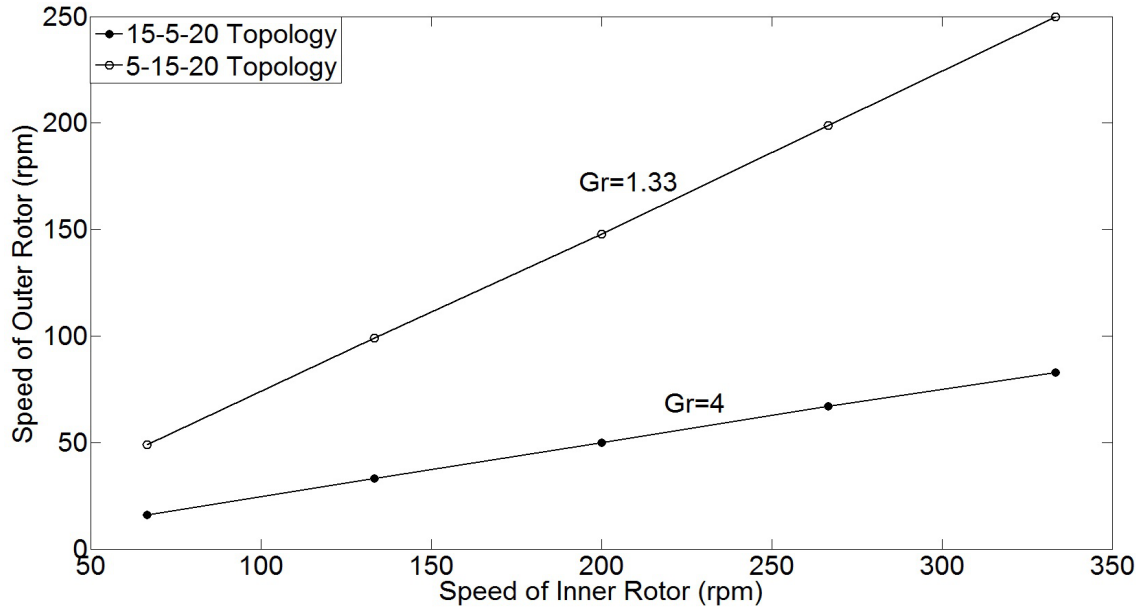
Figure 6.25: Measured gear ratio

Table 6.6: Measured maximum torques.

Topology	Outer rotor (Nm)	Inner rotor (Nm)
5-15-20 topology	2.4	1.0
15-5-20topology	1.2	0.4

The measured values are between 86% to 77% of the simulated values. The discrepancy can be mainly due to mechanical issues. The actual air gap is affected by the balance of the inner rotor and it is different from the simulated value. Mechanical friction due to the bearings and slip rings play a role in decreasing the measured torque.

In addition, the winding resistance changes with temperature and so does the current. Hence, the actual torques are slightly reduced.
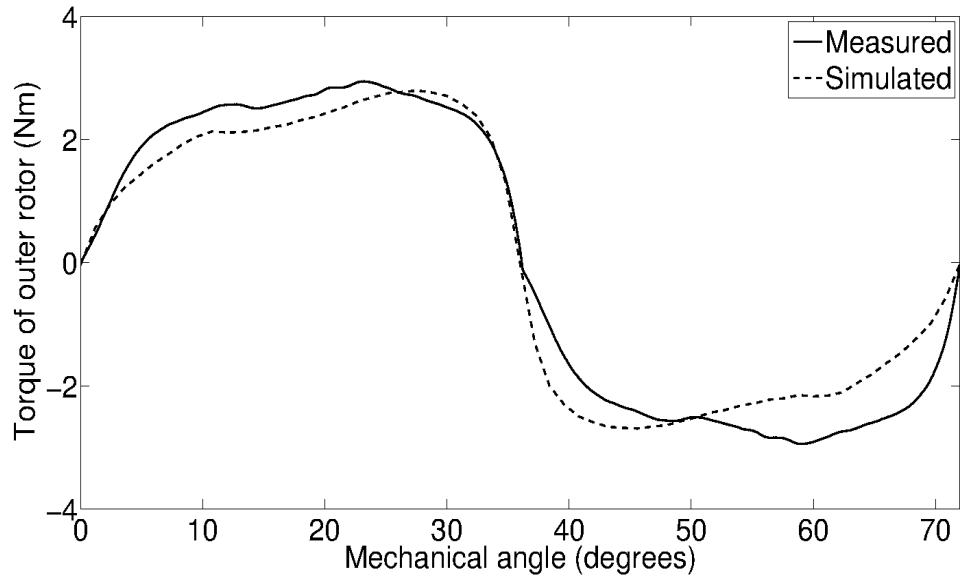
(a)
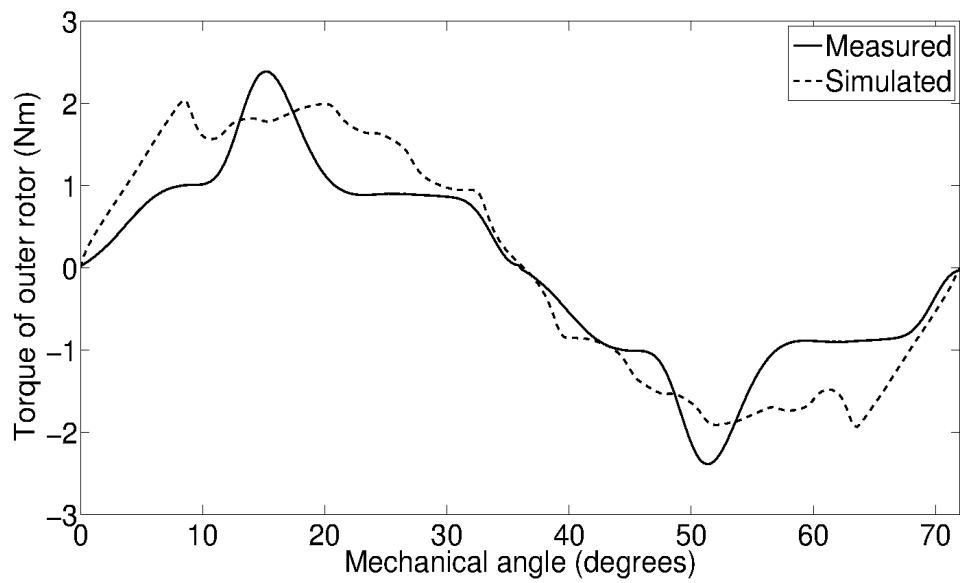
(b)

Figure 6.26: Measured maximum torques of outer rotor (a) 5-15-20 topology (b) 15-5-20 topology
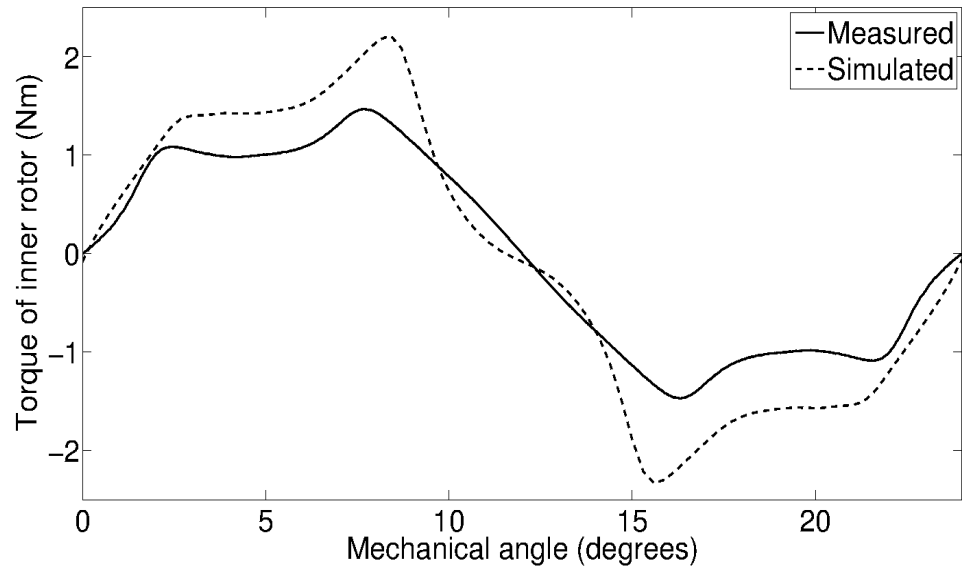
(a)
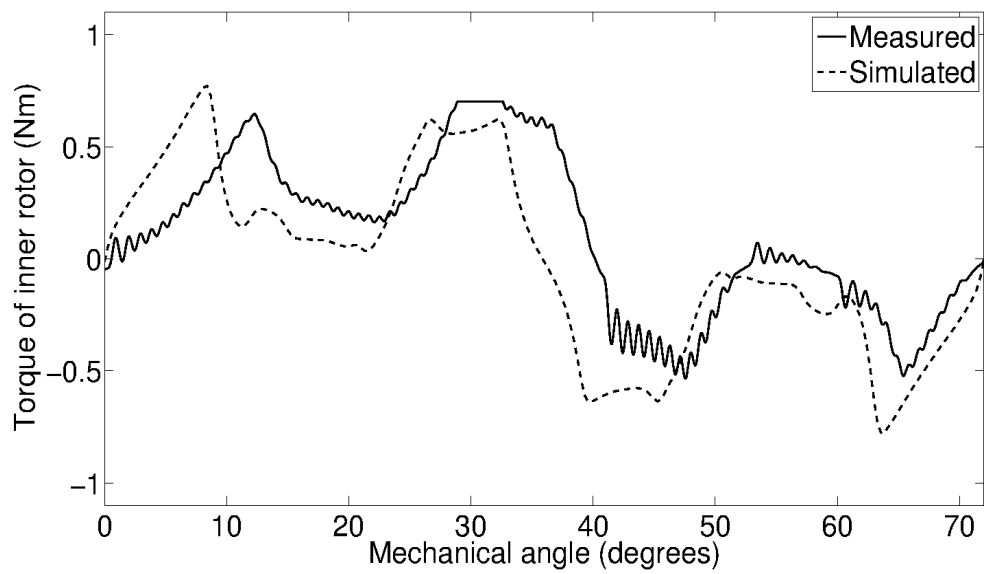
(b)

Figure 6.27: Measured maximum torques of inner rotor (a) 5-15-20 topology (b) 15-5-20 topology
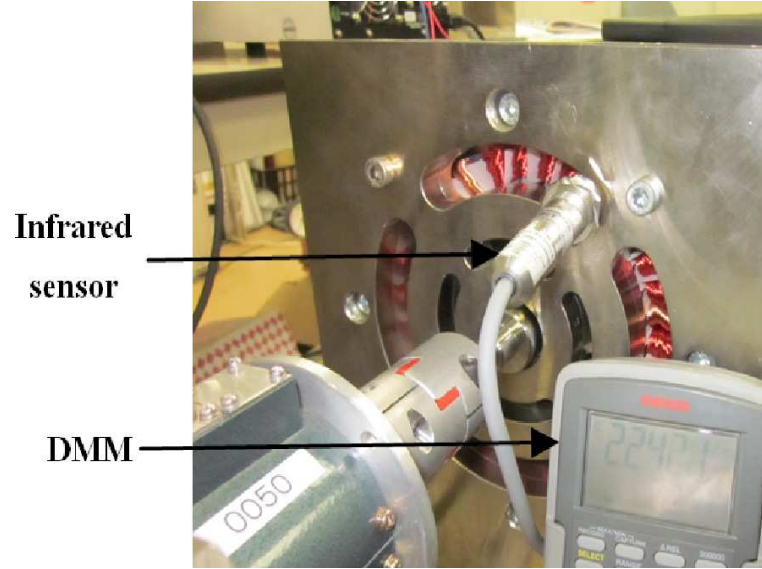
Figure 6.28: Setup of temperature measurement

6.2.5.3 Temperature rise and heat losses

The windings produce heat losses that cause a temperature rise of the prototype. Because the stator is stationary and because it has bigger number of coil turns per slot than the inner rotor, the heat loss in the stator is higher. The temperature of the stator was measured with an infrared sensor and a digital multimeter (DMM). The setup is shown in Fig.6.28. The test was carried out for the 15-5-20 topology which is the most lossy case because all the stator poles are excited.

The graph in Fig.6.29 is the temperature rise of the stator winding when both windings draw rated currents. The stator winding reaches around 75°C after 30 minutes which is below the rated winding temperature of 150°C.

The total heat losses depend on the selected topology. The heat loss of each winding is plotted in Fig.6.30 as a function of current density where the current density is varied from 0 to the rated value of around 8 MA/m^2. A maximum of 5W/slot is dissipated in the stator and 1.5W/slot in the inner rotor.
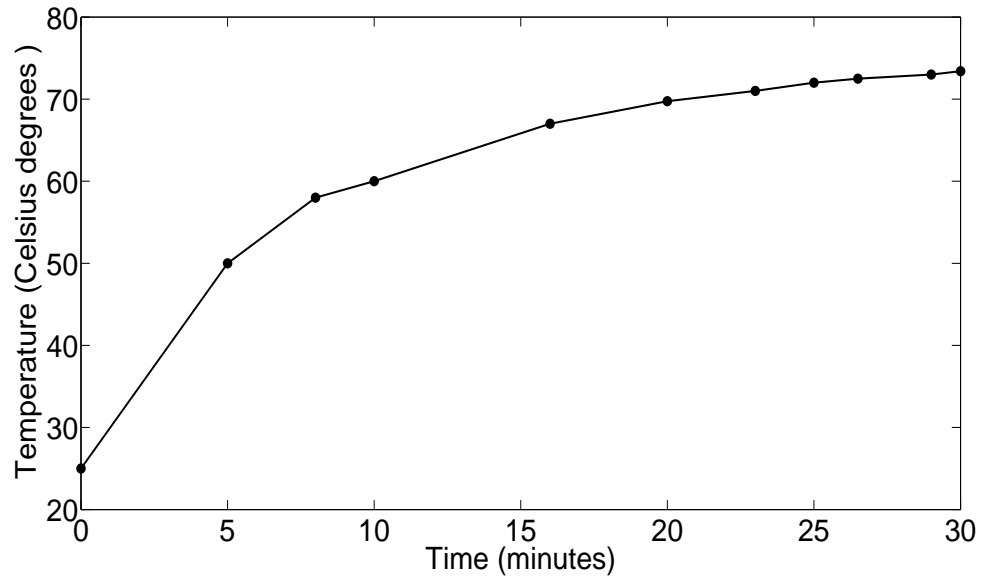
Figure 6.29: Temperature rise of stator winding at rated current
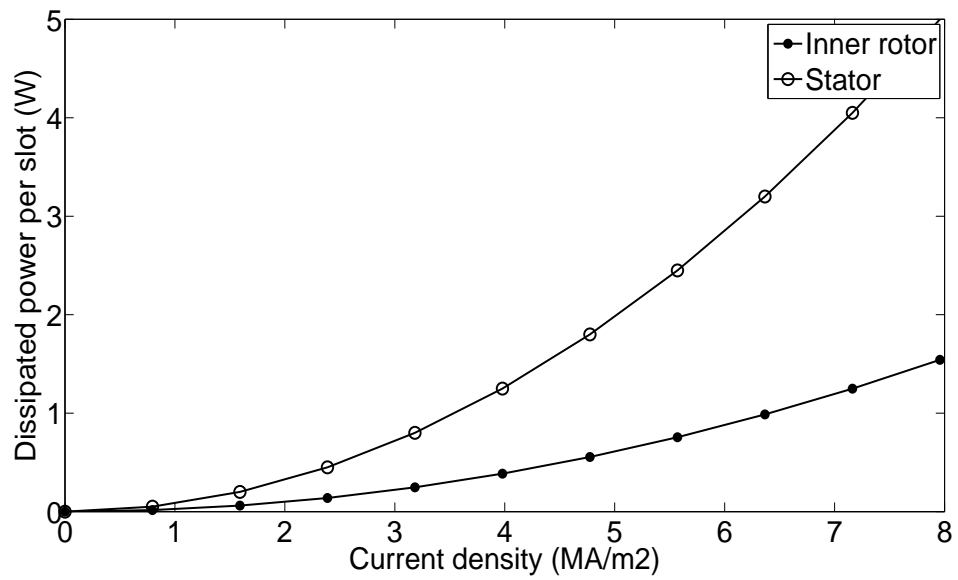
Figure 6.30: Heat losses per slot
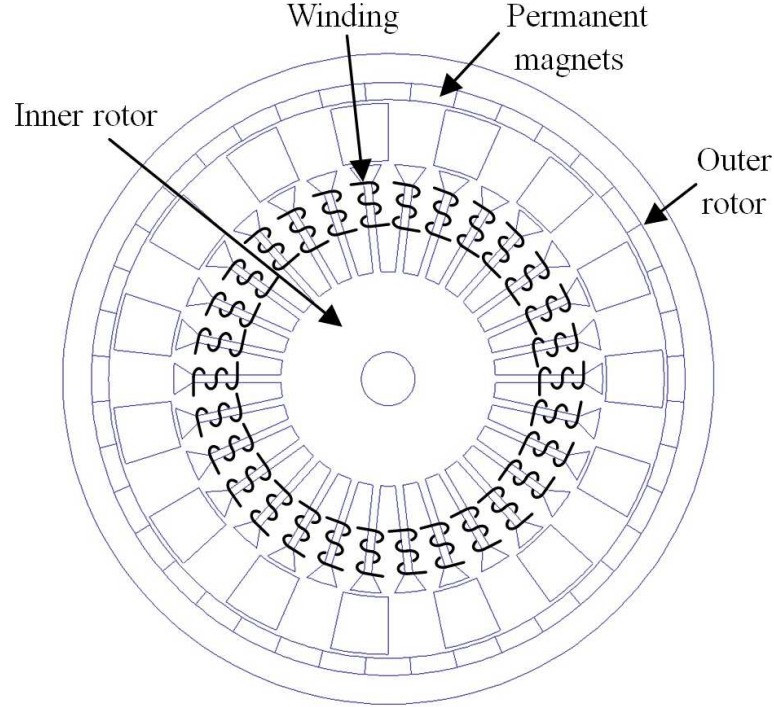
Figure 6.31: Schematic diagram of hybrid magnetic gear

6.3 Method 2: Hybrid magnetic gear

The hybrid magnetic gear has not been realized. The following discussions cover design aspects only. A mechanism for practical realization is proposed.

6.3.1 Construction

Using the same size of the electromagnetic gear, the hybrid magnetic gear was designed based on the guidelines set in Chapter 4. The schematic diagram is shown in Fig.6.31, and the design parameters are listed in Table 6.7. The gear consists of three basic parts: a stator, outer rotor and inner rotor. The outer rotor is made up of permanent magnets, the stator consists of ferromagnetic pole pieces, and the inner rotor contains a dc concentrated winding wound around salient poles. The number of pole pairs of the outer rotor is P_o=20, the number of pole pieces is P_s=15, and the the number of pole pairs of the inner rotor is P_i=15.

Table 6.7: Design parameters of hybrid magnetic gear.

Diameter of outer rotor	170 mm
Diameter of inner rotor	112 mm
Air-gap length	1 mm
Stack length	100 mm
Number of poles of outer rotor	40
Number of pole pieces	15
Number of poles of inner rotor	30
Remanence of permanent magnets	1.28
Pole arc-to-pitch ratio of outer rotor	100%
Pole arc-to-pitch ratio of pole pieces	50%
Pole arc-to-pitch ratio of inner rotor	70%
Number of turns per slot of winding	500
Rated winding current per slot	0.5A

Table 6.8: Topologies of hybrid magnetic gear.

P_o	20	20
P_i	5	15
P_s	15	5
G_r	4.00	1.33

6.3.2 Principle of operation

The gear was designed to operate at two gear ratios of 4:1 and 1.33:1 as presented in Table 6.33. The gear ratio is calculated from Eq.(3.1). The number of poles of the outer rotor is fixed. The gear ratio is changed by changing the number of pole pieces and the number of poles of the inner rotor. The method of changing the number of poles of the inner rotor is the same as that used for the electromagnetic gear.

The number of pole pieces is changed by pulling some of the pole pieces out of the gearbox. This can be achieved by mechanical or electromechanical methods. An electromechanical solenoid actuator is proposed, and it is illustrated in Fig.6.32. Each of these pole pieces is attached to a plunger that is housed inside
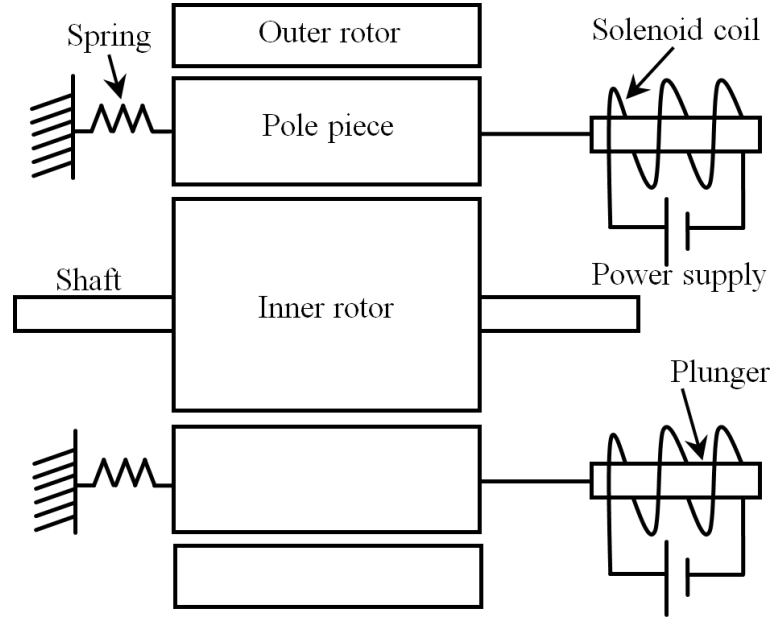
Figure 6.32: Mechanism of pulling pole pieces

a solenoid coil.

To switch from the 20-5-15 topology to the 20-15-5 topology, ten symmetrically-positioned pole pieces are pulled out when the solenoid coils are energized, and twenty symmetrically-positioned poles on the inner rotor are de-energized. The topologies are depicted in Fig.6.33.

The pull force generated by the solenoid can be calculated using several FEM models of the hybrid gear. The force is maximum when the pole pieces are entirely inside the gearbox, and it decreases gradually as the pole pieces are pulled out [HHN11]. The force is initially 60 N, and thus the solenoid should be designed to be capable to handle this value. Practically, the pole piece should be of a circular cross section so that the solenoid stroke is fast and smooth.
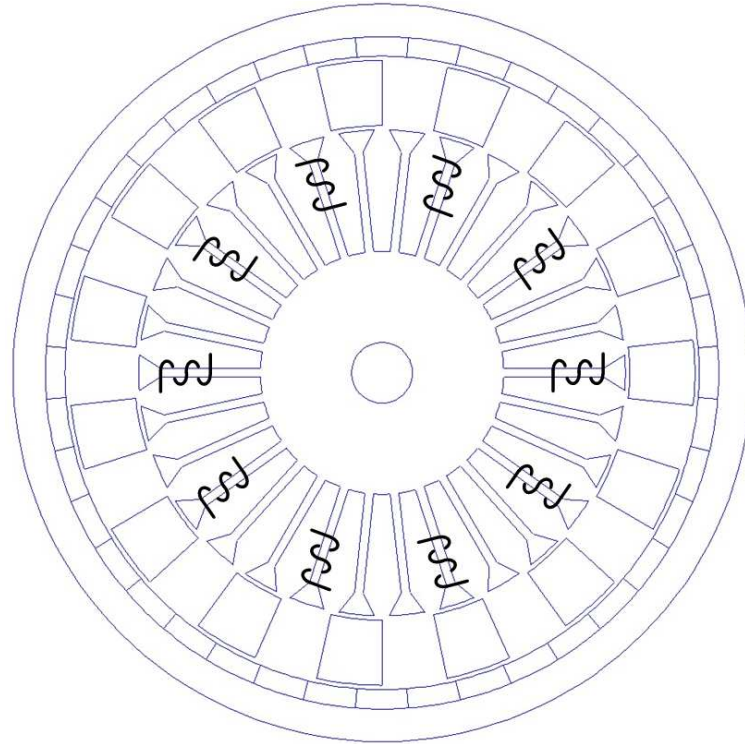
(a)
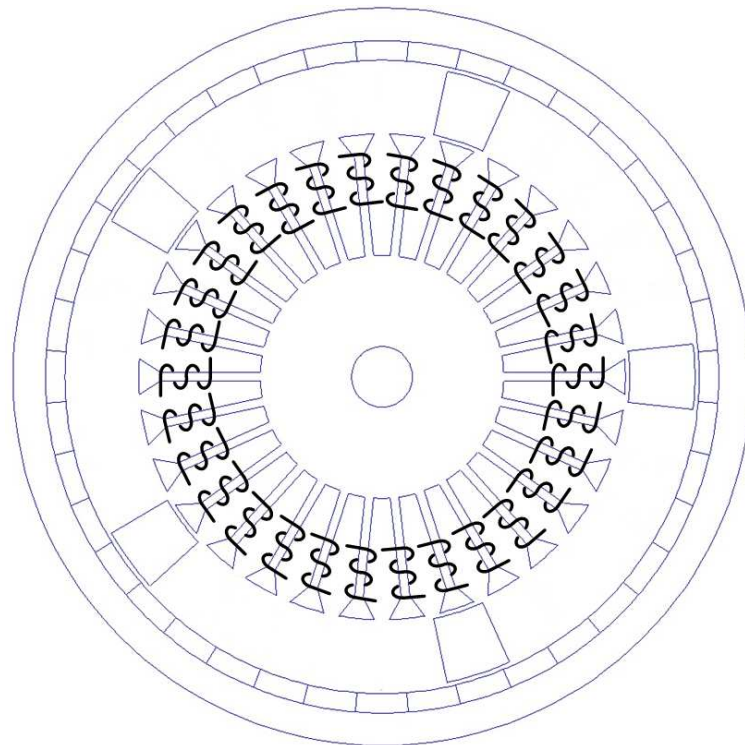
(b)

Figure 6.33: Topologies of hybrid magnetic gear (a) 20-5-15 topology (b) 20-15-5 topology

Table 6.9: Maximum torques of hybrid magnetic gear

Topology	Outer rotor (Nm)	Inner rotor (Nm)
20-5-15	4.00	0.1
20-15-5	11.96	0.56

6.3.3 Transmitted torques

The initial validation of the above method can be judged from the waveforms of the maximum transmitted torques using static analysis. The effective values are listed in Table 6.9, and the waveforms are presented in Fig.6.34.

The waveforms show variable torque transmission by pole changing, and they change in amplitude and period. The torque of the outer rotor changes from 4 Nm in the 20-5-15 topology to 12 Nm in the 20-15-5 topology. The torque of the inner rotor changes from 0.1 N.m in the 20-5-15 topology to 0.56 Nm in the 20-15-5 topology.

The torque density of the hybrid gear is 5.3 kNm/m^3 and that of the electromagnetic gear is 1.4 kNm/m^3. In addition, the hybrid gear produces less torque pulsations than does the electromagnetic gear but the electromagnetic gear is simpler to realize.
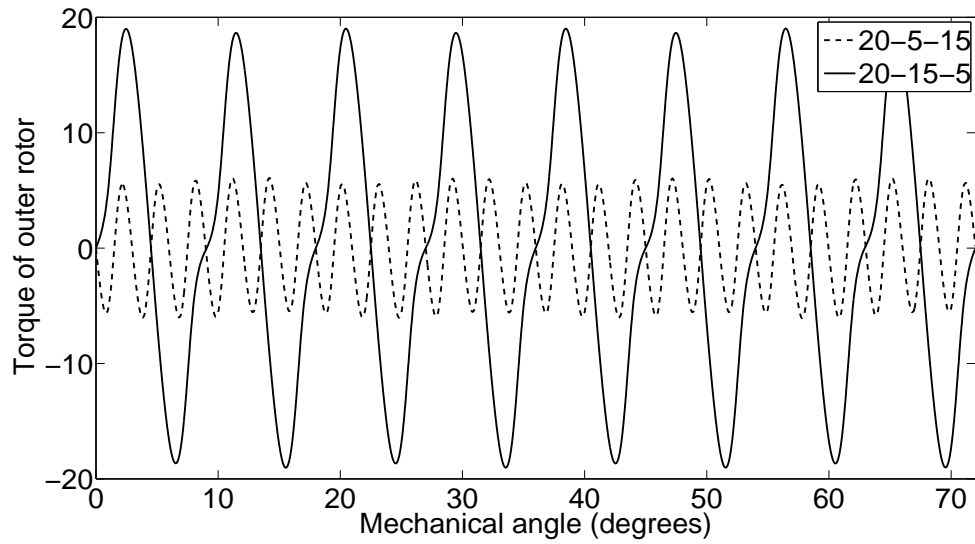
(a)
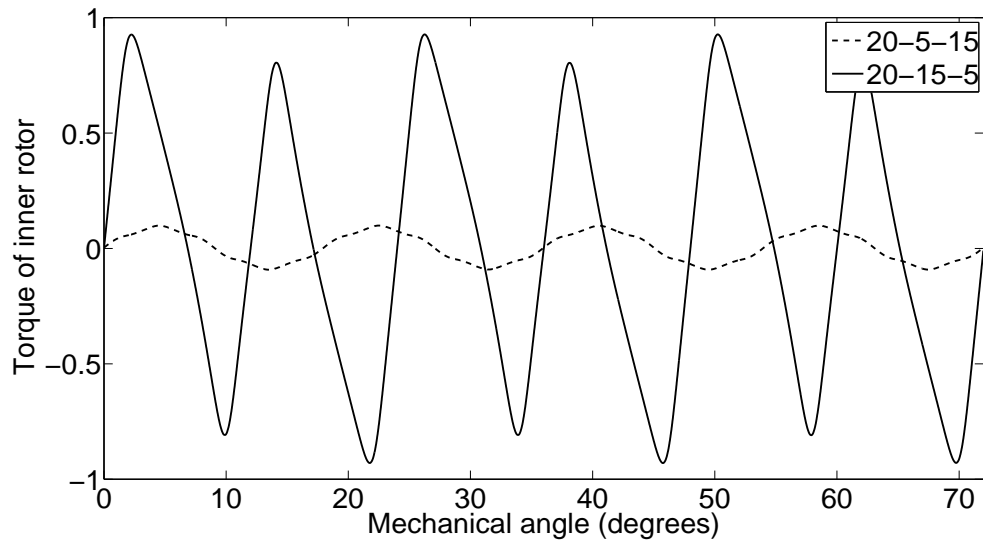
(b)

Figure 6.34: Maximum transmitted torques (a) Outer rotor (b) Inner rotor

Chapter 7

Magnetic Variable Transmission by Multi-element Design

7.1 Introduction

In the light of the concept of pole changing described in Chapter 6, another method of magnetic variable transmission is proposed. Pole changing is executed axially by incorporating several hybrid magnetic gears of different ratios in a single gearbox (Fig.7.1).

Two gears were used to illustrate the method but several gears could be added. Each gear is referred to as an element. The method has not been realized practically, and the aim of this chapter is to describe the method and propose new methods for reducing cogging torque. Compared to the method patented by Atallah et al, the multi-element method is much less costly because it does not employ an electronic drive or a control motor.

Due to the absence of permanent magnets, adopting elements of Neuland's design has the advantages of lower cost and lower cogging torques but it has the disadvantage of extremely low torque density. Adopting hybrid gears would create significant cogging torques as a result of the interaction of the permanent magnets with the stator slots and the spacing between the pole pieces. The proposed method is different from that investigated by Hesmondalgh et al because their gearbox has a constant gear ratio.
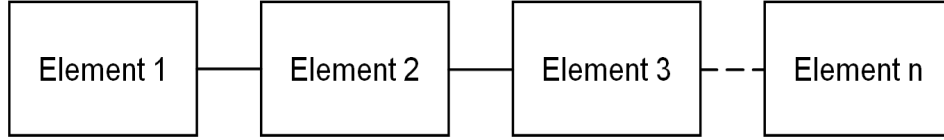
Figure 7.1: Block diagram of multi-element magnetic gear

7.2 Construction and operating principle

A 3D partial model of the proposed gear is presented in Fig.7.2, and the design parameters are included in Table 7.1. There are 20 pole pieces in each element, and each set of pole pieces act as an outer rotor. Element 1 has 15 pole pairs on the inner rotor and 5 pole pairs on the stator. Element 2 has 5 pole pairs on the inner rotor and 15 pole pairs on the stator.

The elements are separated by 20mm in order to allow some clearance between the end windings and to reduce magnetic interference. The axial length of each element is 40 mm and the axial length of the whole gearbox is 100 mm. The inner rotors are coupled by the input shaft and the outer rotors are coupled by the output shaft.

Only one winding is excited at a time. If the winding of Element 1 is excited, a gear ratio of 4.00 is obtained. This value can be changed to 1.33 if the winding of Element 2 is excited after switching off that of Element 1.

Because Element 2 has many slots, it is predicted that its cogging torques are higher than those of Element 1. For best performance, the gearbox should be designed such that the ratio of the cogging torque to the corresponding transmitted torque, K_R, is small. The electromagnetic torque developed by any rotor should be much higher than the sum of its cogging torque and that of the rotor of the adjacent elements.
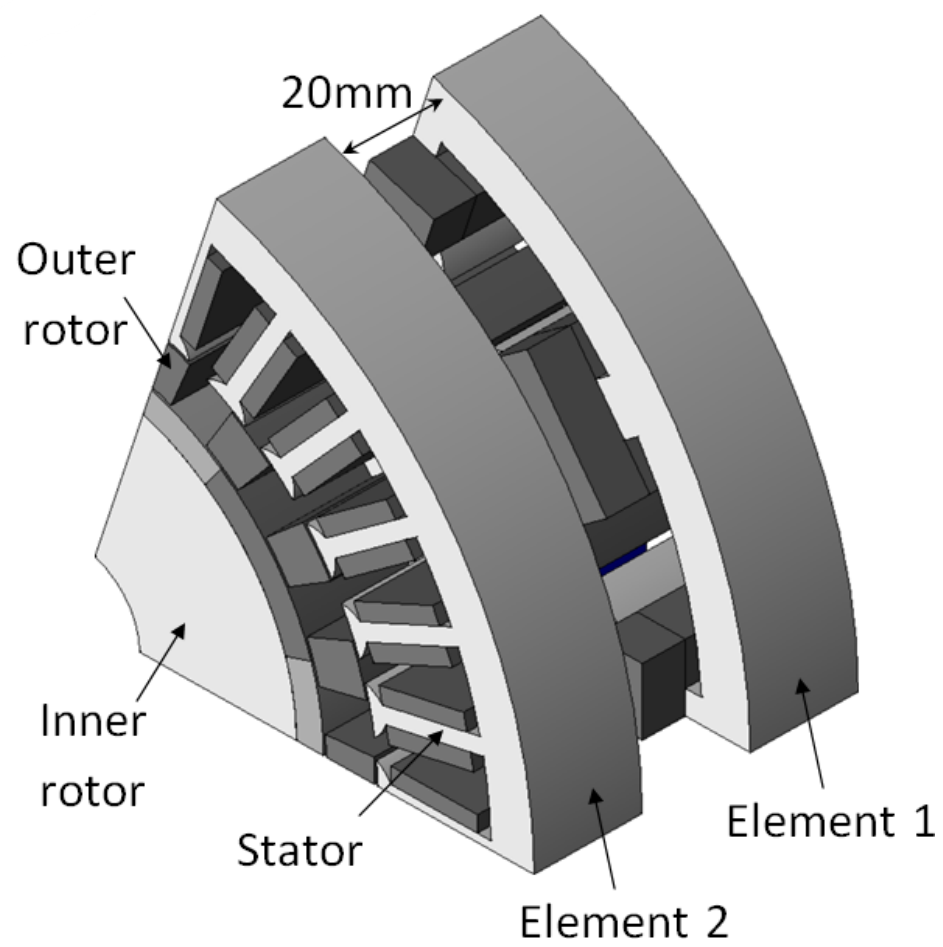
Figure 7.2: Partial model of multi-element magnetic gear

Table 7.1: Design parameters of multi-element magnetic gear.

Diameter of stator	170 mm
Diameter of inner rotor	46 mm
Air-gap length	0.5 mm
Stack length	100 mm
Distance between elements	20mm
Element 1	
Number of poles of stator	30
Number of pole pieces	20
Number of poles of inner rotor	10
Remanence of permanent magnets	1.28
Number of turns per slot of winding	1200
Winding resistance per slot	60 ohms
Rated winding current per slot	0.5A
Element 2	
Number of poles of stator	10
Number of pole pieces	20
Number of poles of inner rotor	30
Remanence of permanent magnets	1.28
Number of turns per slot of winding	1800
Winding resistance per slot	120 ohms
Rated winding current per slot	0.5A

Element 1			
Torque	Transmitted (Nm)	Cogging (Nm)	K_R (%)
Inner rotor	16.9	3.9	23
Outer rotor	28	4.7	17
Element 2			
Torque	Transmitted (Nm)	Cogging (Nm)	K_R (%)
Inner rotor	8.6	3.85	45
Outer rotor	14.3	3.25	23

Table 7.2: Effective torques of multi-element gear

7.3 Simulation results

Cogging and transmitted torques are the main quantities to be considered during the initial design stage. 2D simulations of each element were conducted. The effective torques are listed in Table 7.2. The transmitted and cogging torques of each rotor of each element are plotted in one graph (Fig.7.3-7.4).

Element 1 exhibits better characteristics. The torque waveforms of Element 1 are symmetrical and have smaller ripples than Element 2. The transmitted torque of the inner rotor is roughly 16.9 Nm with a cogging torque of 3.9 Nm; the cogging ratio is 23% which is better than Element 2. The outer rotor produces 28 Nm as transmitted torque and a cogging torque of 4.7 Nm; the cogging ratio is nearly 17%.

The inner rotor of Element 2 generates a transmitted torque of 8.6 Nm and a cogging torque of 3.85 Nm. The cogging ratio is nearly 45% which is too high. The outer rotor produces a transmitted torque of 14.3 Nm and a cogging torque of 3.25 Nm which gives a cogging ratio of around 23%.

The effective values of the torques are represented by bar graphs so that the effect of cogging torques is clearly observed (Fig.7.5).
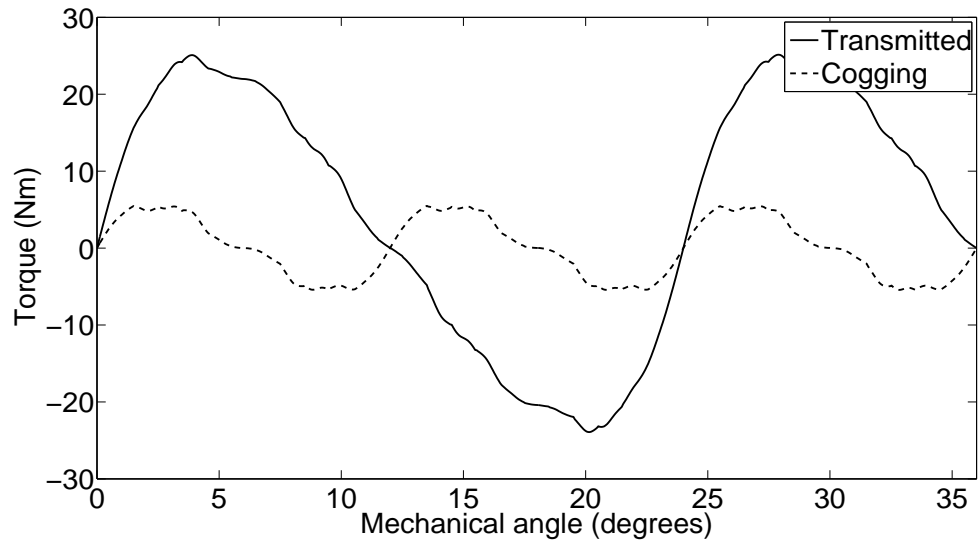
(a)
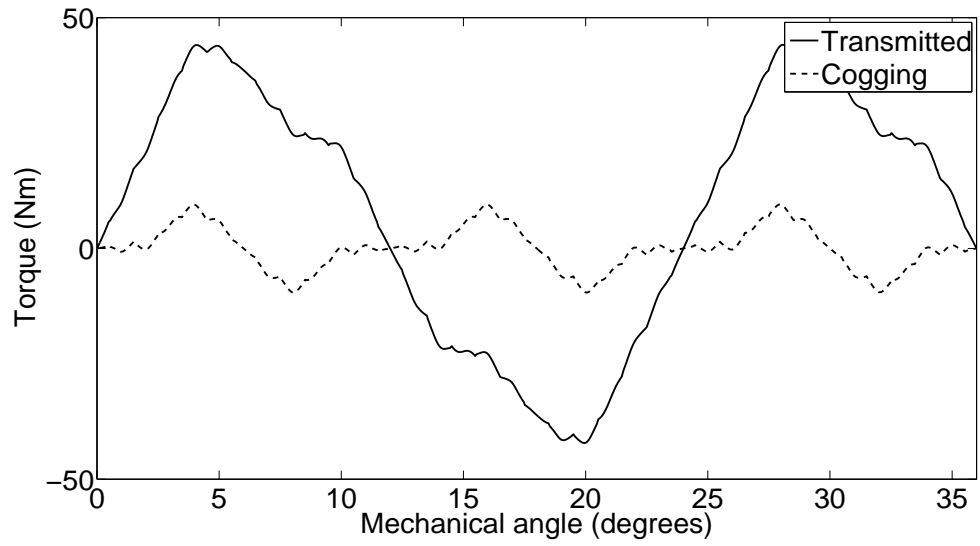
(b)

Figure 7.3: Torques of Element 1 (a) Inner rotor (b) Outer rotor
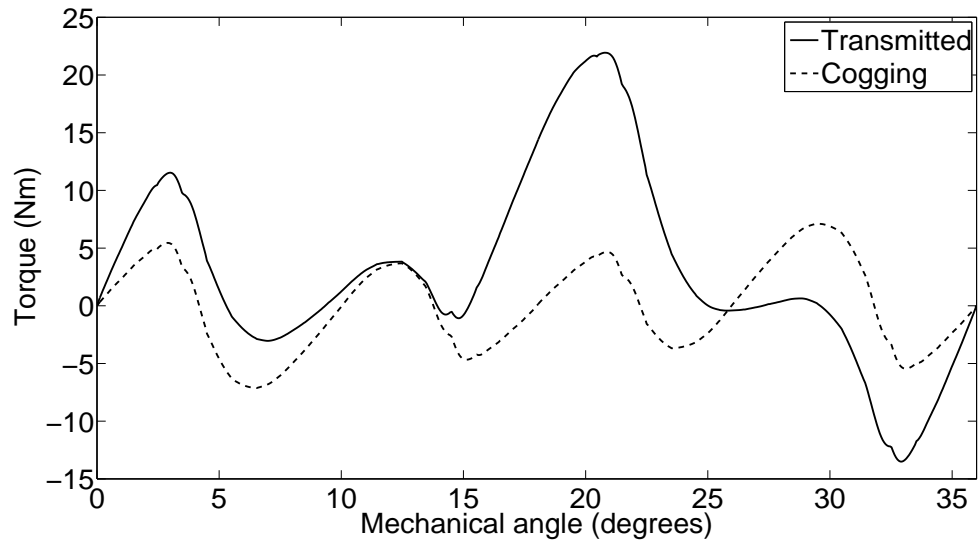
(a)
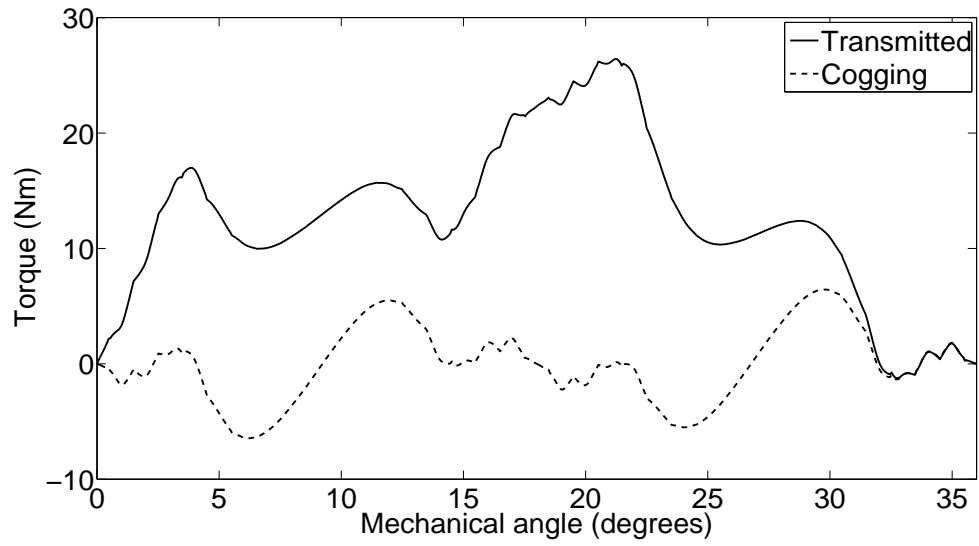
(b)

Figure 7.4: Torques of Element 2 (a) Inner rotor (b) Outer rotor
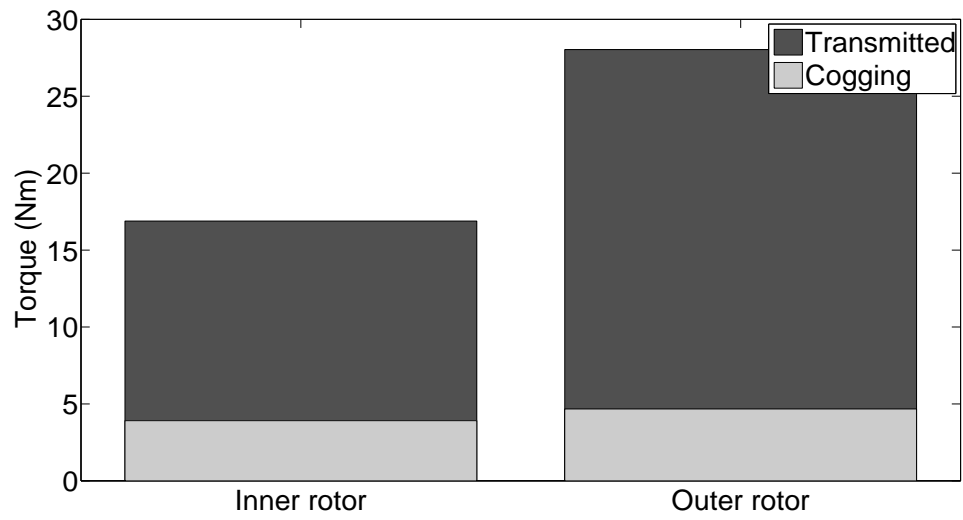
(a)
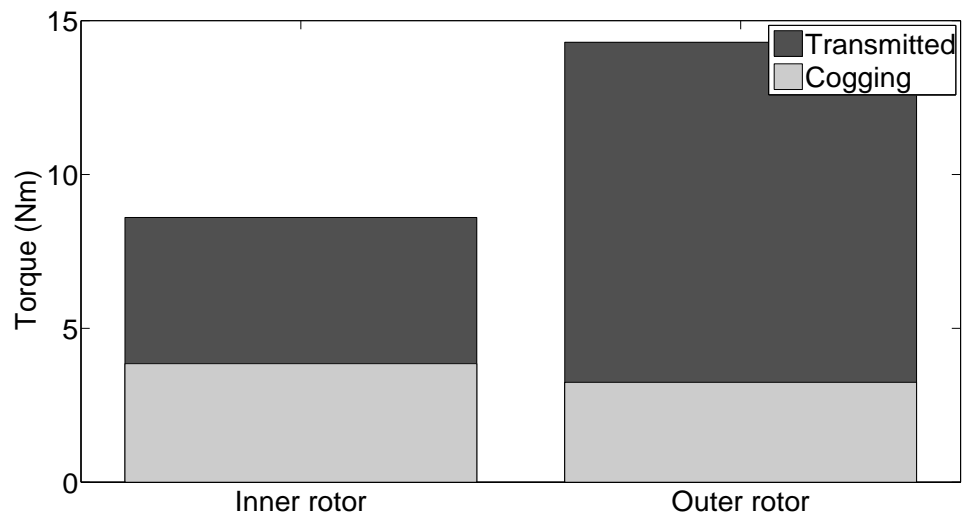
(b)

Figure 7.5: Effective values of torques (a) Element 1 (b) Element 2

7.4 Cogging torque reduction methods

The cogging torques produce vibrations and they might cause malfunctioning effects such as locking the shafts during start up. Remedies must be applied to overcome such issues without reducing the transmitted torques significantly.

7.4.1 Conventional methods

The interaction of the magneto-motive forces of permanent magnets with slots produces cogging torque. Only one research is found that thoroughly investigates this phenomenon in magnetic gears [NH12a]. Further analysis was contributed by the same authors for magnetic-geared ac motor [NH12b]. Cogging torques were reduced by skewing the magnets and pole pieces in several steps.

Many researches on the analysis and reduction of the cogging torque are found in the literature ([LS88], [IS93], [ZH00], [BB02], [Kur03], [DSR07]). The developed methods of reducing the cogging torque of different types of electric machines are listed below

1. Magnet and/or stator skewing
2. Magnet shaping
3. Magnet shifting
4. Stator-pole notching
5. Magnet arc shortening
6. IPM

Skewing the magnets and pole pieces might complicate the structure of the multi-element gear. Magnet shaping, stator notching and arc shortening would not reduce the cogging ratio. Using segmented IPM would eliminate the cogging torques but at the expense of considerable reduction of the transmitted torques.

7.4.2 Proposed methods

The cogging torque may be expressed in terms of the magnetic flux and air-gap reluctance as

$$T_{cog} = -\frac{1}{2}\phi_g^2 \frac{dR_g}{d\theta} \tag{7.1}$$

It can be reduced by decreasing the air-gap flux or the rate of change of the air-gap reluctance with the mechanical angle θ. A slight change of flux would result in significant change of the cogging torque and the transmitted torques as well. It is favored to reduce the change of reluctance.

As the inner rotor rotates, the reluctances seen by the inner rotor change from high values in slot regions to low values in core regions. This change can be decreased by decreasing the number of slots, the width of slots or the spacing between the pole pieces.

The following methods are proposed:

1. Introduction of double bridge between pole pieces

Two bridges are introduced between the pole pieces (Fig.7.6a). The bridges introduce low reluctances that cause some reduction of the resultant reluctance in the air gap.

2. Wedge-shaped pole pieces

Some of the reluctances that arise due to the introduction of the pole pieces can be reduced by re-designing the pole piece as wedge-shaped without affecting the modulating function (Fig.7.6b). .

3. Split IPM

By using interior magnets and splitting each pole into several segments, the cogging torques can be reduced to very small values but this also results in big reduction of the transmitted torques (Fig.7.7).

Table 7.3 shows the simulation results of the proposed methods. 'NA' means the used method is not applicable because of either high cogging ratio or very low transmitted torques.

The double-bridge method reduces the cogging torque by 72%-81% for Element 1. For Element 2, the cogging torque of the inner rotor is reduced by 31% but it has no effect on the outer rotor.
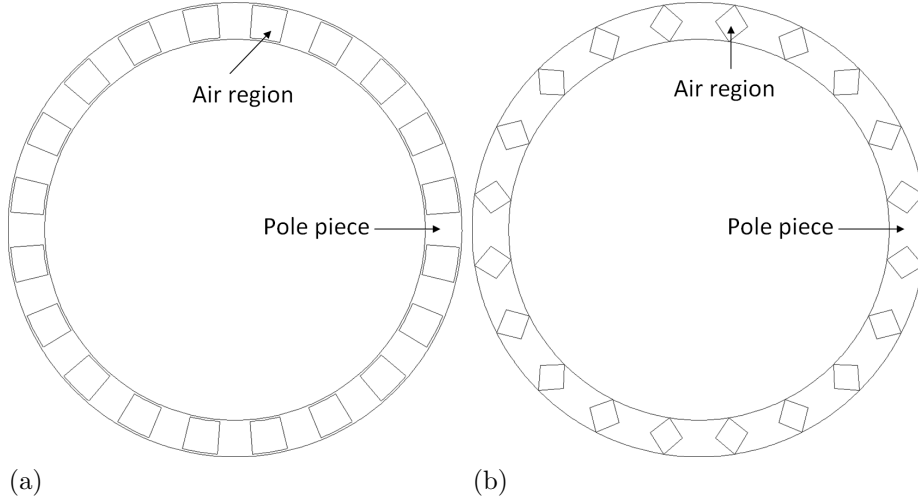
Figure 7.6: Cogging torque reduction method (a) bridges between pole pieces (b) wedge-shaped pole pieces

The wedge-shape method reduces the cogging torque of the inner rotor of Element 1 by 78% but the torque of the inner rotor is reduced by nearly 40%. The cogging torque of the outer rotor is reduced by 81% and the transmitted torque is reduced by 33%.

By using IPM, the cogging torques of both elements are reduced to very low values but the transmitted torque are also low. In Element 1, the cogging torques are reduced to roughly 0.2 N.m which implies a reduction by 96%. The transmitted torques are reduced by 63%-72%. In Element 2, the cogging torques are reduced by 96%-98%, and the transmitted torques are reduced by 76%-88%. Despite achieving low cogging torques, this method is not efficient because of the big reduction of the transmitted torques.

The wedge-shape method is suitable for Element 1. For Element 2, the effects of skewing the stator and pole pieces need to be investigated throughly according to the guidelines developed by [NH12b].

(a)   (b)
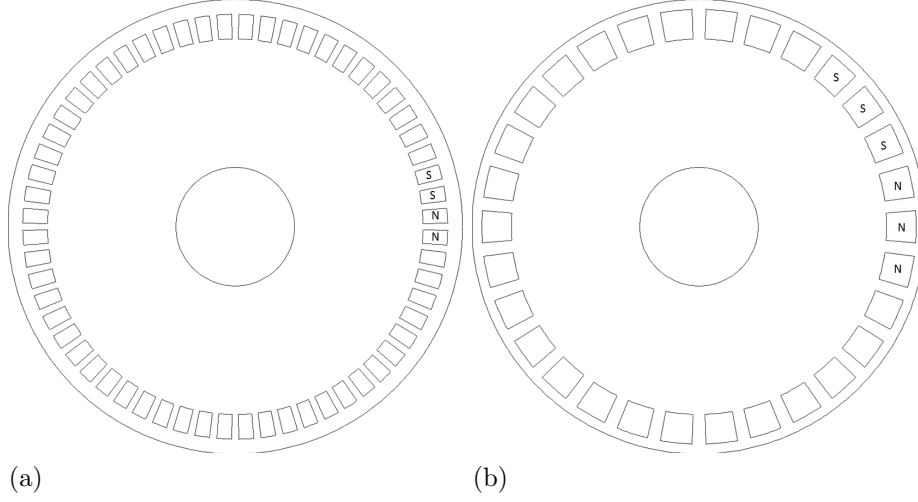
Figure 7.7: Used IPM for (a) Element 1 (b) Element 2

Element 1						
Method	T_i (Nm)	T_{cog} (Nm)	K_R (%)	T_o (Nm)	T_{cog} (Nm)	K_R(%)
Double bridge	13.8	1.1	7.97	20.6	0.9	4.37
Wedge shape	10.24	0.86	8.4	18.7	0.87	4.63
Split IPM	4.76	0.16	3.36	10.27	0.16	1.56
Element 2						
Method	T_i (Nm)	T_{cog} (Nm)	K_R (%)	T_o (Nm)	T_{cog} (Nm)	K_R(%)
Double bridge	9.96	2.65	26.6	8.74	3.24	37.1
Wedge shape	NA	NA	NA	NA	NA	NA
Split IPM	1.04	0.08	7.7	3.42	0.13	3.8

Table 7.3: Cogging torque reduction methods

Chapter 8

Conclusions

8.1 Research contribution

Finding methods for realizing magnetic variable transmission was the focus of this research. Only one method was developed by other researchers, and so this study may be considered as the second contribution in the field of magnetic variable transmission.

The techniques of magnetic gearing were studied and utilized to develop two methods one of which was practically realized. The two methods are based on the concept of pole changing.

In the first method, an electromagnetic gear was designed to have a 5-step variable gear ratio from 1.33 to 4.00. The design was optimized thoroughly, and a general design guideline was developed and could be applied to the magnetic gear and its derivatives. A torque density of 1.2 kNm/m^3 and a transmission efficiency of up to 90% were achieved. The main merit is the simplicity of the design and control circuit. The method was validated by finite element analysis and by conducting experiments on a prototype. The simulation and experimental results agree at an accuracy of up to 87%.

The second method was developed after comprehending the method of pole changing. Several magnetic gears of different topologies incorporated in one unit form a multi-element gear, and each element can be operated at a time which results in variable-transmission operation. This method produces a torque density

of roughly 12 kNm/m^3 which is ten folds higher than the previous method. However, cogging torque is a serious issue and several remedies have been proposed.

8.2   Recommendations for further research

The developed electromagnetic gear can be operated in three modes

1. Direct-current mode
2. Frequency mode
3. Induction mode

The direct-current mode was validated. In the frequency mode, the design of the hybrid magnetic gear is employed with some changes. The stator is composed of a 3-phase winding and the inner rotor is made up of permanent magnets. The pole pieces act as the outer rotor. By varying the frequency, the speed of the revolving field is varied and hence the speed of the outer rotor can be varied. A similar approach is being investigated by other researchers [ZNH12] using a vernier-type machine.

Martin described the possible operation of the magnetic gear if the inner rotor is replaced with a squirrel-cage rotor. This is an induction-mode operation. Using the realized electromagnetic gear, one winding must be connected to a direct-current supply and the other winding must be short circuited. This method reduces electric losses and simplifies the design. Once successful, a new design can be made in which the windings can be replaced by a cage rotor and permanent magnets in the stator.

The multi-element method requires improvement. Other topologies that can produce low cogging torques and high torque density should be investigated.

Appendix A

Electric Circuit of Electromagnetic Gear

The electric circuit of the realized electromagnetic gear consists of two circuits: power circuit (Fig.A.1) and control circuit (Fig.A.2). Each winding is arranged in 5 similar groups, and Fig.A.1 shows only one group. The power circuit is the connection between the windings and the power supply. The control circuit performs the process of pole changing.

The initial operation is in the 15-5-20 topology and the control circuit is de-energized. If the ON push button of the control circuit is pressed, the relay KM1 is energized. Then, the power contact 3-4 disconnects and so the poles of the stator decrease to 10 poles. Simultaneously, the power contact 5-6 closes and so all the poles of the winding of the inner rotor are energized (30 poles). The latching contact 1-2 keeps the relay energized after the ON button is released. Now the gear operates in the 5-15-20 topology. To switch back to the 15-5-20 topology, the OFF button must be pressed.
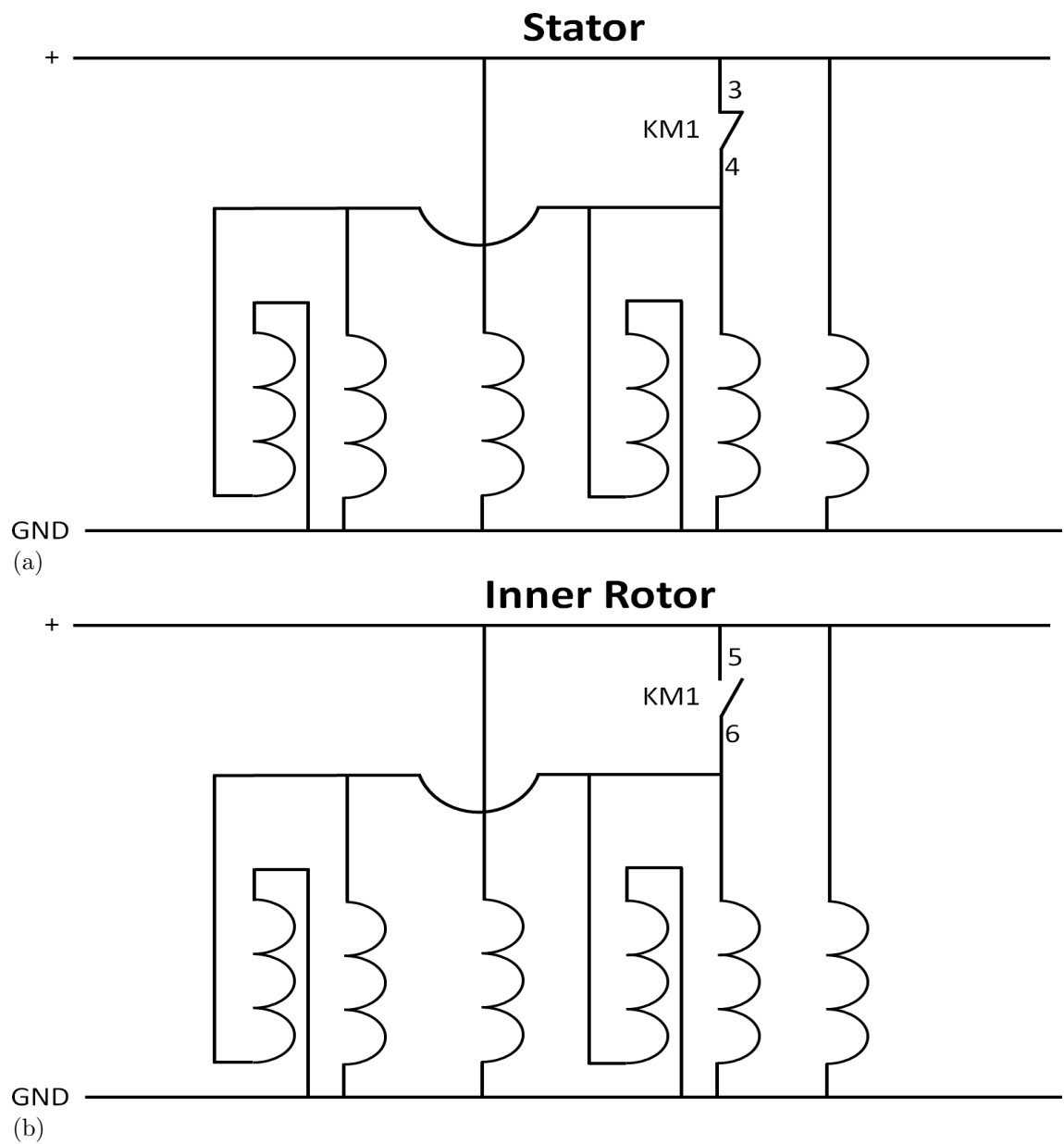
Stator

(a)

Inner Rotor

(b)

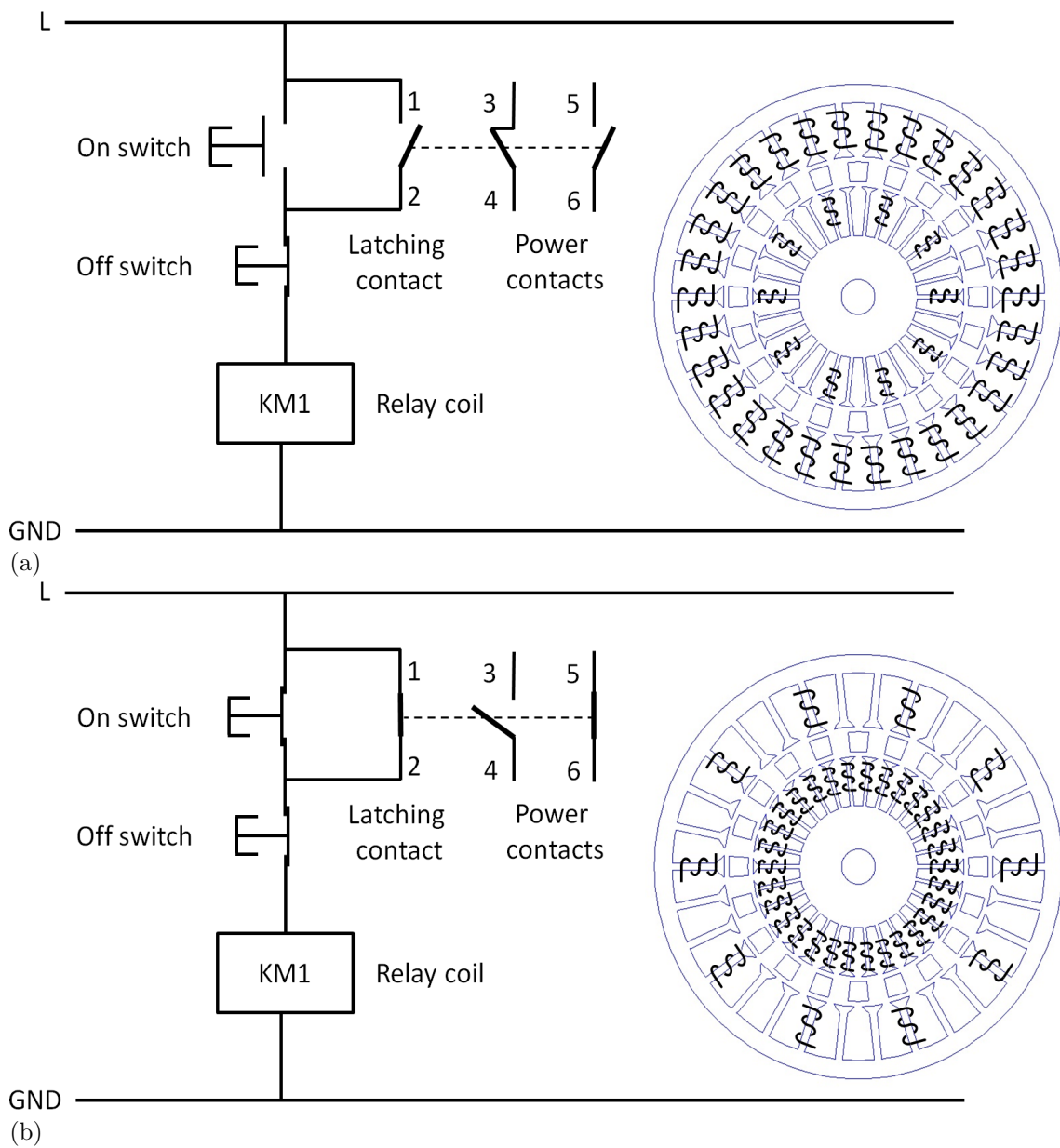Figure A.1: Part of power circuit (a) stator (b) inner rotor

Figure A.2: Control circuit (a) 15-5-20 topology (b) 5-15-20 topology

References

[AH01] K. Atallah and D. Howe. A novel high-performance magnetic gear. *IEEE Transactions on Magnetics*, 37(4):2844–2846, 2001. 4, 7

[Arm01] C.G Armstrong. Power transmitting device. *United States Patent Office*, US 687292, 26^{th}November, 1901. x, 1, 3

[AS69] F.J. Allen and S.A. Swann. A magnetic gear. *Proceedings of the 4th Universities Power Engineering Conference*, paper 8.3, Nottingham University Library, 1969. 4

[Atk58] W. Atkins. An improved electromagnetic analogue. *Proceedings of IEE*, 105C:151–154, 1958. 23

[AWCD12] K. Atallah, J. Wang, S.D. Calverley, and S. Duggan. Design and operation of a magnetic continuously variable transmission. *IEEE Transactions on Industry Applications*, 48:1288–1295, 2012. 12

[BB02] N. Bianchi and Silverio Bolognani. Design techniques for reducing cogging torque in surface-mounted pm motors. *IEEE Transactions on industry applications*, 38(5):1259–1265, 2002. 108

[BC04] V.S Beam and C.L Clarke. Power transmission. *United States Patent Office*, US 771802, 11^{th}October, 1904. 11

[Cor12] JSOL Corporation. Jmag designer. Version 11.01, 2012. 7

[CRA09] R. Clark, J. Rens, and K. Atallah. Wind turbine power train. *World Intellectual Property Organization*, PCT/GB2009/000477, 27^{th}August, 2009. 12

[DSR07] R. Dutta, S. Sayeef, and M. Rahman. Analysis of cogging torque and its effect on direct torque control in a segmented interior permanent magnet machine. *IEEE specialists conference on power electronics*, pages 2568– 2574, 2007. 108

[Fau41] H.T Faus.   Magnetic gearing.   *United States Patent Office*, US 2243555, 27thMay, 1941. x, 2, 3

[FNI11] M. Fukuoka, K. Nakamura, and O. Ichinokura. Dynamic simulation of planetary type magnetic gear based on reluctance network analysis. *Proceedings of the 2011-14th European Conference on Power Electronics and Applications (EPE 2011)*, pages 1 – 7, 2011. 7

[FT10] N.W. Frank and H.A. Toliyat. Analysis of the concentric planetary magnetic gear with strengthened stator and interior permanent magnet (ipm) inner rotor. *IEEE Energy Conversion Congress and Exposition (ECCE)*, pages 2977– 2984, 2010. 7

[Hef40] Karl Hefel. Electrical transmission gearing. *United States Patent Office*, US 2223210, 26thNovember, 1940. 12

[HHN11] M. Husain, K. Hirata, and N. Niguchi. Novel proposals for the realization of variable-transmission magnetic gear. *IEEJ Special Issue on Rotating Machinery*, 131(11), 2011. 96

[HR04] Martin Hoeijmakers and Marcel Rondel. The electrical variable transmission for a city bus. *35th Annual IEEE Power Electronics Specialist Conference*, 4:2773–2778, 2004. 12

[HT80] D.E Hesmondhalgh and D. Tipping. A multi-element magnetic gear. *IEE Proceedings*, 127:129–138, 1980. x, 4, 6, 15, 21

[IS93] T. Ishikawa and G. Slemon. A method of reducing ripple torque in permanent magnet motors without skewing. *IEEE transactions on magnetics*, 29(2):2028 – 2031, 1993. 108

[JC10]   Linni Jian and K.T. Chau. A coaxial magnetic gear with halbach permanent-magnet arrays. *IEEE Transactions on Energy Conversion*, 25(2):319 – 328, 2010. 7, 12

[Kur03]   Panu Kurronen. Torque vibration model of axial-flux surfacemounted permanent magnet synchronous machine. *PhD thesis, Lappeenranta University of Technology*, pages 71– 111, 2003. 108

[LCJY09]   Xinhua Liu, K.T. Chau, J.Z. Jiang, and Chuang Yu. Design and analysis of interior-magnet outer-rotor concentric magnetic gears. *Journal of Applied Physics*, 105(7):07F101–07F101–3, 2009. 7

[Leo91]   H.W Leonard. Electrical transmission of power. *United States Patent Office*, US 463802, 24thNovember, 1891. 11

[LS88]   T. Li and G. Slemon. Reduction of cogging torque in permanent magnet motors. *IEEE transactions on magnetics*, 24(6):2901–2903, 1988. 108

[Mar68]   T.B Martin. Magnetic transmission. *United States Patent Office*, US 3378710, 16thApril, 1968. x, 4, 5

[Mee12]   D.C Meeker. Finite element method magnetics. Version 4.2, 2012. 7

[Neu16]   A.H Neuland. Apparatus for transmitting power. *United States Patent Office*, US 1171351, 8thFebruary, 1916. x, 2, 5

[NH12a]   N. Niguchi and K. Hirata. Cogging torque analysis of magnetic gear. *IEEE Transactions on Industrial Electronics*, 59(5):2189 –2197, 2012. 108

[NH12b]   N. Niguchi and K. Hirata. Cogging torque characteristics of magnetic-geared motor. *The International Journal for Computation and Mathematics in Electrical and Electronic Engineering (COMPEL)*, 31(5):1470–1481, 2012. 108, 110

[Per02]   Jarmo Perho. *Reluctance network for analyzing induction machines.* PhD thesis, Helsinki University of Technology, Laboratory of Electromechanics, 2002. 42

[RA09]   J. Rens and K. Atallah. Variable magnetic gears. *World Intellectual Property Organization*, PCT/GB2009/000476, 27thAugust, 2009. 12

[RAJN03]   P.O Rasmussen, T.O. Andersen, F.T. Joergensen, and O. Nielson. Development of a high-performance magnetic gear. *38th IAS Annual Meeting Industry Applications Conference*, 3:1696–1702, 2003. 7

[SCW11]   Laxman Shah, Andrew Cruden, and Barry W. Williams. A variable speed magnetic gear box using contra-rotating input shafts. *IEEE Transactions on Magnetics*, 47(2):431–438, 2011. 12

[TK87]   K. Tsurumoto and S. Kikuchi. A new magnetic gear using permanent magnets. *IEEE Transactions on Magnetics*, 23(5):3622–3624, 1987. x, 4, 6

[WAC11]   Jiabin Wang, K. Atallah, and S.D. Carvley. A magnetic continuously variable transmission device. *IEEE Transactions on Magnetics*, 47:2815–2818, 2011. 12

[Yao00]   Yeong-Der Yao. Method of designing optimal bi-axial magnetic gears. *United States Patent Office*, US 6047456, 11thApril, 2000. x, 2, 3

[ZH00]   Z.Q Zhu and D. Howe. Influence of design parameters on cogging torque in permanent magnet machines. *IEEE transactions on energy conversion*, 15(4):407–412, 2000. 108

[ZNH12]   A. Zaini, N. Niguchi, and K. Hirata. Continuously variable speed vernier magnetic gear. *IEEE transactions on magnetics*, 48(11):3104–3107, 2012. 113